

SHRP-S-324

Condition Evaluation of Concrete Bridges Relative to Reinforcement Corrosion

Volume 2: Method for Measuring the Corrosion Rate of Reinforcing Steel

Janusz Flis, Akshey Sehgal, Dan Li,
Young-Tai Kho, Scott Sabotl,
Howard Pickering, Kwadwo Osseo-Asare

Philip D. Cady
Pennsylvania Transportation Institute
The Pennsylvania State University
University Park, PA



Strategic Highway Research Program
National Research Council
Washington, DC 1993

SHRP-S-324
ISBN: 309-05258-0
Contract C-101

Program Manager: *Don M. Harriott*
Project Manager: *Joseph F. Lamond*
Copy Editor: *Katharyn Bine Brosseau*
PTI Technical Editor: *Joanne M. Fox*
Program Area Secretary: *Ann Saccomano*

September 1992

key words:
bridges
concrete resistance
corrosion current
corrosion rate
electrochemical measurements
field testing
half-cell potentials
polarization resistance
reinforced concrete

Strategic Highway Research Program
National Academy of Sciences
2101 Constitution Avenue N.W.
Washington, DC 20418

(202) 334-3774

The publication of this report does not necessarily indicate approval or endorsement of the findings, opinions, conclusions, or recommendations either inferred or specifically expressed herein by the National Academy of Sciences, the United States Government, or the American Association of State Highway and Transportation Officials or its member states.

© 1993 National Academy of Sciences

Acknowledgments

The research described herein was supported by the Strategic Highway Research Program (SHRP). SHRP is a unit of the National Research Council that was authorized by Section 128 of the Surface Transportation and Uniform Rehabilitation Assistance Act of 1987.

The authors acknowledge the Nippon Steel Corporation and K. C. Clear, Inc., for providing their instruments for the laboratory and field testing, and they thank M. Garcia for carrying out measurements with the GECOR device. The authors are grateful to the Florida Department of Transportation, the Pennsylvania Department of Transportation, and the Virginia Department of Transportation for their assistance in the planning and performance of the field studies. Many thanks also are due to Edward J. Gannon of the Pennsylvania State University for his considerable contribution to this research.

Contents

Abstract	1
Executive Summary	3
1. Introduction	5
Objectives	5
Scope	6
2. Background	7
Technology Assessment	7
General Research Approach	9
3. Preliminary Testing	11
Preparation of Specimens	11
Corrosion Rate Devices	12
Experimental Procedures	17
Results and Discussion	18
4. Current Distribution in the Measurement of Corrosion Rate of Reinforcing Bars in Concrete	45
Investigation Method	45
Results and Discussion	49
5. Field Validation Studies	65
Introduction	65
Devices Used for Corrosion Rate Measurements	66
Test Sites	66

Testing Procedure	73
Results	78
Discussion	93
6. Summary and Conclusions	95
Basic Laboratory Studies	95
Current Distribution Studies	97
Field Validation Studies	98
Test Procedure	99
References	101

List of Figures

3-1. Concrete specimen geometry showing the exposed part of the rebar	13
3-2. Schematic illustration of the mortar specimen used in the macrocell test	14
3-3. Variation of corrosion potential after wetting the concrete surface	21
3-4. Current and potential distribution in concrete showing the effect of probe position	22
3-5. GE/CE: (a) top view; (b) cross sectional view	25
3-6. Corrosion caused by anodic polarization of rebar using: (a) CE only; (b) CE and GE	29
3-7. The extent of corrosion by anodic polarization of rebars	30
3-8. Influence of corrosion spot on R_p measurements	32
3-9. Polarization resistance values along the rebar	33
3-10. Comparison of polarization resistance values obtained with EIS and the NSC device	39
4-1. Schematic representation of polarizing electrodes and steel-in-concrete system . . .	50
4-2. Potential/current distribution in the longitudinal direction of the rebar	51
4-3. Potential/current distribution around the cross section of the rebar without GE	52

4-4. Potential/current distribution around the cross section of the rebar with GE	53
4-5. Effect of polarization resistance on current distribution	55
4-6. Effect of separation distance on signal distribution	56
4-7. Effect of concrete cover thickness on signal distribution	57
4-8. Effect of GE size on signal distribution	59
4-9. Potential/current distribution	60
4-10. Potential/current distribution showing effect of macrocells along rebar	62
4-11. Potential/current distribution showing effect of macrocell along rebar without GE	63
5-1. NSC device on a bridge on US Route 220 in Pennsylvania	67
5-2. The 3LP instrument on a bridge deck on US Route 220 in Pennsylvania	68
5-3. The GECOR device on a distressed pier column of a bridge on US Route 322 in Pennsylvania	69
5-4. Position of test sites H, C, T and L on Assembly 65 and Pile 75 of Bahia Honda Bridge (northbound), Florida	71
5-5. Position of test sites D1 to D4 on bridge decks	72
5-6. Using a rebar locator to determine the position of the reinforcement	74
5-7. Core drilling in order to expose a rebar for making an electrical connection	75
5-8. Drilling a pier column to install wall anchors for affixing an instrument probe to the concrete surface	76
5-9. Taking corrosion potential readings with the copper/copper sulfate half-cell	77

5-10.	Corrosion current i_c versus corrosion potential E_c for Bahia Honda Bridge	79
5-11.	Corrosion current i_c versus corrosion potential E_c for Bridge 322, PA	80
5-12.	Corrosion current i_c versus corrosion potential E_c for Bridge 220, PA	81
5-13.	Corrosion current i_c versus corrosion potential E_c for Bridge 81N-2, VA	82
5-14.	Corrosion current i_c versus concrete resistance R_s for the sites tested	85
5-15.	Standard error if i_c as a function of i_c for Bahia Honda Bridge, measured by devices NSC, 3LP, and GECOR on days indicated	87
5-16.	Standard error versus i_c for all the bridges, measured by 3LP device	88
5-17.	Standard error versus i_c for all the bridges, measured by all the devices	89
5-18.	Relationships between i_c values determined by NSC, 3LP, and GECOR for all the field test sites and for laboratory slabs	92

List of Tables

2-1. Various electrochemical methods of corrosion rate measurements	9
3-1. Specifications of specimens tested	15
3-2. Polarization resistance values ($k\Omega\text{ cm}^2$), measured with the NSC device, of medium-size mortar specimens using different probe contact methods	19
3-3. Effect of probe placement on R_p measurements made with the NSC device on large concrete specimens.	23
3-4. Polarization resistance (R_p) values obtained by the NSC device on medium-size mortar specimens with and without GE.	26
3-5. Effect of GE parameters on measured polarization resistance (R_p) values obtained using the NSC device on medium-size mortar specimens.	27
3-6. Polarization resistance (R_p) measurements showing the effect of macrocell.	36
3-7. Comparison of two corrosion rate measuring methods with steel coupons in $0.2\text{NH}_2\text{SO}_4$ solution.	40
3-8. Polarization resistance ($k\Omega\text{ cm}^2$) results obtained with large specimens using various devices.	41
4-1. Input parameters for numerical simulation (1-m-long [3.28-ft-long] segments). . .	49
5-1. Distances for test sites on bridge decks and the height of test sites on piers and abutments.	70

- 5-2. Values of A and B in equation $\log EM \text{ (Bridge)} = A + B \log i_c$ for data from all the devices for each bridge separately; R^2 is the coefficient of determination 90
- 5-3. Values of C and D in equation $\log EM \text{ (Device)} = C - D \log i_c$ for data from all the bridges for each device separately; R^2 is the coefficient of determination 90

Abstract

Laboratory studies examined the myriad parameters effecting corrosion rate measurements made by electrochemical means. The most important parameters found were: good electrical contact between the probe and the concrete surface; symmetric positioning of the probe over the rebar; presence of a stable open-circuit (corrosion) potential; use of a guard ring of appropriate size and spacing (relative to the counter electrode) to define the polarized area; and the necessity of ensuring that measurements are carried out over the active part of macrocells.

Three commercially developed corrosion rate devices were evaluated in the laboratory and the field. Two, GECOR and 3LP, operate on the linear polarization principle. The third, an NSC device, operates on the principle of superimposed current pulses of high and low frequency with current confinement. All gave comparable qualitative results for actively corroding conditions. Field tests were carried out at sites representing sub-tropical marine, mild and severe winter (deicing chemical) exposure conditions.

Reproducibility was comparable among the three devices. The corrosion currents measured correlate with each other, although rather significant differences exist in magnitude.

Executive Summary

Three commercially developed devices were used to measure the polarization resistance of reinforcing steel in concrete. Two devices operated on the principle of linear polarization with or without current confinement (the GECOR and 3LP devices, respectively), while the third was based on the principle of superimposed current pulses of high and low frequency with current confinement (the NSC device). For comparison, impedance measurements were also made with the use of a Solartron frequency response analyzer.

It was found that the instruments gave comparable results in the laboratory for small mortar specimens and large slabs with actively corroding steel; however, these instruments were unable to confine signal distribution for large slabs with passive steel.

The polarizing current reaches the steel rebar over an area far beyond that of the counter electrode (CE) of the probe. Thus, for a proper evaluation of the corrosion rate it is important to define the polarized area of the rebar. This can be achieved by applying a guard electrode (GE) for current confinement. The GE is situated concentrically around the CE and is maintained at the same potential as the CE. As a result, the signal distribution from the CE is limited to an area not greater than the midpoint of the separation between the CE and the GE, when both the electrodes are of the same width and assuming the concrete can be treated as a homogeneous medium.

Ring GEs of various sizes were examined to obtain the optimal current confinement. It was found that the signal confinement was improved by decreasing the separation between the CEs and GEs and by increasing the width of the GE. Experiments showed that most of the half of the rebar that faces the probe is polarized during the measurements instead of the entire circumference of the rebar. The assumption of the polarization of the entire circumference leads to an underestimation of the corrosion rate by up to half of its real value.

Numerical techniques were used to determine current distributions in concrete with embedded steel rebars. The current distribution was calculated for a variety of parameters, including geometry of the CE/GE system, polarization resistance, concrete resistance, and cover thickness.

Numerical calculations showed that the most significant parameter in specifying the polarized area is the concrete cover thickness; the polarized area increases significantly with increasing cover thickness. The other two important parameters are the polarization resistance and the separation between CE and GE. If the GE length is larger than the cover thickness, then the polarized area does not change much with increasing GE length.

The electrochemical measurements were performed with the use of three devices (NSC, 3LP, and GECOR) on bridges chosen in areas representing a marine environment and regions with mild and cold winters where the use of deicing agents was low or more extensive, respectively. Corrosion currents (i_c) were low and almost independent of corrosion potentials (E_c) when the potential was nobler (more positive) than about -0.25 V relative to the copper/copper sulfate half-cell, whereas they increased as E_c shifted in the negative direction. The i_c versus E_c relationship is in agreement with the qualitative estimation of corrosion activity based on the corrosion potential measurements alone (ASTM C876-87). Values of i_c were inversely proportional to the concrete resistance.

On the basis of the laboratory findings and field work, a draft Standard Test Method for Determining Instantaneous Corrosion Rate of Uncoated Steel in Reinforced Concrete has been prepared.

1

Introduction

Corrosion damage is a multibillion dollar problem in the United States and other countries (1-4). In a 1986 report, the Strategic Highway Research Program (SHRP) estimated that the unfunded liability to correct corrosion-induced distress in bridges in the United States was \$20 billion and was increasing by about \$0.5 billion annually (5). While the collapse of the Berlin Congress Hall (6) and a parking garage in Minnesota (7,8) has been widely publicized, corrosion problems in numerous unpublicized reinforced structures produce significant maintenance and replacement costs (4). The United States Secretary of Transportation's report to Congress in 1982 estimated that there are nearly 213,000 deteriorating bridge structures alone with a repair cost of \$41.1 billion (9). By 1986, the number of deteriorating bridge structures had gone up to nearly 244,000, with a total repair/rehabilitation/replacement cost of \$51.4 billion (10).

A rapid, nondestructive field test method for measuring the corrosion rate of reinforcing steel in concrete structures would provide key information for the evaluation of structure life-cycle costs. Equipment that would provide this information is being developed. Therefore, the emphasis of the research was placed on working cooperatively with the developers of available, promising devices.

Objective

The overall objective of the work described in this report was to develop a methodology for the nondestructive measurement of the corrosion rate of steel embedded in concrete. The

information on the corrosion rate is needed to determine the present condition of concrete structure components and to predict future deterioration rates.

Scope

The scope of the research effort described in this volume involves the identification of the appropriate electrochemical technique(s), their enhancement and development, and the verification necessary to meet the objective.

The desired characteristics of the candidate methods for corrosion rate measurement of reinforcing steel in concrete bridge components are:

- They should provide a *quantitative* measure of instantaneous corrosion rate;
- They should permit *rapid* corrosion rate data acquisition;
- They should be simple in terms of equipment and operation; and
- They should be portable and durable.

2

Background

Technology Assessment

Since corrosion is an electrochemical process, it is rational to monitor it with electrochemical techniques. Most of the electrochemical techniques for determining the corrosion rate involve measurement of polarization resistance (R_p) since it is inversely proportional to the corrosion current, which in turn is directly proportional to the corrosion rate. This assumes that the measurement of R_p is made under open-circuit conditions, i.e., in the absence of any other polarization such as cathodic protection, stray electrical fields, etc. However, a number of questions arise:

- How quickly can R_p be measured?
- How reliable is the measurement technique over the range of environmental variables?
- How expensive is the equipment needed to do the job?
- How portable and field-durable is the equipment?

The second question above poses particular problems for measuring the corrosion rate of steel in concrete. For example, the resistivity of concrete can vary by about eight orders of magnitude (10^0 to 10^7 ohm-cm), depending on the degree of saturation of the concrete and the ions contained in the pore solution. Furthermore, several implicit assumptions are

involved in linking polarization resistance with corrosion rate, and that in some systems there may not even exist measurable polarization resistance. However, polarization resistance measurement has been found to generally work well with the steel in concrete system throughout the wide range of conditions encountered in practice.

Electrochemical techniques for measuring corrosion rate can be categorized into two broad classifications--transient and steady state. Examples of steady-state methods include Tafel slope extrapolation (to determine the corrosion current) and linear polarization measurements (to determine the polarization resistance) and, subsequently, the corrosion current. In both of these methods, the potential is varied and the current is allowed to come to steady state. There is a wide variety of transient methods, including potential step, small amplitude cyclic voltammetry, impedance, and current step. The first three involve the application of a potential (step, ramp, and AC, respectively) and measuring current response. The fourth involves the application of a current step and measurement of the potential response. Corrosion currents can then be extracted in each case using the appropriate models, and corrosion rates can be calculated by the application of Faraday's Law.

Thus, there is a wide variety of potential electrochemical procedures that might be used to provide information on the rate of corrosion of steel in concrete. Table 2-1 lists the advantages and disadvantages of some of the procedures.

For the steady-state techniques, an important consideration is the time needed to attain the steady-state condition. Because polarization resistance is much greater than concrete resistance (under the usual moisture conditions of concrete in the field), use of potential step requires less time to reach steady-state than use of current step. Therefore, especially for steady-state techniques, potential step methods should be considered.

In small amplitude cyclic voltammetry, a voltage ramp is applied and then reversed and current response is measured. The nature of the signal received is highly dependent on the scan rate, and, at the lower limit, information on concrete resistance is lost.

The AC impedance method involves measuring impedance while scanning frequencies. A plot of the absolute values of the imaginary versus the real component of the impedance values is, ideally, a semi-circle, of which the diameter is the polarization resistance and the intercept on the real component axis at the low impedance (high frequency) end is the concrete resistance. In practice, the plot often deviates greatly from a semicircular shape. Also, under conditions of low corrosion rate and high concrete resistance, the low-frequency impedance limit may be undefined, as would be the corrosion rate. With the high polarization resistances encountered with steel in concrete, very low frequencies are needed

Table 2-1. Various electrochemical methods of corrosion rate measurements.

TECHNIQUES	ADVANTAGES	DISADVANTAGES
Polarization Curves	<ul style="list-style-type: none"> · Give information about steel's behavior at potentials other than E_{corr} 	<ul style="list-style-type: none"> · Sometimes destructive · Takes long time
Tafel Slope Extrapolation	<ul style="list-style-type: none"> · Simultaneous determination of β_a and β_c 	<ul style="list-style-type: none"> · IR-drop effect is significant
Linear Polarization	<ul style="list-style-type: none"> · Fast method (short measuring time) · Small perturbation (minimal disturbance of interface) · Simple method and low equipment cost 	<ul style="list-style-type: none"> · Sweep rate dependence of R_p · Separate measurement of Tafel slope required · IR-drop effect is significant
AC Impedance	<ul style="list-style-type: none"> · Suitable for low conductivity media · Simultaneous determination of R_c and R_p · Determines C, R_c and R_p 	<ul style="list-style-type: none"> · Long measuring time (for low frequency region) · Interpretation of results is difficult · Extrapolation is needed sometimes · Equipment is costly

in order to establish the polarization resistance value. From the practical viewpoint of field application, a complete frequency scan is simply too time-consuming. Since only very low- and very high-frequency response data are needed in order to define the corrosion rate, a method developed for field use should scan only those regions.

General Research Approach

There are two major problems that occur in the translation of these methods from the laboratory to the field. The area of the field-model working electrode (WE) is much larger than that of the CE. The current path between the electrodes therefore is not defined precisely. As a result, neither the amount of the signal received by the WE nor the area of the WE that receives the signal is known.

There are two ways to solve these problems. One approach uses a "guard ring" second concentric CE surrounding the first CE. It is at the same potential as the central CE. This

causes the current paths between the central CE and the WE to be essentially straight. Thus, the area of the WE polarized by the central CE is, in theory, equal to the area of the central CE. The second approach is to electronically model the system on the basis of a transmission line, since the reinforcement is very long in comparison with the effective polarization range of the CE.

Instrumentation for determining corrosion rates of steel in concrete was under development. Therefore, the emphasis was placed on working cooperatively with the developers of the most promising devices. Three devices were selected based on their level of development and availability.

The general research approach consisted of:

- Laboratory evaluations of the parameters that affect measurement of the corrosion rate of steel embedded in concrete;
- Computer modeling of the current distribution in the linear polarization process to aid in evaluating probe design and measurement geometry;
- Laboratory and field evaluations of three commercially available devices developed for measuring the rate of corrosion of steel embedded in concrete; and
- Development of a draft standard test method for determining the instantaneous corrosion rate of uncoated steel in reinforced concrete.

3

Preliminary Testing

Preparation of Specimens

Mortar specimens with dimensions of 2.5 x 2 x 1 in. (6.5 x 5.0 x 2.5 cm) were made using an ASTM A36 steel coupon with dimensions of 3 x 1 x .25 in. (7.7 x 2.5 x 0.6 cm). The steel coupons were thoroughly cleaned with a metallic brush to remove surface scale. Epoxy paint was applied to the top, bottom, and back surfaces in order to prevent crevice corrosion and expose a known area of the steel surface. For the mortar mixture, standard graded sand (ASTM C778), portland cement, and distilled water were used. The sand : cement : water ratio was 2.75 : 1.0 : 0.6 by mass. The specimens were cured (in air) in a wooden mold for 48 hours, after which they were removed from the mold and cured for 4 weeks in a 100-percent relative humidity (RH) chamber. Medium-sized mortar specimens with dimensions of 11.8 x 5.9 x 3.5 in. (30 x 15 x 9 cm) were made using no. 4 rebar (0.5 in. [1.3 cm] in diameter) and a sand : cement : water ratio of 2.75 : 1.0 : 0.6. After molding, the specimens were cured for 4 weeks in a 100-percent RH chamber. Some of the medium-size specimens contained 2 wt percent chlorides, which were added to the mortar mix. This was done to compare results obtained from corroding (chloride containing) and noncorroding (no chlorides) specimens.

Three large concrete specimens were made. Two of the large concrete slabs with dimensions of 78.7 x 31.5 x 3.9 in. (200 x 80 x 10 cm) were made using a coarse aggregate : fine aggregate : cement : water ratio of 3.85 : 2.75 : 1.0 : 0.6 (by mass) without any chloride additives. The third large concrete specimen was made with 2 wt percent chlorides (NaCl as chloride additive) to the concrete mix. The steel rebar (A-36 grade, no. 4 size, 0.5 in.

[1.3 cm] in diameter) had a concrete cover of 1.8 in. (4.6 cm), and each specimen had three parallel rebars along its length. In one of the specimens without chloride, a well-defined corrosion spot was created by inserting a plastic cup over the central rebar during casting. The rebar at that point had no concrete cover and was directly exposed to the atmosphere. The rebar was corroded by pouring HCl into the cup, thus creating a well defined corrosion area. The specimen geometry is shown in Figure 3-1. The specimens were cured for 4 weeks in a 100-percent RH chamber.

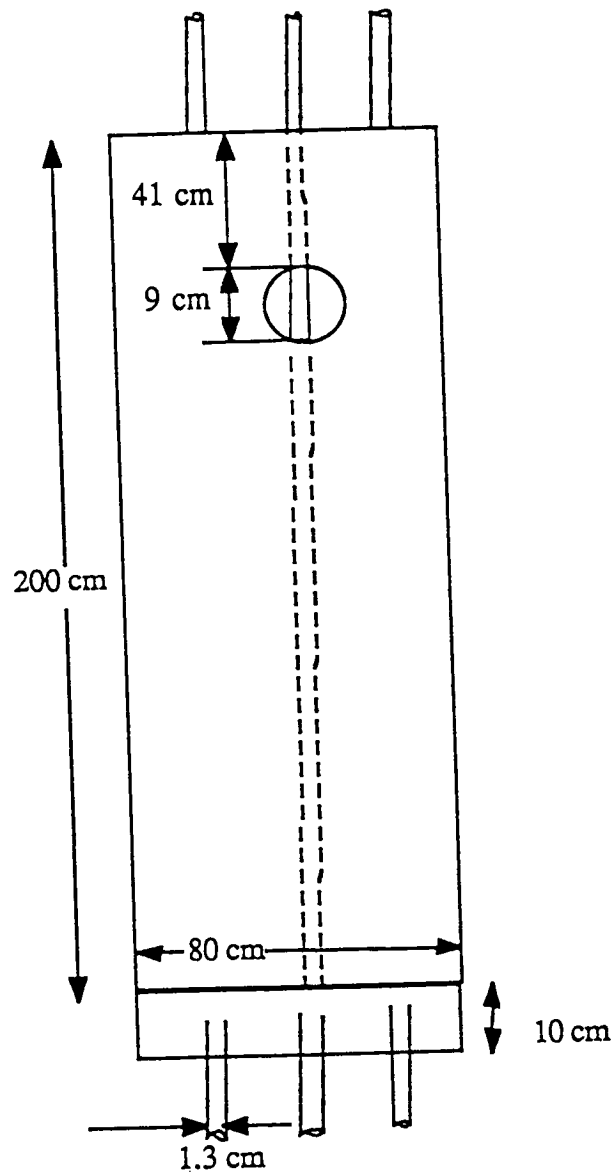
To study the macrocell effect, a mortar specimen with dimensions of 43.3 x 24 x 3 in. (110 x 61 x 7.6 cm) with a cover thickness of 1 in. (2.5 cm), and a sand : cement : water ratio of 2.75 : 1.0 : 0.6 and 15 wt percent chloride additives (NaCl), was made. Alternate bars of copper and steel were arranged in two rows. Each of the bars was 3.9 in. (10 cm) long and had a diameter of 0.5 in. (1.3 cm). These bars were uniformly spaced 3.9 in. (10 cm) apart while the two rows were 6 in. (15.2 cm) from the edge of the specimen and were separated by 11 in. (28 cm). The bars were placed on plastic anchors and tied to the anchor with plastic strings so that the bars would not be displaced when the mortar mix was poured and subsequently cured. Copper wires were soldered to each end of the rebar and the ends coated with plastic spray to avoid galvanic corrosion. These wires were permitted to protrude from the specimen surface and were used to make electrical connections with each other and the corrosion rate measuring device.

The specimen geometry is shown in Figure 3-2. Carbon paste electrodes were painted on the specimen surface. This was done to compare the effect of mortar cover (1 in. [2.5 cm] for the paste electrode and 11 in. [28 cm] between the two rows) and any possible effect of a corroding CE on the measurements. The paste electrodes were actually painted right over the embedded bars on the specimen surface and are shown displaced in Figure 3-2 only to show the shape and size of the bars embedded in mortar. The curing procedure followed was the same as described above.

The laboratory concrete specimen specifications are summarized in Table 3-1.

Corrosion Rate Devices

Three commercially developed prototype devices were chosen from the instruments reported in the literature (11). They were provided by Nippon Steel Corporation, K. C. Clear, Inc., and GEOCISA. The devices are designated in this report as NSC, 3LP, and GECOR,



Note: 1 cm = 0.39 in.

Figure 3-1. Concrete specimen geometry showing the exposed part of the rebar.

Table 3-1. Specifications of specimens tested.

Specimen	Composition (by mass)	Dimensions, in. (cm)	Tests
Steel Coupons	N/A ^a	0.9 x 0.9 x 0.04 (2.25 x 2.4 x 0.1)	Weight Loss; Polarization Resistance
Small-Size Mortar ^b	Sand: Cement: Water = 2.75:1.0:0.6	2.5 x 2 x 1 (6.5 x 5.0 x 2.5)	Polarization Resistance
Medium-Size Mortar ^b	Same as Above ^c	11.8 x 5.9 x 3.5 (30 x 15 x 9)	Polarization Resistance; Electrical Contact; Surface Morphology; Wetting; Probe Placement; GE Confinement and Parameters
Large-Size Concrete ^b	N11 and N12 Same as Above Cl 11 ^d	78.7 x 31.5 x 3.9 (200 x 80 x 10)	Locate and Determine Extent of Corroding Area; Compare Various Devices/ Techniques
Large-Size Mortar Macrocell ^b	Same as Above ^e	43.3 x 24 x 3 (110 x 61 x 7.6)	Macrocell Effect

^aNot applicable

^bCuring was carried out for 28 days in a 100-percent RH chamber.

^cSome specimens contained 8 wt % NaCl.

^dContained 3.3 wt % NaCl

^eContained 15 wt % NaCl

respectively (12). For information regarding procurement or operational details of these devices, see Notes 1-3 in the standard test method presented in Appendix A of Volume 8 ("Procedure Manual") of this report series.

NSC (Nippon Steel Corporation)

The Portable Corrosion Monitor Model 1 and/or Model 3 was used. A CE (1.4-in. [36-mm] outer diameter and 0.24-in. [6-mm] inner diameter) was surrounded by a ring GE (2.4-in. [60-mm] outer diameter).

This device operates by using a galvanostatic double pulse. Two current pulses of different frequencies are superimposed. The higher frequency provides a measure of the concrete resistance (R_c). The lower frequency measures the sum of concrete resistance and polarization resistance. Thus, the difference between the two provides polarization resistance (R_p), from which the corrosion current and corrosion rate can be calculated. The technique used here differs from the AC impedance technique in that it does not sweep frequencies, but uses only two. The two frequencies can be selected, or the operator may use the values incorporated in the "automatic" operational mode (1300 and 0.02 Hz). The lowest selectable frequency is 1 mHz, which may not be low enough to measure polarization resistance in the passive state. The probe consists of a central silver/silver chloride reference electrode and concentric platinum CE and GE. The CE and GE are maintained at the same potential using a voltage follower.

3LP (K. C. Clear, Inc.)

The instrument is named 3LP because it uses a three-electrode linear polarization technique (13). A cathodic current sweep is applied until the rebar is cathodically polarized to 12 mV. During this process, the current flow values at polarization levels of 4, 8, and 12 mV are recorded. Upon reaching the 12-mV polarization level, the system is depolarized and must return to within 2 mV of the original potential for a valid determination. The probe consists of a pencil copper/copper sulfate reference electrode and a copper mesh CE 6.75 in. (17.1 cm) long. It is not equipped with a GE. Approximately 3 minutes are needed to take one reading.

GECOR (GEOCISA)

This equipment is manufactured in Spain (14,15). It consists of the corrosion meter model no. LG-ECM-03 and the probe model no. LG-ECS-04. The probe uses two sensor electrodes (3.1 in. [80 mm]) in diameter and external CEs. The diameter of the current confinement area is 5.5 in. (140 mm). Before applying current to the system, the corrosion potential is measured with a solid silver/silver chloride reference electrode placed at the center of the probe. Any potential difference existing between the two sensor electrodes is also determined. Current is applied from the CE in the center of the probe, changing the potential difference between the two sensor electrodes. Current is then applied from the external counter (guard) electrode until the potential difference between the two sensor electrodes returns to the original value. This procedure effectively confines the current to an area directly below the central CE, permitting calculation of true polarization resistance. The device stores data for up to 3,500 tests in an internal RAM. The data can subsequently be downloaded to an auxiliary data-processing PC through an RS-232 interface cable.

Experimental Procedures

Preliminary testing to compare the various corrosion rate measuring devices was conducted using a steel coupons in acid (0.2N H_2SO_4 , pH 1.5) and ammoniacal (2M NH_4NO_3 + 2M NH_4OH , pH 9.6) solutions. This was done to compare the results obtained using the NSC device with those obtained by standard electrochemical techniques such as linear polarization and electrochemical impedance spectroscopy (EIS). The impedance measurements were carried out using a 1286 Solatron frequency response analyzer in conjunction with a commercial impedance software package, M388, marketed by EG&G Princeton Applied Research Corporation (PARC).

Small mortar specimens were immersed continuously in solution or subjected to alternate wetting and drying cycles. The solutions used were a noncorrosive solution, i.e., 0.1N Na_2SO_4 (pH 6.3), and a corrosive solution (0.1N NaCl , pH 6.5). The first batch of specimens was subjected to a 48-hour cycle of alternate wetting and drying with drying being carried out in air, while the second batch was subjected to a 12-hour cycle, which included drying in an oven at 150°C for 5 hours to study the effects of different cycle times and conditions. EIS was carried out in the frequency range of 100 kHz to 20 mHz using a Solatron 1286 frequency response analyzer. The NSC device was used at two frequencies in this experiment, namely 1.6 kHz and 120 mHz. The linear polarization test was carried out using a Model 273 EG&G PARC potentiostat along with commercial linear polarization software, M342, marketed by EG&G PARC. The tests were carried out in a potential

window of ± 7 mV around the open circuit potential at a scan rate of 0.1 mV/sec. This scan rate has been reported to provide good correlation with gravimetric corrosion measurements in many rebar systems (16-18). For all of the remaining testing, measurements with the NSC device were made using high and low frequencies of 1280 and 0.02 Hz, respectively.

Results and Discussion

Factors Affecting the Polarization Resistance Measurements

All of the corrosion rate measuring techniques for the steel-in-concrete system use the Stern Geary relation (19) for nondestructive determination of the corrosion rate, i_c , from the equation:

$$i_c = B/R_p \quad (3-1)$$

where B is constant and R_p is the polarization resistance, which is determined experimentally. It was found that the success of R_p measurements depends on the attainment of good electrical contact between the probe and concrete surface. A poor contact results in a large IR drop at the concrete surface, which makes it difficult to obtain reliable results and reproducible R_p measurements. In order to investigate the effect of contact, the following interface media were used: dry contact (no water), wet contact (water), and conducting paste (Aquasonic™, Parker Laboratories Inc.).

Table 3-2 shows the effect of various contact methods on the R_p values measured using the NSC device. The R_p values obtained by using water or conducting paste are larger than those obtained by dry contact. Moreover, it was observed that the reproducibility was poorer in the dry and paste contact cases. This may be due to an overdosage of conducting paste, which resulted in electrical shorting between the CE and GE. However, a decrease of the paste dosage so that the load of the probe did not squeeze out the paste from under the CE and GE, did not improve the results.

Table 3-2. Polarization resistance values ($k\Omega \text{ cm}^2$), measured with the NSC device, of medium-size mortar specimens using different probe contact methods.

Specimen	R_p ($k\Omega \text{ cm}^2$)		
	Dry	Wet	Paste
1	1.55	3.65	3.01
2	1.50	3.64	--- ^a
3	1.30	3.10	2.78

^aNo reading.

It has been suggested for high resistance overlays that as the signal goes into a medium of lower resistivity it is refracted at the interface (20). Since the resistivity of the medium is smaller than that of the overlay, the current is refracted away from the normal, thus increasing the path length for the signal. This is because at the interface of two layers M and $M+1$, there must be a continuity of potential, E , and current normal to the boundary. Therefore:

$$E_M = E_{M+1} \quad (3-2)$$

and

$$\sigma_M \frac{dE_M}{dY} = \sigma_{M+1} \frac{dE_{M+1}}{dY} \quad (3-3)$$

where $\sigma = 1/\rho$ is the conductivity.

These relationships show that when current passes from a highly resistive layer to a lower resistive layer ($\sigma_M < \sigma_{M+1}$) the change of potential with distance (dE/dY) becomes smaller,

i.e., the path increases. A similar explanation can be given for conducting overlays with path length decreasing as the signal enters a more resistive medium, resulting in the signal being refracted towards the normal. The presence of a highly resistive top layer results in a wider signal distribution and a larger polarized area. Therefore, dry contact results in lower R_p values compared to conducting paste or wet contact cases, as shown in Table 3-2.

The results (obtained with the NSC device) of a series of measurements on medium-size specimens having different surface morphologies (roughness) showed that reasonable and reproducible R_p values were only obtained when the concrete surface was relatively flat. Improving the contact helps to attain better signal distribution in concrete owing to a reduction of the IR drop in the medium. For active systems in which the polarization resistances are relatively small, reduction of the contact IR is significant, whereas in passive systems, it is relatively small compared to the impedance of the rebar/concrete interface.

The R_p measurement made on dry surfaces was found to be nonreproducible and a large scatter was observed in the results obtained. After wetting the specimen surface, the corrosion potential, E_c , changed as shown in Figure 3-3. The potentials just after wetting were considerably higher (nobler) than the steady-state potentials. The most likely reason for this change is the penetration of water into the surface. A possible explanation of the potential shift is that the oxygen needed for the cathodic reaction is supplied by the diffusion of oxygen into the system through the pores in the concrete. When water is added for wetting, it fills up the pores of the concrete and thus cuts off access to the atmosphere (and oxygen) for part of the rebar. However, water contains a limited amount of dissolved oxygen, which decreases as it is consumed in the cathodic reaction and time passes. This results in the potential becoming more negative as the oxygen content decreases. Similar shifts of potential, up to 200 mV, have been reported by other investigators (24).

Figure 3-3 also shows that longer times are required for the potential to reach steady state as the cover thickness increases. Further, it was observed that the time to attain stability depends on the state of the concrete. Dry concrete (high resistivity) takes longer for the E_c to stabilize than moist concrete or specimens immersed in water (low resistivity). These effects may be due to the fact that larger cover thickness and dry concrete need larger amounts of water for wetting. This means that these concrete systems have a greater amount of oxygen available for the cathodic reaction, and, due to the larger amount of water (resulting in greater amount of dissolved oxygen), the system takes a longer time to achieve steady state. Non-reproducible values of E_c lead to a larger scatter in the R_p values obtained. The scatter was decreased by allowing E_c to achieve steady state before starting R_p measurements.

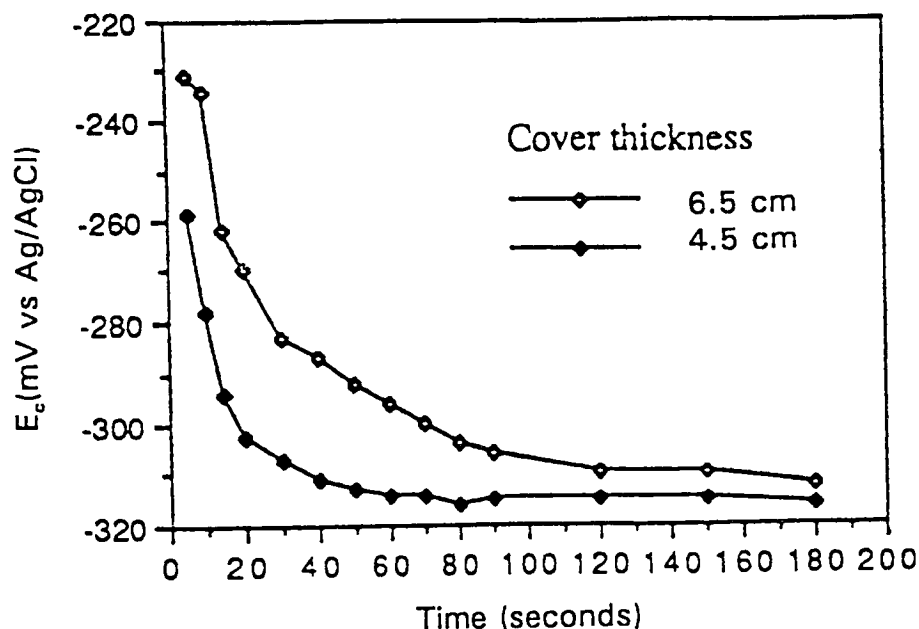


Figure 3-3. Variation of corrosion potential after wetting the concrete surface.

It is a known fact that a small portion of the top concrete surface loses its moisture and has a relatively high resistivity. This results in a large IR drop at the concrete surface and in some cases may even act as an open circuit preventing any signal transmissions from the CE to the rebar. Therefore, proper wetting is essential for reasonable and reliable R_p values. It can be concluded from the above observations that wet electric contact (using water) is the best method among the various contact methods examined. However, it should be noted that reliable results could only be obtained when measurements were made after a stable open circuit potential was attained following wetting. The procedure that gave the most reliable and reproducible results involved wetting an area of the concrete surface not larger than the probe itself with water. Use of a sponge of the same dimensions as the probe between the probe and concrete surface was found to give the same scatter in results as obtained by contacting the probe directly with the concrete surface.

Figure 3-4, based on the computer modeling of current and potential distribution (see Chapter 4), illustrates the importance of the probe position with respect to the underlying rebar. It shows that the displacement of the probe from the center of the rebar results in a larger polarized area; the proportion of the rebar circumference polarized in Figure 3-4(b) is larger than that in Figure 3-4(a). This was verified by R_p measurements, made with the NSC device, which are reported in Table 3-3. By displacing the probe, R_p values decrease, which implies an increase in polarized area. Since the rebar, which is the only conducting material in a highly resistive concrete medium, is of finite dimensions, different probe positioning should result in different current and potential distributions, as shown in Figure 3-4. This factor in part may account for poor reproducibility in R_p measurements.

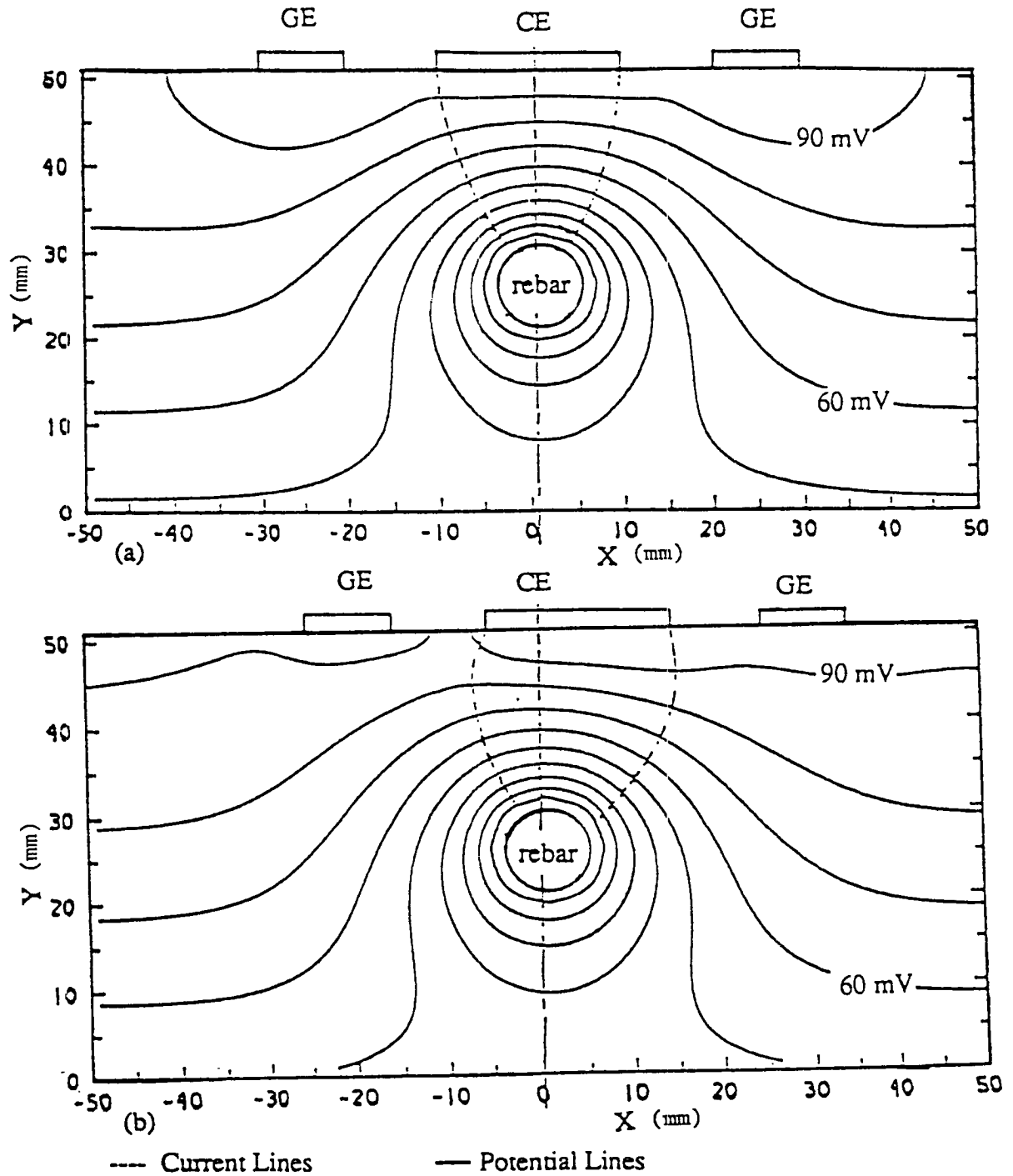


Figure 3-4. Current and potential distribution in concrete showing the effect of probe position: (a) probe is positioned symmetrically over the rebar; (b) probe is displaced from the center of the rebar.

Table 3-3. Effect of probe placement on R_p measurements made with the NSC device on large concrete specimens.

Measurement Site	R_p ($k\Omega\text{ cm}^2$) ^a	
	Symmetrical ^b	Displaced ^c
A	48.35	40.27
B	64.33	52.39
C	74.61	49.46
D	41.32	29.38

^aAverage of three results reported.

^bProbe centered symmetrically over rebar.

^cProbe displaced 0.5 cm (0.2 in.) from the rebar center.

Polarized Area

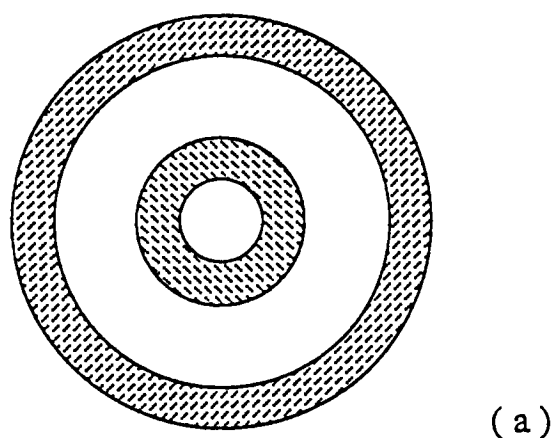
The Stern-Geary relation has been used for nondestructive determination of the corrosion rate of rebars in concrete (25). However, for large reinforced concrete structures, it is not possible to polarize the entire steel surface in concrete, because the CE, through which the signal is applied, is considerably smaller than the rebar (the WE). This results in a nonuniform signal distribution over the rebar with the signal decreasing in intensity and eventually vanishing as one moves away from the CE. This nonuniform distribution is dependent on such factors as the state of the rebar (larger distribution for a passive rebar), electrical resistivity of the concrete (larger distribution for lower resistivity), the CE size (as the CE size increases, the measured R_p approaches the R_p value based on actual current distribution) (26), and the frequency when alternating perturbation is used.¹

¹Macdonald, et al (27,28) have reported that when the WE area \gg CE area, the polarized area is also dependent upon the frequency of perturbation, with the polarized area increasing with decreasing frequency. As stated earlier in this report, the NSC device uses only one low frequency instead of a frequency sweep, and, therefore, its measurements are not affected by the above-mentioned dependence. The 3LP and GECOR devices use linear polarization and hence this frequency dispersive area effect is not applicable to them.

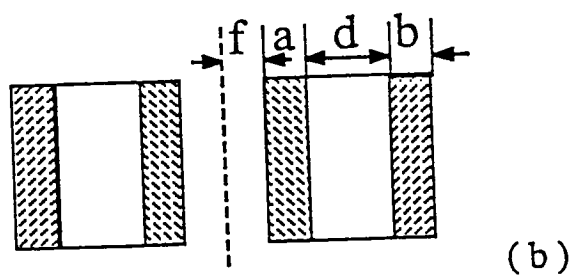
To define the polarization area of the rebar during a measurement, a second electrode, the GE, has been successfully used (29-31). The GE is situated concentrically around the CE and is maintained at the same potential as the CE. As a result, the signal distribution from the CE is limited to an area not greater than the midpoint of the separation between the CE and the GE, when both electrodes have the same width in vertical cross section ($b = c$ in Figure 3-5) and the concrete is treated as a homogeneous medium. It is important to notice also that the rebar should behave as an electrochemically uniform boundary for ideal confinement to occur. In order to achieve the best possible confinement and verify the current/potential (I/E) distribution obtained from modeling work (see Chapter 4 of this volume), a GE was constructed and a systematic analysis of its parameters was carried out.

A GE is maintained at the same potential as a CE by using a voltage follower. This obviates any restrictions on the shape and size of the CE and the GE. Computer modeling has shown that the focusing ability of a GE is markedly increased by arranging the GEs in a circular configuration (20). So the GEs used were cylindrical, which can be imagined as an infinite number of point size GEs in contact with each other. Similarly designed cylindrical probes have been used in highly resistive media with considerable success (32,33). The GE/CE assembly is shown in Figure 3-5. The annular space in the CE is for placing the reference electrode and allows the reference electrode to pick up the signal response from the area of the rebar polarized by the CE. GEs of different sizes were constructed, according to the design shown in Figure 3-5, using graphite cylinders as electrodes and polyethylene or glass as an insulator. The reference electrode was placed in a glass tube in order to electrically insulate it from the CE. Insulation between the CE and GE was achieved by filling the annular space between them with low-density polyethylene powder. The electrode assembly was heated in a vacuum at a temperature of 150°C, which is higher than the melting temperature of polyethylene. Afterwards, the electrical resistance between various parts of the GE assembly was checked using a multimeter to ensure that good insulation between the inner graphite cylinder and the reference electrode chamber was achieved. The graphite was not oxidized, and its conductivity was not impaired (as evidenced by the low resistance values measured between two points on the graphite cylinder). In order to prevent the cracking of the GE elements during the cooling process following the melting of polyethylene, it was necessary to cool the probe slowly. Rapid cooling in air resulted in cracking of the glass element and of the outer surface of graphite, probably due to significant differences in thermal expansion of the materials.

Measurements were made on medium-size mortar specimens using the NSC device with and without a GE. The results are shown in Table 3-4. It can be seen that R_p values increase by an order of magnitude when a GE is used. This shows that the signal applied from the CE




(a)



(b)

 Graphite Counter Electrode

 Insulation

 Graphite Guard Electrode

f : Radius of annular space

a : Width of counter electrode

d : Separation between CE and GE

b : Width of guard electrode

Figure 3-5. GE/CE assembly: (a) top view; (b) cross sectional view.

reduced the polarized area by an order of magnitude. These results are in agreement with results obtained by other investigators and show the effectiveness of the GE in confining the signal distribution (20,31). However, this is the first work to have experimentally quantified the confining effect of the GE. During the experiments, the specimens were kept in air, and R_p measurements were made after ensuring a flat surface (by using a grinder) and following the wetting procedure outlined earlier in this report. These laboratory results can be extrapolated to field determinations of R_p in large concrete structures (which are also dry and have a WE area > CE area), and the GE may be expected to reduce the polarized area by an order of magnitude. This effect was confirmed during the field validation testing (Chapter 5).

Table 3-4. Polarization resistance (R_p) values obtained by the NSC device on medium-size mortar specimens with and without GE.

Specimen	Polarization Resistance ($k\Omega\text{ cm}^2$)		Low Frequency Used (Hz)
	w/o GE	w/GE	
1	1.42	17.12	0.01
1	1.06	11.69	0.04
2	0.94	13.77	0.01
2	0.59	9.95	0.04
3	1.16	18.74	0.01
3	0.90	14.35	0.04

The R_p values obtained by using the NSC device are shown in Table 3-5. As can be seen from these results, better confinement is achieved when the separation between the CE and the GE is reduced and the length of the GE is increased. These results are in agreement with results obtained by other investigators (29,34-37). Assuming ideal confinement of the signal by using a GE, which helps to confine signal distribution from the CE, as discussed earlier, the appropriate reading is at the midpoint of the separation between the CE and the GE. However, many researchers have assumed that the signal from the CE is confined directly

Table 3-5. Effect of GE parameters on measured polarization resistance (R_p) values obtained using the NSC device on medium-size mortar specimens.

Separation distance, d ^a (mm)	Width of GE, b ^a (mm)	R_p (k Ω cm ²)
6.3	6.3	65
6.3	15.8	118

^aSee Figure 3-5.

below the CE and that the entire circumference below the rebar is polarized. The polarized area, A , is defined by the equation $A = 2 \cdot \pi \cdot r \cdot L$, where r is the radius of the rebar and L is the length of the CE. Matsuoka et al. (31) applied a finite element analysis to determine L while assuming that all of the rebar circumference is polarized during an R_p measurement. During experimental and computer simulation studies, it was found that the rebar could not be polarized around its entire circumference. If a single CE is intended to polarize the entire circumference of the rebar, the equipotential lines must be parallel to the surface. Therefore, the current lines, which are perpendicular to the potential lines, must go straight down in order to polarize the entire surface of a finite/infinite electrode. This can only be achieved by using an electrode of infinite length (very large compared to rebar size), which is not a practically feasible idea. When a GE is used, the CE and GE are maintained at the same potential, and, therefore, the rebar areas polarized by them cannot overlap, i.e., the signal separation between the CE and GE results in distinct and separate polarized areas. Even the use of the "external" CE (15) on the GECOR device (which is used to confine the signal from the CE) results in well-defined and separated signals being applied from the two CEs to the rebar. These separate signals can only polarize different parts of the rebar. Hence, the entire surface of the rebar cannot be polarized during R_p measurements.

To verify the actual sites of polarization, the steel rebars of the mortar specimens were anodically polarized using Model 173 and 273 EG & G PARC potentiostats, applying a constant current density of 0.9A/ft² (1mA/cm²), based on the entire circumferential area of the bar, for 4 weeks. Figure 3-6(a) shows a rebar corroded by an anodic current through a CE. Figure 3-6(b) shows a rebar corroded by current passed through both the CE and the GE. Figure 3-7(a) and 3-7(b) shows the top view of the corroded rebars. As can be seen, only the top part of the rebar, which is nearest to and facing the electrode(s), underwent

corrosion; the bottom part is not corroded. It can be seen that the rebar shown in Figure 3-6(b), which was polarized by both the CE and the GE, is more severely corroded than the one with the current applied only from the CE (Figure 3-6(a)). In Figures 3-6(b), 3-7(a), and 3-7(b) extensive corrosion products can be seen to have leached into the mortar matrix around the rebar polarized by both the CE and the GE. This is because the CE and the GE are at the same potential, and, therefore, the rebar is additionally polarized by the current applied from the GE, resulting in greater corrosion of the rebar.

These results show that the actual area polarized during an R_p measurement is much smaller than the entire circumference of the rebar, as is commonly assumed. From experimental, computer modeling and theoretical considerations, it is essentially only the top half of the rebar (facing the electrodes) that becomes polarized when a GE is used. Therefore, the polarized area, A , is better approximated by $\pi \cdot r \cdot L$ instead of $2 \cdot \pi \cdot r \cdot L$. The polarized area is used to convert the measured polarization resistance, R'_p (Ω), to an apparent polarization resistance, R_p (Ωcm^2), by multiplying by the area polarized during the measurement. The assumption that the entire circumference of the rebar is polarized, instead of only the top half, leads to an underestimation of the corrosion rate by up to a factor of two (100 percent error). Assuming ideal confinement of the signal by using a GE, an area up to the midpoint of the separation of the CE and the GE is polarized, not the length of the rebar under the CE, as is commonly assumed. The additional error introduced (apart from the circumference error) would depend on the particular probe used. Presently, unquantifiable error lies in assuming the polarized area to be restricted to the area of the rebar under the CE when the 3LP device is used, since it does not use a GE to confine the signal distribution. Gonzalez et al. (16,17) and Sagües (35) have discussed the errors in using the electrochemical techniques for steel-in-concrete systems, but have not considered what the actual polarized area in an R_p measurement is and the error introduced by using an incorrect polarized area. Therefore, it is important to use only half of the circumference of the rebar as the polarized area to get meaningful results from R_p measurements.

Use of R_p Measurements to Locate Corroding Areas

Potential mapping is currently in wide use to identify corroding areas in concrete structures (39-41). Its use and interpretation are described in ASTM C876-80 (42). However, the interpretation of the resulting potential contour map is ambiguous, since the absolute potential value for corrosion identification as proposed in ASTM C876-80 is in question (41,43,44).

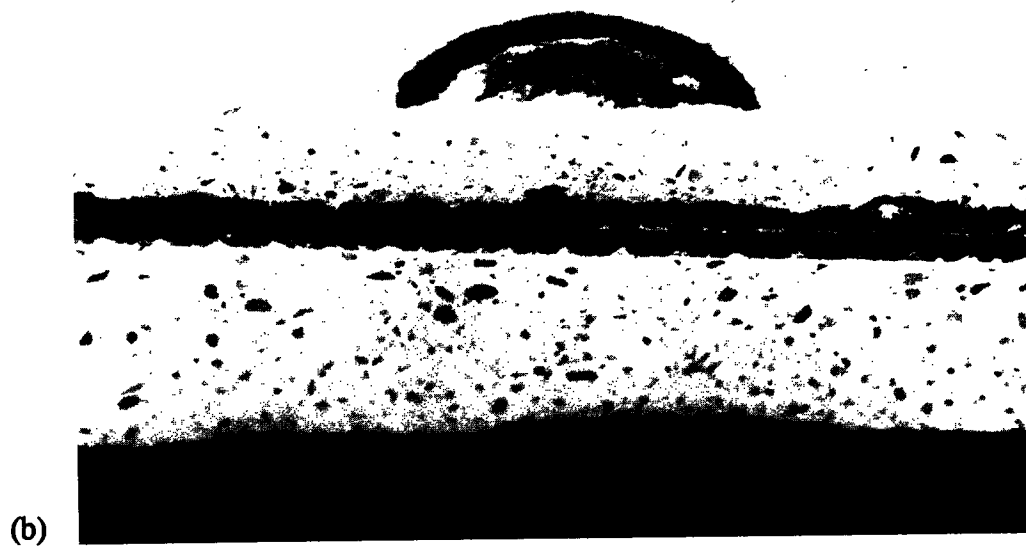


Figure 3-6. Corrosion caused by anodic polarization of rebar using: (a) CE only; (b) CE and GE.

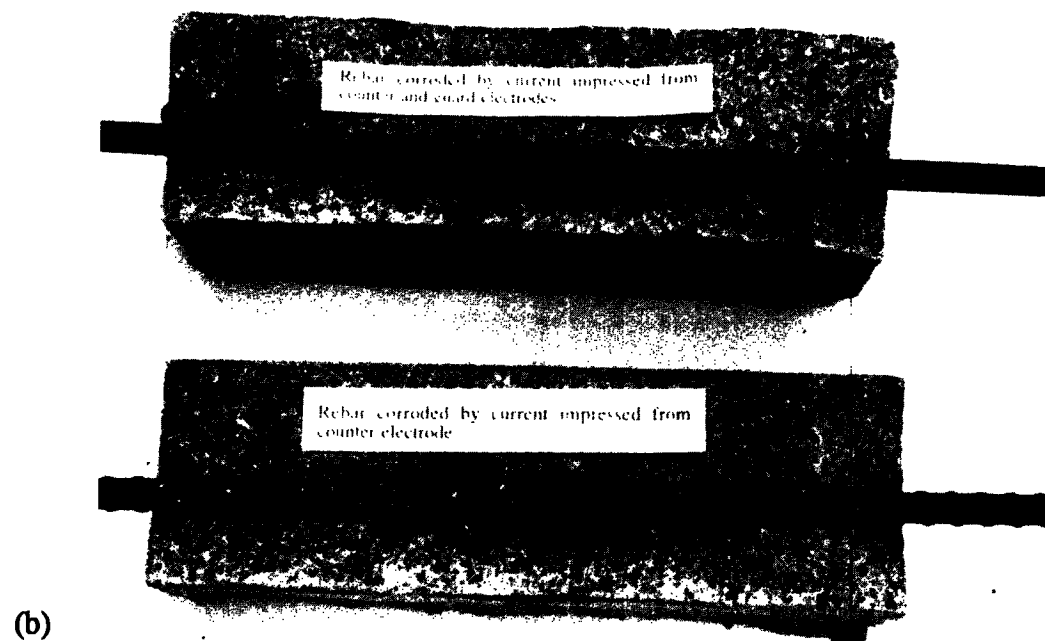
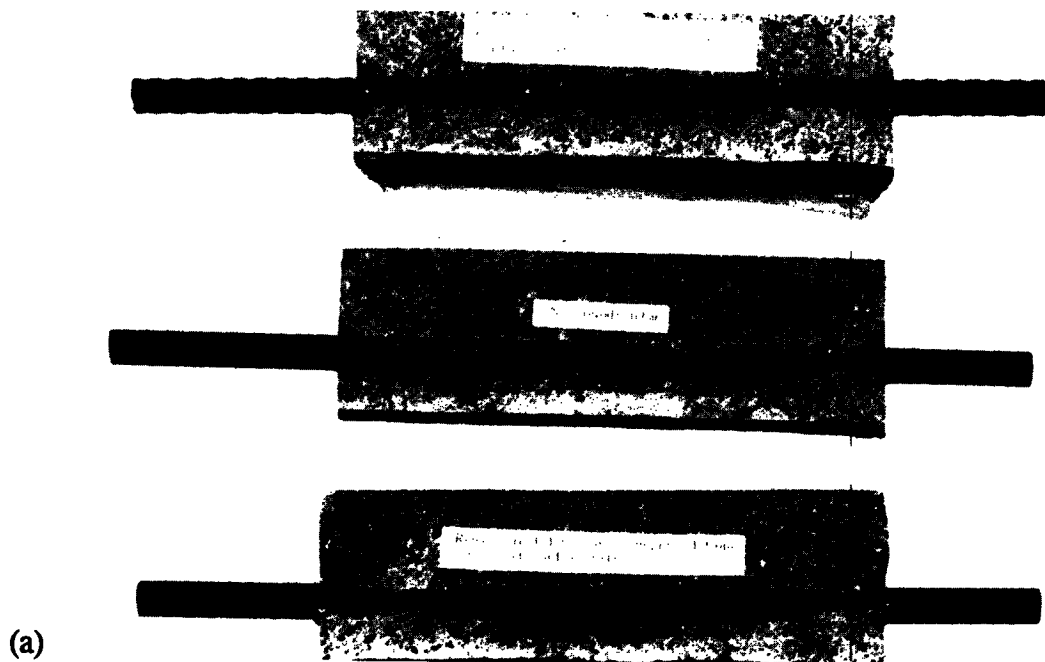


Figure 3-7. The extent of corrosion by anodic polarization of rebars: (a) comparison of corroded and noncorroded rebars; (b) only the portion of the rebars facing the electrodes is polarized.

Therefore, an experiment was carried out on a specimen with a well-defined corrosion spot (see Figure 3-1). The purpose of the experiment was to determine whether the signal-confining effect of the GE can be used to locate corroding areas, as shown in Figure 3-8. At points *A* and *B*, the confined signal "sees" a passive rebar and therefore measures a high R_p . However, near the corroding spot, the signal tends to deviate from its expected path because of the proximity of the corrosion spot, and, therefore, the GE is unable to confine the signal. Similar confinement failures have been reported in other systems (34,45). At *D*, the probe is situated directly over the corrosion spot and measures the lowest R_p . At *E*, a point far away from the corroding area, the signal "sees" only a passive rebar and measures a high R_p . This change of R_p is used to identify the location and extent of the corroding area.

Similar attempts using R_p measurements to identify and estimate the extent of the corroding area have been reported by Wenger et al. (46), although these authors reported difficulties in applying this procedure to reinforced concrete beams. It was concluded (46) that the corrosion potential measurement method would be easier and quicker to use. However, electrochemical impedance spectroscopy measurements, as used by Wenger et al., take a long time, and interpretation of the results is difficult (27,46). The NSC device, which was used for our experiments, employs only two frequencies instead of a frequency sweep (as is done in impedance measurements), and this results in measurements that are quicker.

The R_p measurement results obtained for different probe positions and distances from a corroding area are shown in Figure 3-9. Comparing the R_p values obtained near the cup, the R_p values decrease sharply when the cup is filled with electrolyte and suddenly increase near the edge of the cup when there is no electrolyte in the cup. When there is no electrolyte, i.e., with air in the cup, the signal cannot pass through the cup, since there is no medium available for signal transmissions. In contrast, with electrolyte in the cup, the signal can pass in and through the area defined by the cup, resulting in a considerably larger signal distribution (also allowing signal transmission to the corroded part of the rebars), and, therefore, a lower R_p is measured.

The increase in R_p values near the edge of the specimen (170, 192 cm [66.9, 75.6 in.]) can also be explained as due to limited space availability for signal distribution. However, similar effects are not observed at the other edge of the specimen (8, 15 cm [3.1, 5.9 in.]). The R_p values at the edges are nearly the same irrespective of whether any electrolyte is present in the cup. Probably some corrosion has occurred in that part of the rebar, or the GE is unable to confine the signal, which spreads to the corrosion spot. Since the same results are obtained for all electrolytes, the former explanation seems to be the most likely, because with no electrolyte in the cup the signal cannot go into the cup. These observations can only be explained if the corrosion has spread beyond the exposed part of the rebar.

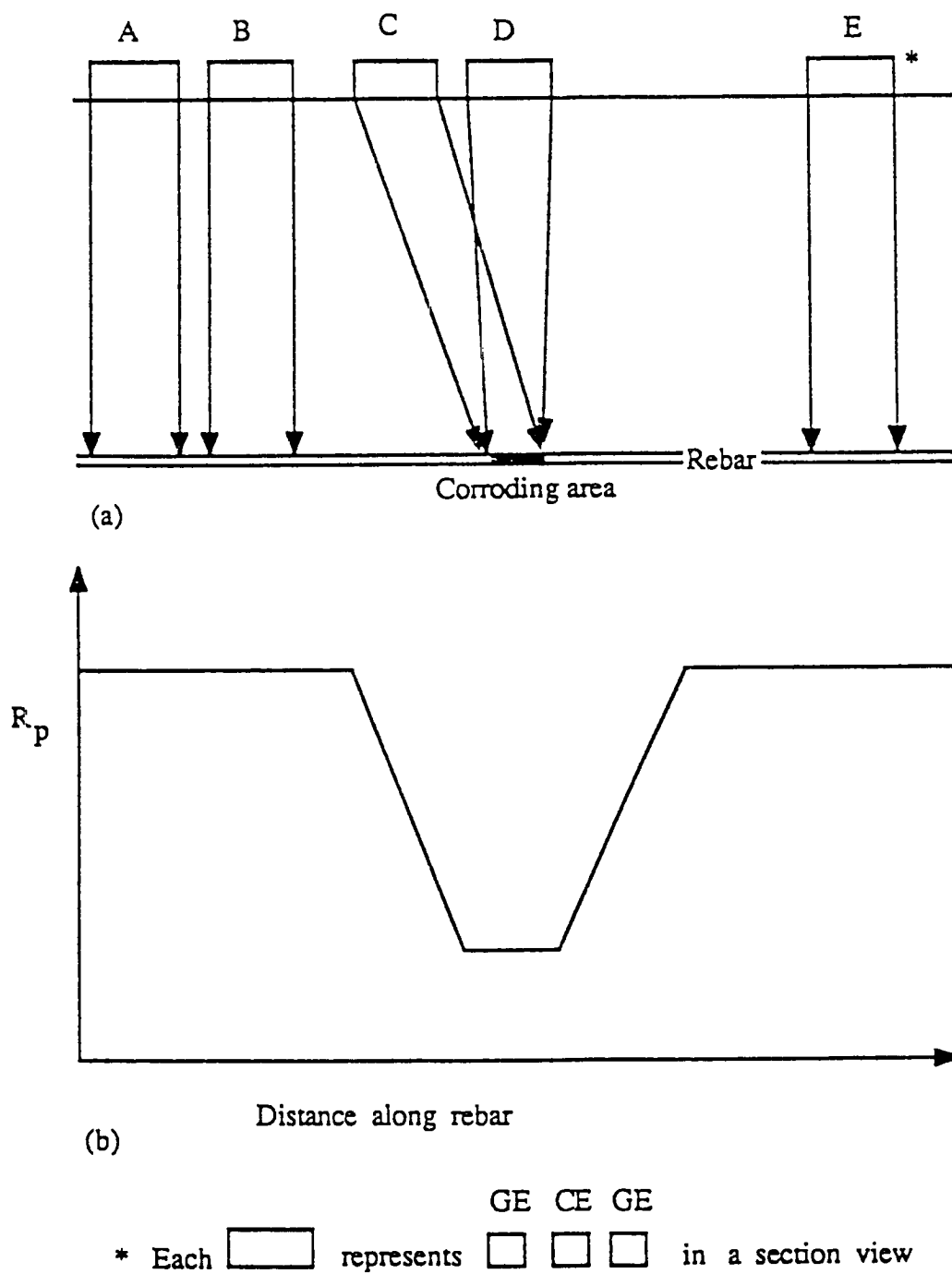
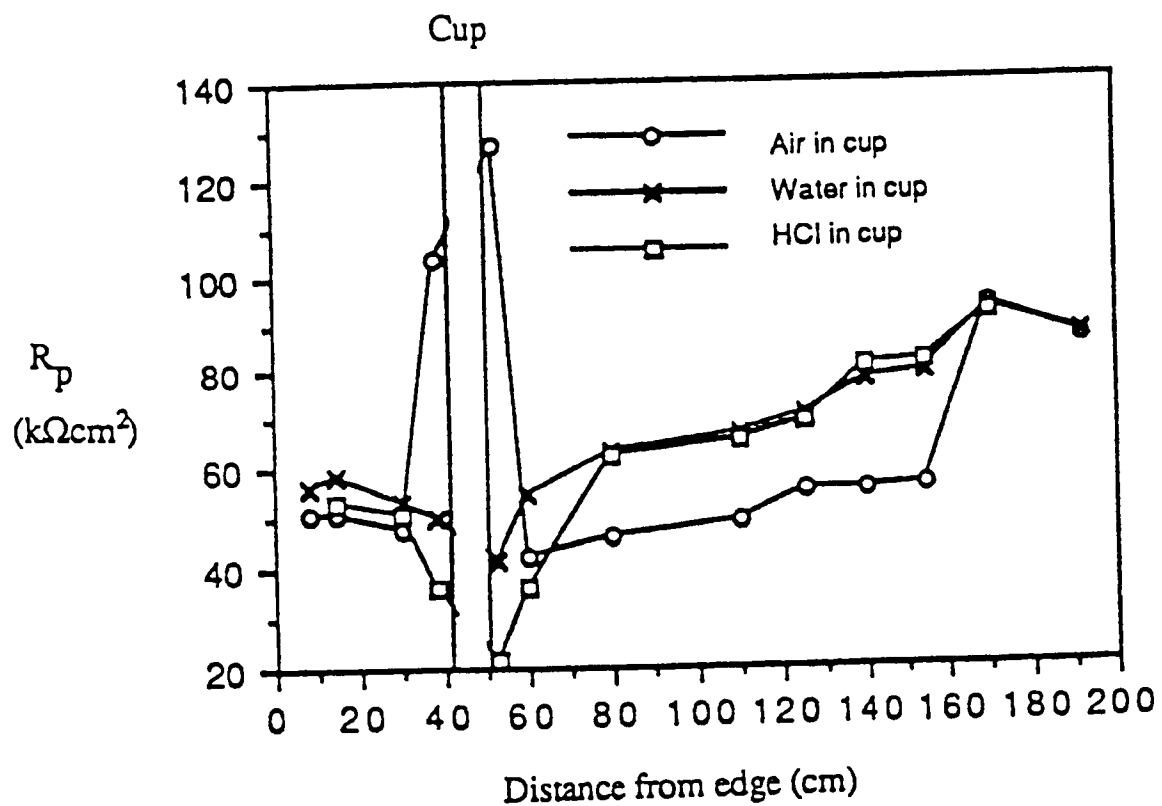


Figure 3-8. Influence of corrosion spot on R_p measurements: (a) effect of corrosion spot on signal distribution; (b) effect of corrosion spot on measured R_p values.



Note: 1 cm = 0.39 in.

Figure 3-9. Polarization resistance values along the rebar.

The expected R_p versus position plot depicted in Figure 3-8 is similar to the plots obtained experimentally (Figure 3-9) with an electrolyte in the corrosion cup (except at the edges), but does not match the curve obtained with no electrolyte in the cup. However, as shown in Figure 3-9, a gradual reduction in R_p occurs with decreasing distance from the corrosion spot, rather than the sharp transition visualized in the conceptual model of Figure 3-8. The influence of the corrosion spot appears to extend to a distance of 125 cm (49.2 in.) and 140 cm (55.2 in.), respectively, with the absence and presence of an electrolyte. The increases in R_p values at 170 cm (66.9 in.) suggest that the GE is unable to confine the signal from a 6-cm (2.4-in.) probe closer than 30 cm (11.8 in.) from the edge of the specimen.

Comparing the results obtained with the two different electrolytes (water and HCl) and no electrolyte, the R_p values are essentially the same for both electrolytes. Generally, the values obtained with HCl in the cup are slightly lower than for water, which is reasonable, considering the fact that HCl is the more corrosive environment. However, away from the cup, the R_p values for air in the cup are lower than those for water and acid. Possibly some change occurred in the ambient humidity leading to drying of the specimen before the latter measurements were carried out.

Assuming that the corroded area in the specimen extends from about 30 to 80 cm (11.8 to 31.5 in.), (the cup extends from 41 to 50 cm [16.1 to 19.7 in.]) and comparing the results obtained from various media (air, water, and acid) in the cup, it can be concluded that unambiguous results for corrosion rate values can only be obtained for the highly active corrosion sites, situated at an adequate distance from barriers in current flow such as outer edges, cracks, and joints. Even with an ineffective GE, the R_p measurements allow good identification and estimation of the extent of corrosion area for a corroding rebar. Since R_p measurements involve measurement of corrosion potential, both of the measurements can be used to identify "hot spots" and areas beginning to corrode during field testing of reinforced concrete structures.

Effect of Macrocells on R_p Measurements

It is known (47) that actual reinforced concrete structures experience localized attack (via development of macrocells due to the varying environmental conditions along the rebar) rather than uniform corrosion. In microcell (or pitting) corrosion, the anode is immediately adjacent to the cathode. In a macrocell, the anode and cathode are separated by some distance. The anode/cathode pair in a macrocell can occur on the same rebar, on different rebars in the same reinforcement layer, or in different layers. In the latter case, one layer becomes anodic (generally the top layer, since chlorides and moisture enter the concrete from

the top) while the other layer becomes cathodic (the bottom layer being drier and therefore having more access to oxygen).

Macrocell experiments have been carried out previously to study the effect of an inhibitor (47), electrolyte resistance, water/cement ratio, etc. (48) and to compare the polarization resistance technique to the macrocell technique (49). Berke et al. (49) found that the polarization resistance technique was much more accurate than the macrocell technique. However, some of their specimens had the top rebar as the anode and the lower rebar as the cathode. The remaining specimens had the top rebar as the cathode and the lower rebar as the anode. Macrocells are commonly found in large reinforced structures. Therefore it is important to make representative specimens, with known active and passive areas, to study the macrocell effect. This needs to be done since it is imperative to know the effect of macrocells on signal confinement, current/potential distribution, and measured R_p values. For this purpose, a macrocell specimen was made by arranging alternate bars of steel (active) and copper (passive) in two rows in a chloride-containing mortar specimen. The specimen configuration was presented earlier in Figure 3-2. Experiments were carried out using the NSC device. The results are reported in Table 3-6. The average of two measurements is reported.

In the first experiment, III (steel = active/A) was used as the WE, and 3 (copper = passive/P) as the CE. On adding II and IV (copper = P) to III (steel = A) and making II, III, and IV the WE, the corrosion potential, E_c , shifts to nobler potentials, which is the result of coupling a noble metal to a corroding metal (50). But the shift in the corrosion potential is not very large and indicates that the WE couple of steel and copper is controlled by steel, and most of the current still goes to the steel. This is also borne out by the apparent R_p value (0.041 k Ω), which is nearly the same as the value obtained by using III alone as a WE. However, the polarized area is taken to be all of the WE area since the separation between the two rows is 11 in. (28 cm) and there is a broad signal distribution over such a large electrode separation. Since all of the bars connected together were the WE in the experiment, the polarized area was assumed to be all of the WE. Even the GE is only able to confine the signal distribution by a factor of four. On further coupling I and V (steel = A) to the WE couple (II, III, IV), E_c is observed to shift to cathodic values, which is the result of coupling a corroding metal to a noble metal (50). But the magnitude of the shift is only 4 mV, which agrees with the previous conclusion that the II, III, and IV couple is controlled by III (corroding steel). When 2 and 4 are used as the GE, E_c shifts in the noble direction as explained above and the signal becomes confined. On further increasing the length of the GE, the confinement improves (in accordance with results presented earlier), but not dramatically, as is evident in the shift of E_c .

Table 3-6. Polarization resistance (R_p) measurements showing the effect of macrocell.

E_c (mV _{SCE})	WE	CE	GE	R'_p (k Ω)	R_p^* (k Ω cm ²)
-376	III	3	---	0.042	0.85
-355	II, III, & IV	3	---	0.041	2.50
-325	II, III, & IV	3	2, 4	0.16	9.73
-348	I, II, III, IV, V	3	2, 4	0.11	11.15
-351	I, II, III, IV, V	3	---	0.017	1.73
-347	I, II, III, IV, V	3	(1+2)+ (4+5)	0.14	14.19
-376	III	Paste	---	0.75	15.20
-237	3	III	---	3.27	66.29
-235	3	Paste	---	2.56	51.89
-349	2, 3, & 4	III	---	0.053	3.22
-347	2, 3, & 4	III	II & IV	0.088	5.35
-337	1, 2, 3, 4, & 5	III	---	0.048	4.86
-336	1, 2, 3, 4, & 5	III	II & IV	0.070	7.10
-331	1, 2, 3, 4, & 5	III	I, II, III, & IV	0.133	13.50

*Multiplied by polarized area ($\pi r l = 1.995$ l), where r is the radius of the rebar, and l is the length of the WE.

--- Not used.

To check the effects of cover thickness on R_p measurements, carbon paste electrodes were painted on the specimen surface and used as a CE in the measurements, as shown in Figure 3-2. This electrode has a cover thickness of 1 in. (2.5 cm), while when 3 was used as a CE, the WE and CE electrodes were separated by 11 in. (28 cm). It is observed that lower R_p values are obtained for increasing cover thickness, because the signal distribution in the concrete increases. This is because the signal distribution between two electrodes of different dimensions and configurations will increase as the distance between them increases.

When 3 (copper = P) was made the WE and III (steel = A) was used as the CE, the measured R_p indicated a passive rebar and was two orders of magnitude higher than that indicated by steel. To check any possible effect of a corroding CE on R_p measurement, a carbon paste electrode was painted over the WE (3). The R_p values should have increased due to decrease in signal distribution (cover thickness decrease from 11.0 to 1.0 in. [28 to 2.5 cm]), but instead it was observed to decrease. This effect is not explainable at the present and suggests that the corroding CE did affect the measurement. So experiments were carried out in the same sequence, as was done when III was the WE and 3 was the CE, using both III and the paste electrode as a CE, with 3 as a WE. The results obtained using the paste electrode as the CE are not presented here since those measurements were carried out using combinations of I, II, IV, and V as the GE. When the paste electrode was the CE, and situated directly over the rebar on the specimen surface, the separation between the CE and the WE (bar embedded 1 in. [2.5 cm] inside the mortar) was one order of magnitude smaller than the separation between the CE (paste) and the GE (bars embedded 1 in. [2.5 cm] inside the mortar). The results obtained with paste electrode as the CE and the GE embedded 1 in. (2.5 cm) in the concrete cannot be compared meaningfully to the result obtained when the CE and GE lie embedded 1 in. (2.5 cm) inside the mortar, in a straight line in the specimen. However, the results indicate the same trends, i.e., E_c moving in the cathodic direction when coupled with a corroding electrode, E_c shifting to nobler values when coupled to passive electrodes, current confinement when using the GEs, and better confinement when the length of the GE is increased.

The results obtained by using III as a CE show the same trends as presented above. Coupling 2 and 4 (steel = A) to 3 (copper = P) gives almost the same E_c and R_p values as when II and IV (copper = P) were coupled to III (steel = A). This is an additional confirmation of the fact that this copper/steel couple is controlled by steel, and only a limited amount of signal goes to copper. Therefore, it would be difficult to confine signal distribution in an APA system as is indicated by the small shift in E_c and R_p values. Marginally better confinement is observed in a PAPAP system. However, results obtained with a corroding CE (III) cannot be greatly relied on.

The experimental and modeling results (see Chapter 4) indicate that confinement is only obtained when the measurements are carried out over the active part (which is surrounded by passive areas) of the macrocell. When measurements are made over the passive part (which is surrounded by active areas) the confinement is poor. This has great significance for field testing on large structures and shows that meaningful measurements (which result from confinement and, hence, a well-defined polarized area) can only be made when the probe is placed over the active area of the macrocell.

For field R_p measurements, it is very encouraging to note that, by using a GE, confinement was achieved through a highly resistive mortar separation of 11 in. (28 cm), which is four to five times the typical concrete cover thickness in most reinforced structures. As has been already pointed out, increasing the cover thickness results in larger signal distribution. Therefore, enhanced confinement can be expected during field testing, given the smaller cover thicknesses of the large reinforced structures.

Comparison of Corrosion Rate Measuring Methods

R_p results yielded excellent agreement between electrochemical impedance spectroscopy and the NSC device for corroding steel coupons, as shown in Table 3-7. However, the agreement for passive specimens was not as good. A linear correlation was observed between the R_p results obtained by EIS and the NSC device for small mortar specimens, as shown in Figure 3-10. A possible implication of this correlation is that the NSC device can be used to give reliable qualitative results of corroding specimens in field measurements. Its advantage over the conventional EIS technique lies in a considerably shorter measuring time, as it only uses two frequencies instead of a range of frequencies.

Two large slabs not containing any chloride in the concrete mix (N11 and N12) and one large slab containing 2 wt percent of chloride (CL 11) were tested to compare the various corrosion rate measuring devices. To meaningfully compare the three devices (NSC, 3LP and GECOR devices), the real average R_p values of the lab test specimens were determined (via a two-electrode potentiostatic measurement) by using a CE as long as the WE (test rebar). The R_p values obtained by using CEs that are as long as the test specimen are free from the effect of current distribution and give the average R_p over the whole of the rebar. For the specimens tested (which contained three parallel rebars running along the length of the specimen), the test rebar was the WE, and the rebar parallel to it acted as both the CE and the reference electrode. A constant potential difference of 10 mV was applied between the two rebars, and the resulting current was measured for two different cases, namely with

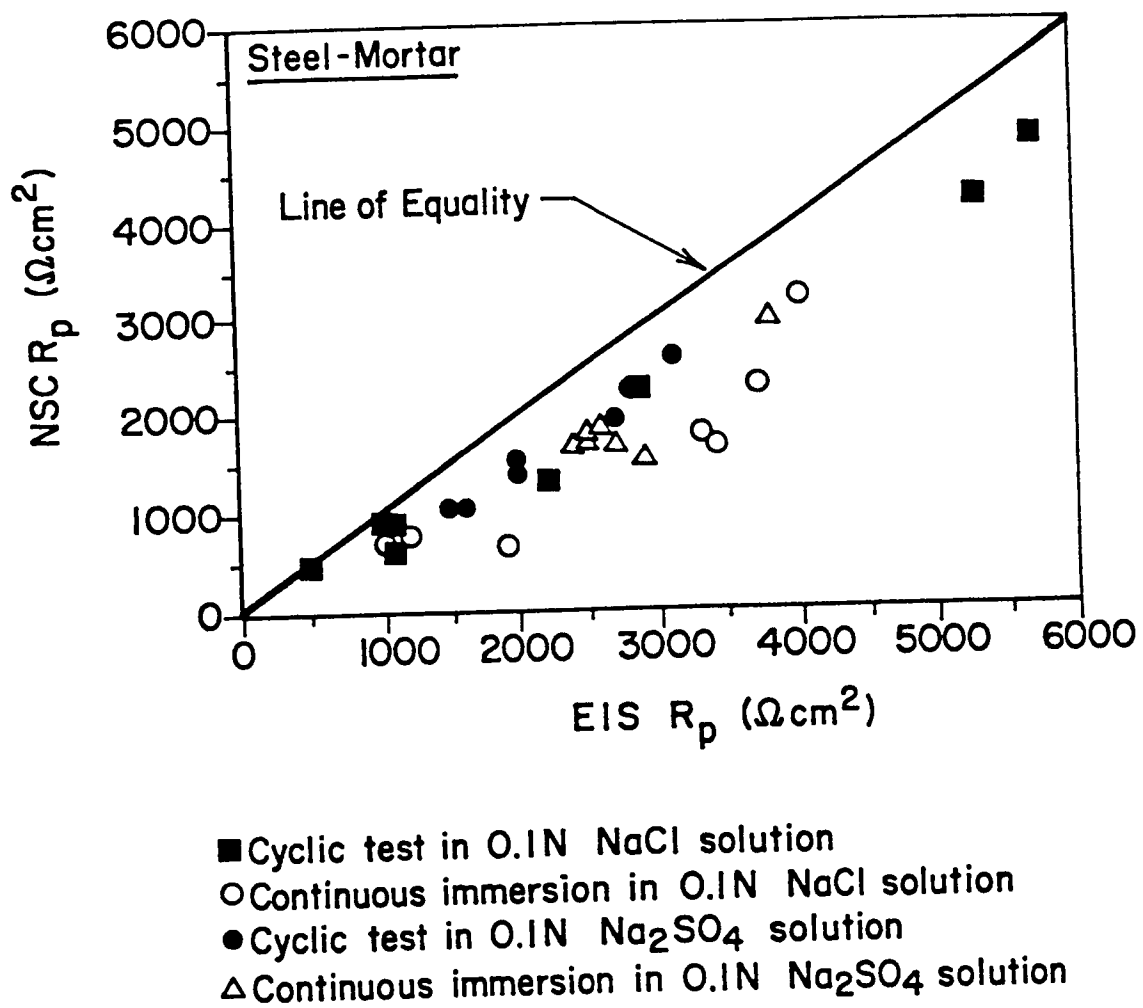


Figure 3-10. Comparison of polarization resistance values obtained with EIS and the NSC device.

Table 3-7. Comparison of two corrosion rate measuring methods with steel coupons in 0.2NH₂SO₄ solution.

Immersion Time in hours	Polarization Resistance (R_p), ohm-cm ²	
	Electrochemical Impedance Spectroscopy	Nippon Steel Corporation Device
0	200	204
12	170	180
18	145	145
24	100	—
36	30	31

and without the use of IR compensation in the potentiostat. Where IR compensation was not used, the uncompensated resistance was subtracted from the measured (i.e., apparent) polarization resistance, R_p' (k Ω). The apparent polarization resistance, R_p' (k Ω), was converted to the true resistance, R_p (k Ω cm²), by multiplying by the total area of the rebar. For the real (average) R_p value, the total area of the rebar was assumed to be polarized, while for the various devices only the area under the CE was assumed to be polarized.

The results of the R_p measurements, obtained with various corrosion rate measuring devices, are reported in Table 3-8 for chloride- and non-chloride-containing specimens. In the aggressive medium of the chloride-containing specimen, the lowest deviation from the "real" average i_c was observed for the GECOR device (below 100 percent); it was much higher for the NSC device (about 1,200 percent); and it was highest for the 3LP device (about 2,200 percent). The high deviation for the 3LP device can be attributed to the absence of a GE to confine current. The large deviation from the average R_p results show that even the use of a GE does not guarantee confinement of signal, as seen in the results obtained with the NSC device.

In the chloride-free specimens (N11 and N12), the deviation from the average values was much higher, below or about 1,000 percent for the GECOR device, and in the range of

Table 3-8. Polarization resistance ($k\Omega\text{ cm}^2$) results obtained with large specimens using various devices.

Specimen	Device	R'_p ($k\Omega$)	R_p^* ($k\Omega\text{ cm}^2$)	i_c^{**} (mAcm^{-2})	% Deviation from "Real" Average i_c
Cl 11	Potentiostat with IR comp.	0.156	155.69	0.167	"Real" Average = 0.156
Cl 11	Potentiostat without IR comp.	0.180	179.31	0.145	
Cl 11 (#1)	GECOR	1.22	86.7	0.3	+92
"	NSC	1.07	15.47	1.68	+977
"	3 LP	0.142	12.21	2.13	+1265
Cl 11 (#2)	GECOR	1.89	134.7	0.19	+22
"	NSC	0.925	13.38	1.94	+1144
"	3 LP	0.086	7.396	3.52	+2156
N 11	Potentiostat with IR comp.	4.14	4127.0	0.0063	"Real" Average = 0.0063
N 11	GECOR	5.09	361.4	0.072	+1043
"	NSC	2.29	33.07	0.78	+12281
"	3 LP	0.77	66.22	0.39	+6090
N 11 (#2)	GECOR	5.74	407.5	0.063	+900
"	NSC	3.93	56.77	0.46	+7202
"	3 LP	0.82	70.35	0.37	+5773
N 11 (#3)	GECOR	5.61	398.3	0.065	+932
"	NSC	4.84	69.97	0.37	+5773
"	3 LP	0.73	62.87	0.41	+6408

Table 3-8. (continued)

Specimen	Device	R'_p (k Ω)	R_p^* (k Ω cm ²)	i_c^{**} (mAcm ⁻²)	% Deviation from "Real" Average i_c
N 12	Potentiostat with IR comp.	3.14	3132.53	0.0083	
N 12	Potentiostat without IR comp.	4.14	4126.98	0.0063	"Real" Average = 0.0073
N 12 (#1)	GECOR	6.32	448.7	0.057	+681
"	NSC	1.85	26.79	0.97	+13188
"	3 LP	0.50	43.00	0.60	+8119
N 12 (#2)	GECOR	7.40	521.0	0.049	+571
"	NSC	1.66	24.0	1.08	+14695
"	3 LP	0.68	58.82	0.44	+5927
N 12 (#3)	GECOR	4.83	342.9	0.075	+927
"	NSC	3.60	52.05	0.50	+6749
"	3 LP	0.78	66.65	0.39	+5242

*Multiplied by polarized area ($2\pi r l = 2\pi \cdot 0.635 \cdot l$ cm²) where r is the radius of the rebar and l is the length of the CE.

** i_c is calculated as $26/R_p$ [V/ohm-cm²].

6,000 to 15,000 percent for the NSC and 3LP devices. These results show that the devices may not be able to confine the signal in a highly resistive (dry), passive steel-in-concrete system. It should be remembered that the applied current travels further down the rebar with increasing R_p (passive steel), and, therefore, the confining power of the probe system must be increased. However, in such passive systems, the results given by these devices (even though two orders of magnitude greater than the actual average rate) indicate the presence of a passive system and in the qualitative sense is correct, and if used this way should not lead to wrong engineering conclusions. The deviations for the NSC device under passive conditions were, surprisingly, higher than those for the 3LP device, despite the lack of a GE in the latter device. This is possibly due to the large size of the CE used in the 3LP device (CE area of 18.8 in.² [121 cm²] compared to the NSC probe (CE area of 1.6 in.² [10 cm²])). Feliu, et al (51) have defined a critical length, L_{crit} , to which the signal spreads along the length of the rebar.² This value of L_{crit} is dependent upon the cross section of the member and the concrete characteristics, and, in general its value is smaller than the length of the concrete member (51). The critical length is very small when the rebars are active, and large when the rebars remain passive (51). Feliu et al. (26) report that upon increasing the CE size, the measured R_p approaches the true R_p value. Thus, even without the use of a GE, the R_p values obtained by the 3 LP device are comparable to those obtained with the NSC device, which uses a GE.

² L_{crit} can be defined as the length at which the current has decreased to some very small arbitrary value.

4

Current Distribution in the Measurement of Corrosion Rate of Reinforcing Bars in Concrete

In corrosion rate measurements, the current distribution determines whether any technique can yield useful information concerning a corrosion process. An overestimation of the corrosion rate can be due to current distribution effects. The highly asymmetric geometry of reinforced structures (i.e., long reinforcing bars) and the embedment of bars in an inhomogeneous resistive medium make it difficult to exactly define the polarized area for the steel-in-concrete system. Thus, the corrosion rate cannot be exactly determined. Use of a GE has been proposed as a possible solution to the current distribution problem. This study investigated the effectiveness and performance of GEs for the purpose of quantifying the corrosion rate. This work involves an investigation of the signal distribution within a concrete matrix and the effects of various physical and geometrical configurations of the concrete and GE system on the signal distribution.

Investigation Method

A corrosion rate measurement involves the induced polarization of a small amplitude step (a few millivolts) of the potential ($\Delta\phi$) while monitoring the current response of the reinforcing bar given as a current (Δi in mA). Correlation of polarization and response intensities results in polarization resistance R'_p , which can be used to evaluate the average corrosion rate of the polarized area, i_c ($mA\ cm^{-2}$), via the Stern and Geary equation:

$$i_c = \frac{1}{2.3R_p A} \frac{\beta_a \beta_c}{(\beta_a + \beta_c)} \quad (4-1)$$

where β_a and β_c are anodic and cathodic constants (Tafel slopes), respectively, and A is the polarized area.

To find the polarized area A we need to know how the signal is distributed in the concrete.

Basic Equations

Macroscopically, electroneutrality must be maintained in the interior of an electrolyte; hence, the Poisson equation reads:

$$\text{div grad} \phi = 0 \quad (4-2)$$

At the conducting boundaries, the current density is controlled by Ohm's Law (21)

$$I = -\sigma \frac{\partial \phi}{\partial n} \quad (4-3)$$

where n is the direction normal to the interface and σ is the electrolyte conductivity. At the insulating boundaries, the gradient of the electrical potential, ϕ , normal to the boundary vanishes (24,52-54).

$$\frac{\partial \phi}{\partial n} = 0 \quad (4-4)$$

Basic Assumptions

In developing the theory presented here, several assumptions are made in the numerical evaluation process.

- Parallel round reinforcing bars are embedded in an infinite concrete matrix. The cross section of bars is very small compared to the longitudinal section. This reduces the problem to a two-dimensional system.
- The electrical properties of the steel and concrete are purely resistive in nature, with the resistivity of the concrete (but not that of the steel) possibly being spatially variable due to macroscopic inhomogeneity within the matrix. The resistivity of the concrete is several orders of magnitude greater than that of the steel. Therefore, the metallic side of the electric double layer is an equipotential surface.
- The impedance of the steel/matrix interface is reactive (55-58), but the effect of a concentration gradient in the electrolyte and the effect of adsorption and desorption of the metal are neglected. The passage of charge across the metal/concrete interface, except for the initial charging of the double layer capacity, results solely from the occurrence of a Faradaic reaction. Since the interfacial impedance for the corroding steel bar, in determining the current distribution, is small compared to the resistance of concrete, the influence of the kinetics of the electrode reaction is negligible in terms of perturbations of the system. Primary current distribution corresponds to this case. This suggests that the potential difference across the double layer is constant over the electrode. Therefore, the solution side of the double layer is an equipotential surface also. The boundary conditions can therefore be written as:

$$\phi = \text{const (at the electrode surface)} \quad (4-5)$$

$$\frac{\partial \phi}{\partial n} = 0 \text{ (at the insulating surface)} \quad (4-6)$$

If the steel bar in the concrete is passive, the influence of activation potential is important. The electroneutrality condition, which is implied in the validity of equation 4-2, can be applied everywhere in the solution except in the electric double layer at the electrode. Therefore, the boundary condition at the solution/metal interface is current density dependent. We now have, instead of the boundary condition described by equation 4-5, the following equation:

$$\phi_e = \phi_m - \Delta\phi = f(i) \quad (4-7)$$

where ϕ_e is the potential at the solution side of the electrode-solution interface, ϕ_m is the constant value of the interior of the steel bar, and $\Delta\phi$ is a function of current density, which is determined by the kinetics of the electrode reaction.

Using a linear approximation, one has for the boundary condition in place of equation 4-5 (53):

$$\Delta\phi = \Delta\phi_0 + \frac{\partial\eta_a}{\partial i}i \quad (4-8)$$

where $\Delta\phi_0$ is a constant and $\frac{\partial\eta_a}{\partial i}$, in fact, is the polarization resistance.

In this parametric study, the geometric parameters, such as the thickness of concrete cover, D , and the diameter of reinforcing rebar, d , were varied. The polarization resistance, R_p , for corroding and noncorroding rebar surfaces were varied from 100 to $10^6 \Omega \text{ cm}^2$ (59), respectively. The resistivity of the concrete was chosen to be $\rho_s = 1,000$ to $3,000 \Omega \text{ cm}.$ ¹

Table 4-1. Input parameters for numerical simulation (1-m-long [3.28-ft-long] segments).

Parameter	Corroding Area	Noncorroding Area
d	1.0 - 5 cm	1.0 - 5 cm
D	1.5 - 10 cm	1.5 - 10 cm
ρ_s	$10^3 - 3 \times 10^3 \Omega \text{ cm}$	$10^3 - 3 \times 10^3 \Omega \text{ cm}$
R_p	$100 \Omega \text{ cm}^2$	$10^4 \Omega \text{ cm}^2$

The input parameters used in this model are summarized in Table 4-1. Schematic presentation of the system studied is shown in Figure 4-1.

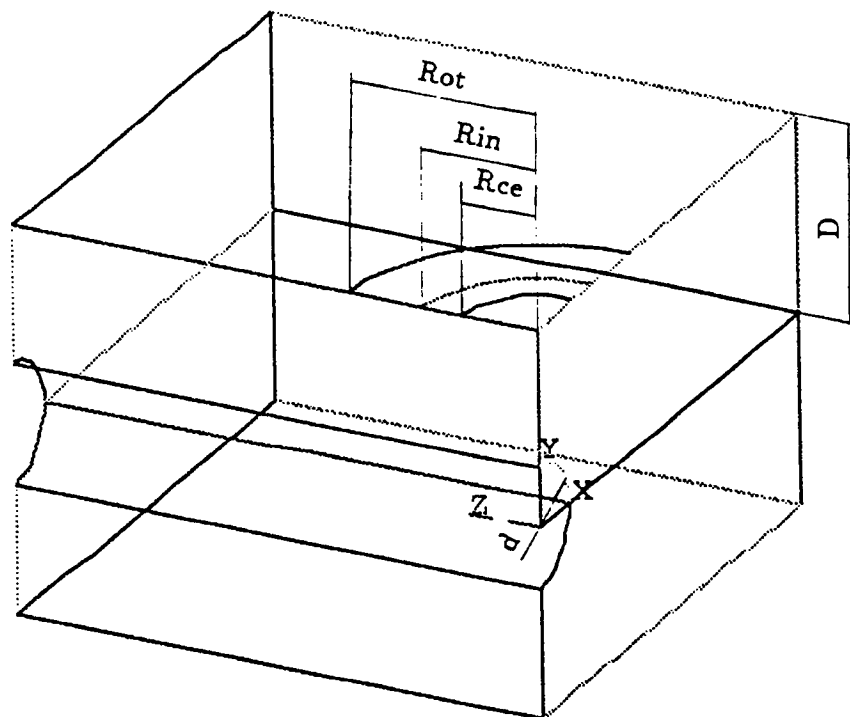
Results and Discussion

Current Distribution Along Longitudinal and Circumferential Sections of Rebar

The potential and current distributions in the longitudinal and circumferential directions of the rebar are presented in Figures 4-2 to 4-4 for corroding (small R_p) and passive (large R_p) rebars.² The applied current distribution is modified considerably along the longitudinal direction of the rebar, but not as much around the circumference of the bar when either using or not using a GE, even in the passive case. In other words, it can be said that only the top portion of the rebar is subjected to polarization. Therefore, the emphasis will be on the two-dimensional signal distribution along the longitudinal direction of the rebar in the sections that follow.

¹For drier concrete, the ρ_s values are higher, in which case $k = \sigma (dE/di)$ (where σ is the concrete conductivity (21-23)) is smaller and the current distribution is more confined as shown elsewhere (60). As a consequence, the spreading of the confined signal from the counter electrode is less compared to wetter concrete (lower ρ_s values), i.e., more confined than shown in Figures 4-2 to 4-4. The resulting signal distribution is more closely confined to the area directly under the CE and, hence, current distribution is of less of a problem in measuring the corrosion rate.

²The 10, 20, and, 30 mV lines are parallel to the circumference within the passive film (not visible for the scale in Figures 4-3b and 4-4b).



Note: R_{ce} --radius of CE
 R_{in} --inner radius of GE
 R_{ot} --outer radius of GE
 D --concrete cover thickness
 d --radius of rebar

Figure 4-1. Schematic representation of polarizing electrodes and steel-in-concrete system.

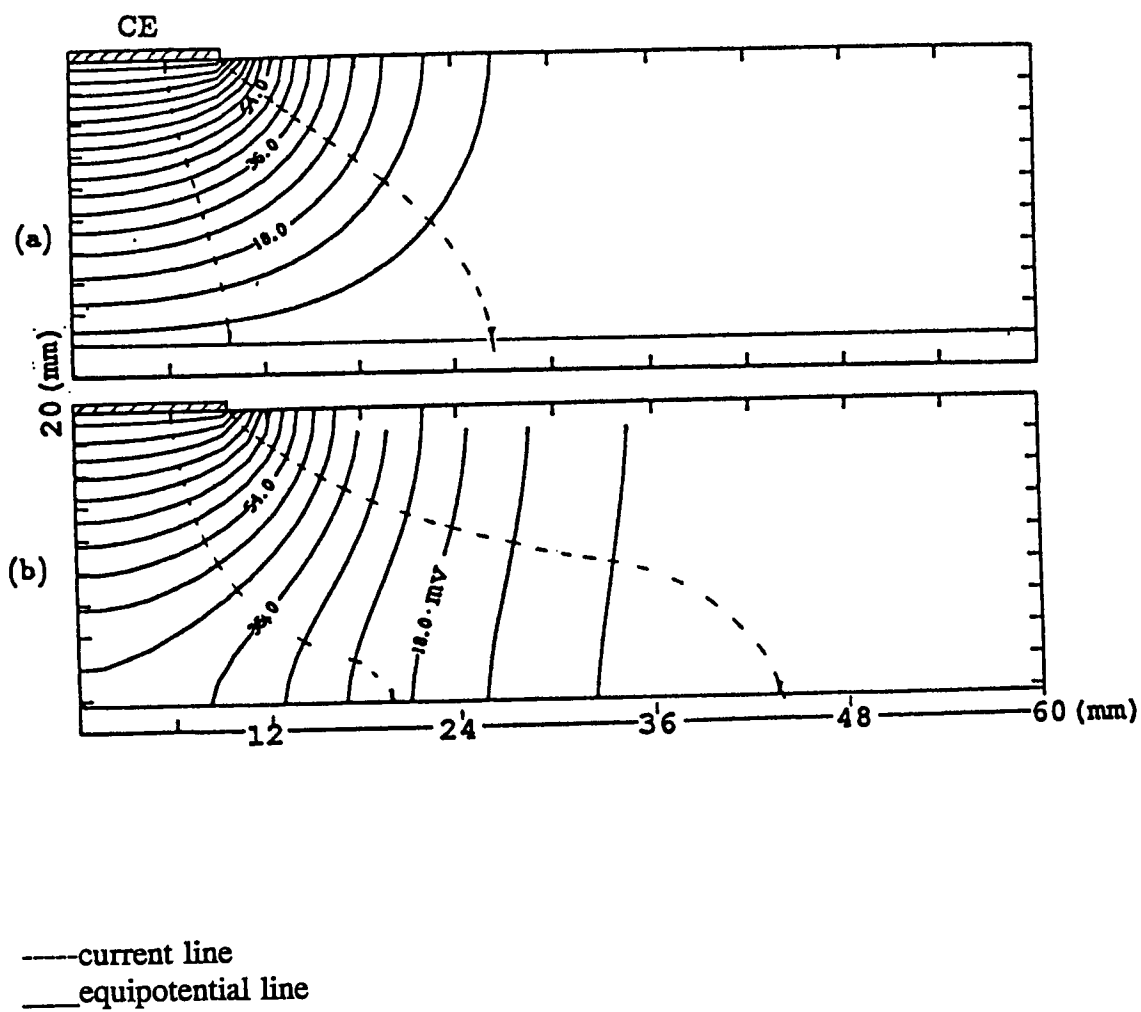
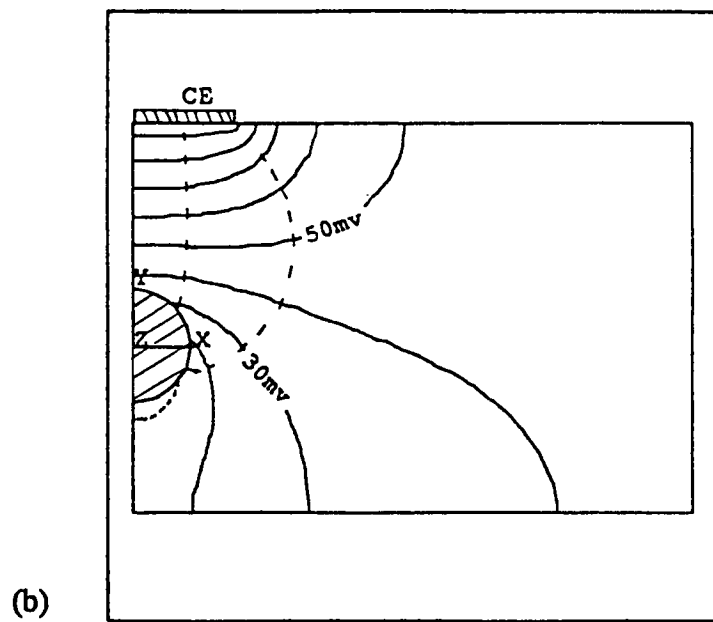
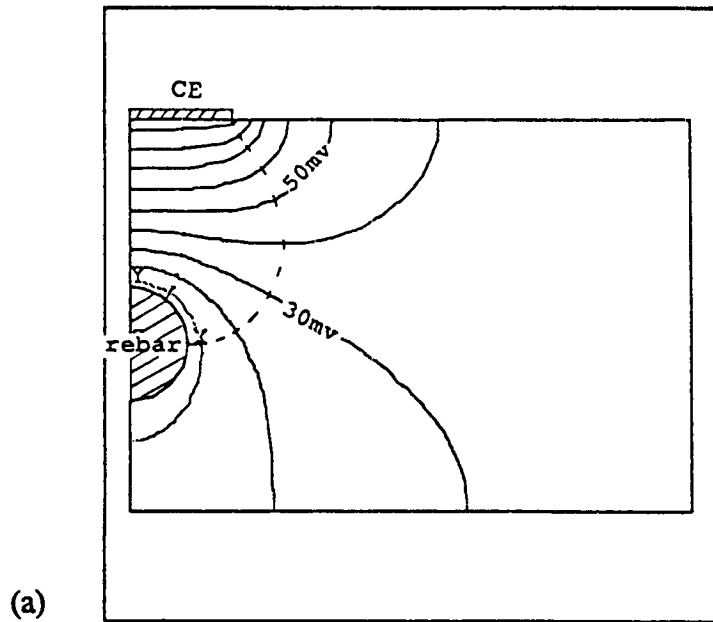
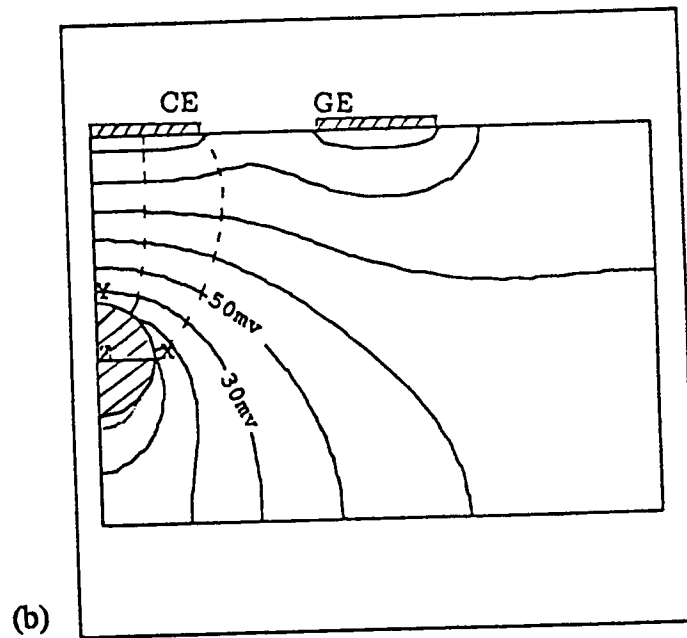
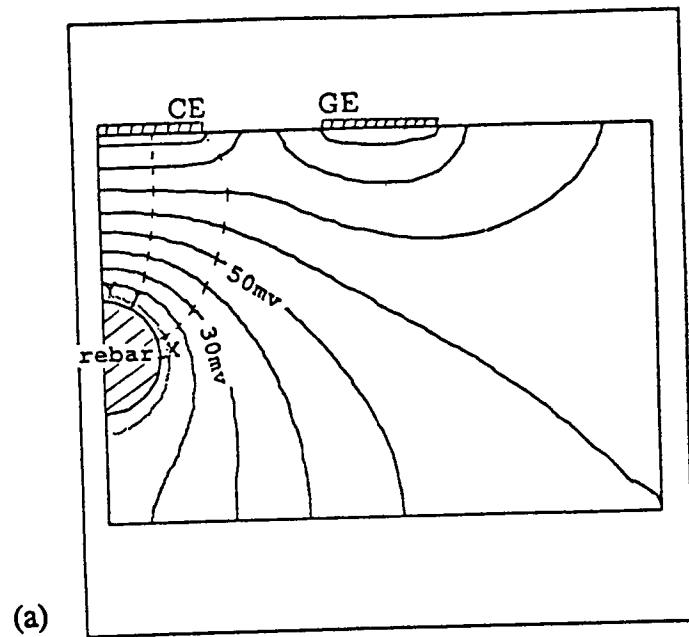


Figure 4-2. Potential/current distribution in the longitudinal direction of the rebar: (a) corroding rebar; (b) passive rebar.



——current line
——equipotential line

Figure 4-3. Potential/current distribution around the cross section of the rebar without GE:
(a) corroding rebar; (b) passive rebar.



-----current line
 _____equipotential line

Figure 4-4. Potential/current distribution around the cross section of the rebar with GE: (a) corroding rebar; (b) passive rebar.

Effect of Polarization Resistance

Effects of polarization resistance, R_p , on signal distribution for the cases where embedded steel is polarized by a single CE and by both CE and GE are shown in Figure 4-5. Wider distribution of the applied current is observed for the larger polarization resistance, i.e., for a passive steel. In other words, the applied signal tends to be distributed further with increasing R_p , resulting in a larger polarized area. This is consistent with an increase in $k = \sigma (dE/di)$, i.e., an increase in (dE/di) (21-23). The occurrence of this increased polarization means that each surface element of an electrode is provided with an equivalent individual resistance in series with the resistance inside the electrolyte. When the R_p value is high, the interfacial resistance dominates, and the variations of the electrolyte resistance due to different geometrical conditions at different points of an electrode become of less importance. A significant potential drop across the rebar/concrete interface leads to a large polarized area. Thus, the capability to confine the electrical signal from the CE to the rebar beneath this electrode tends to deteriorate as the rebar's R_p values increase up to a relatively large R_p value and then levels off, as shown in Figure 4-5.

Using a GE results in decrease in the distribution of current. As a consequence, the polarized area may be more easily defined.

Effect of Separation Distance Between CE and GE

Figure 4-6 shows the effect of the separation distance, S , between the CE and the GE on the signal distribution. The increase in the separation distance leads to greater current distribution and larger polarized area. The reason is thought to be that the electric field produced by the CE and the GE are superimposed on each other. As the GE and the CE get closer, the interaction of their electric fields becomes stronger, better restricting the CE signal. It has been observed that a separation distance that is five times greater than the width of the CE provides no guard effect. Under such conditions, the current distribution is the same as for a single CE.

Effect of Concrete Cover Thickness

Figure 4-7 illustrates the effect of the concrete cover thickness on the signal distribution. The plot shows that the polarized area increases with increasing cover thickness. Evidently, for thick concrete cover, the current spreads further to compensate for the increase in resistance.

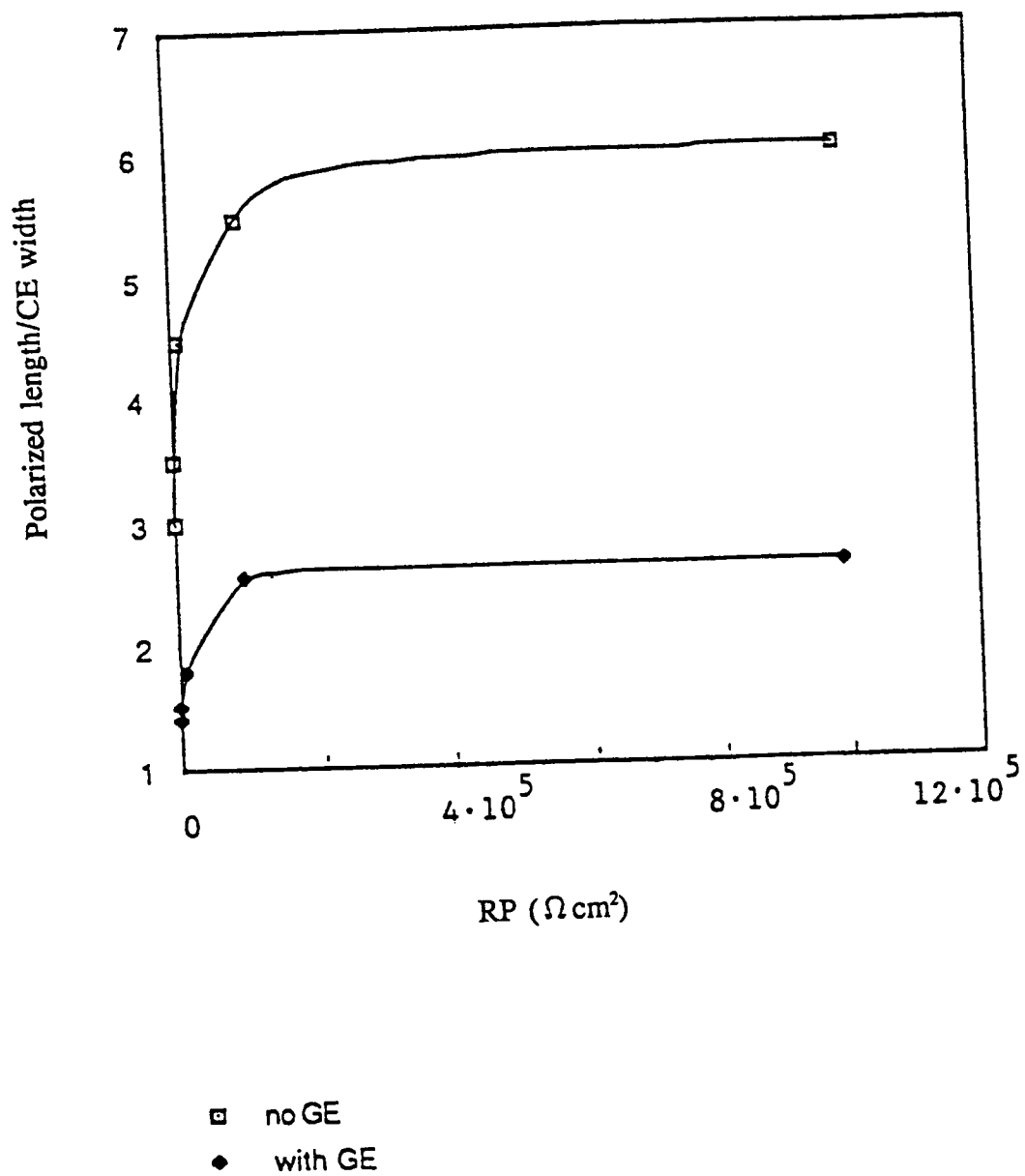
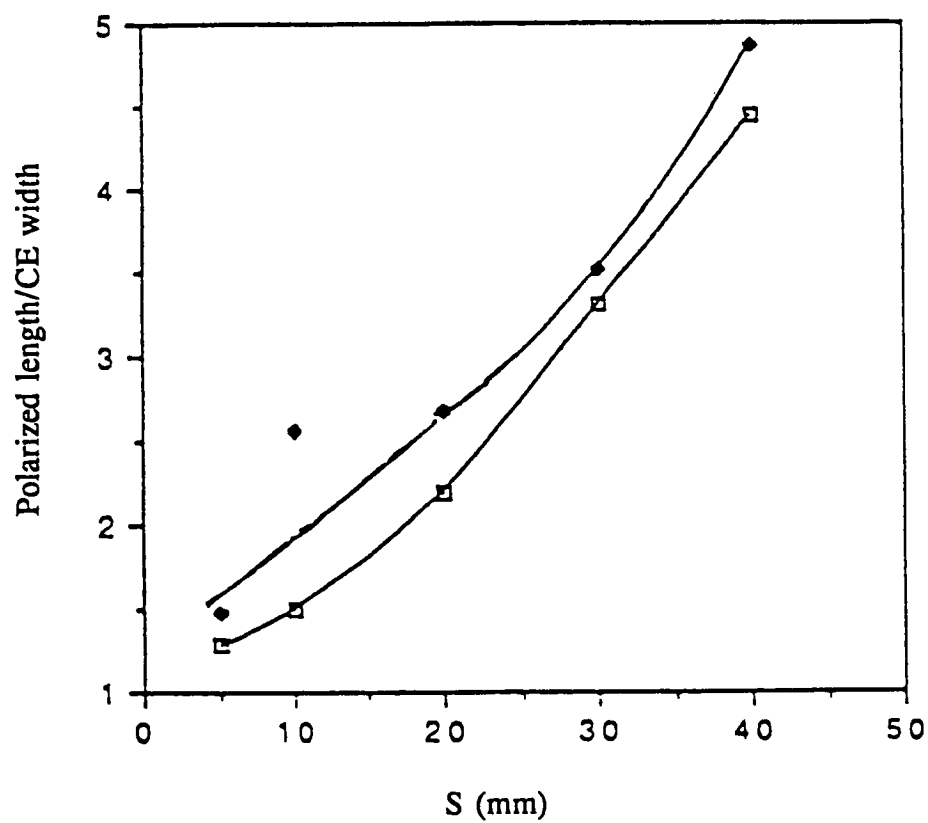


Figure 4-5. Effect of polarization resistance on current distribution.

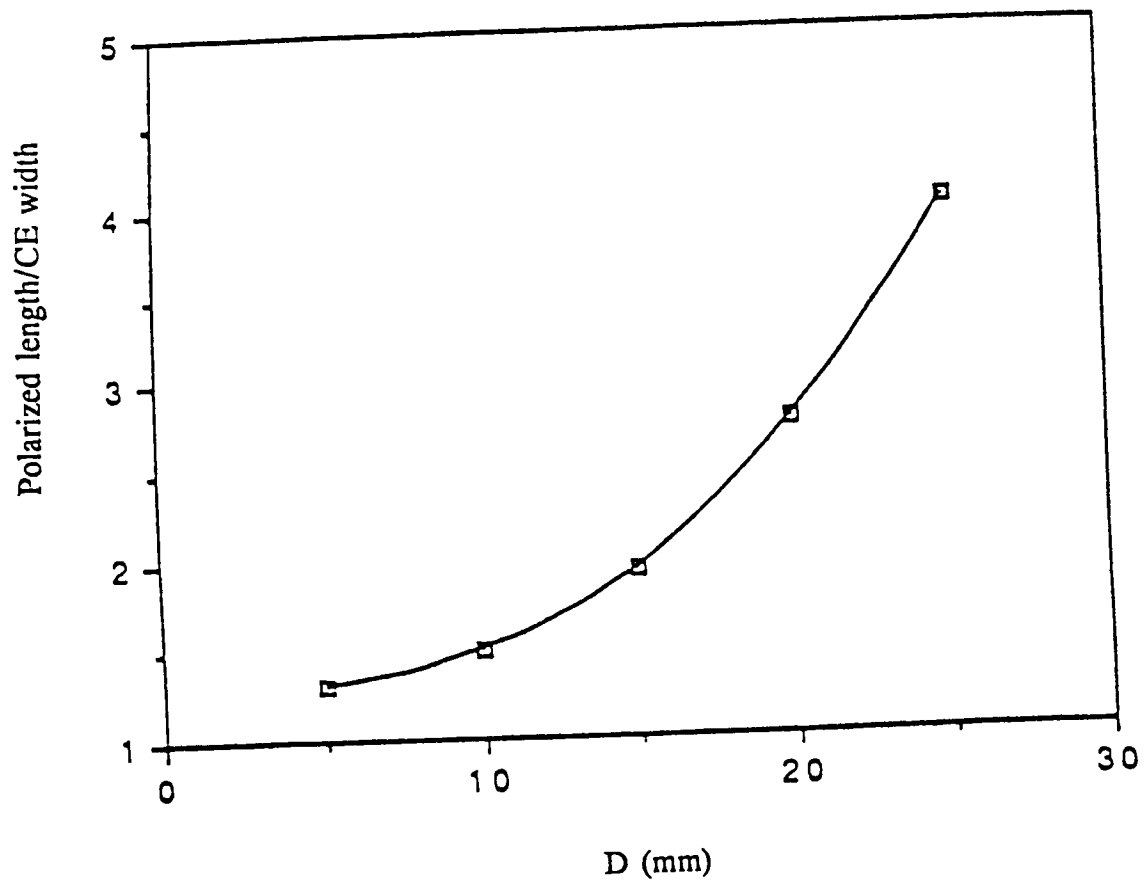


- - $R_p = 10^3 \Omega cm^2$
 ◆ - $R_p = 10^5 \Omega cm^2$

Note:

$R_{ce} = 10 \text{ mm}$
 $R_o - R_i = 10 \text{ mm}$
 $D = 10 \text{ mm}$
 $d = 15 \text{ mm}$
 $\rho_s = 1,000 \Omega cm$

Figure 4-6. Effect of separation distance on signal distribution.



Note:

$$R_{ce} = 1.0 \text{ cm}$$

$$R_{in} = 2.0 \text{ cm}$$

$$R_o = 3.0 \text{ cm}$$

$$\rho_s = 10^3 \text{ } \Omega\text{cm}$$

$$R_p = 10^3 \text{ cm}^2$$

Figure 4-7. Effect of concrete thickness on signal distribution.

Effect of GE Width

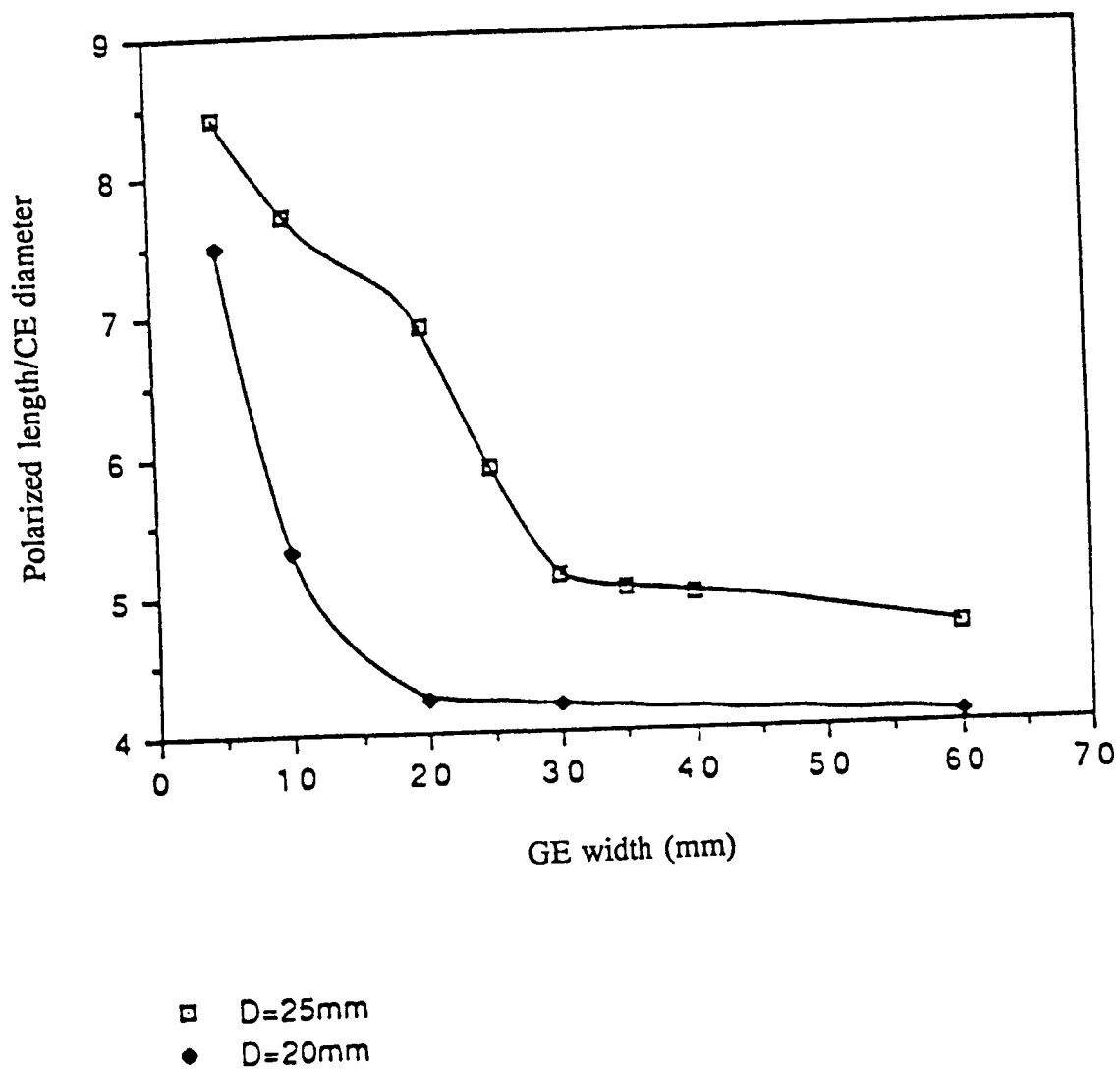
It may be seen in Figure 4-8 that increase of the width of the GE ring (Figure 4-1) relative to the diameter of the CE reduces the length of rebar affected by the current flowing from the CE, i.e., decreases the polarized length. However, above some limiting value (which is apparently a function of cover depth), an increase in the GE width does not appear to have a significant effect on further confinement of the current flow. As shown elsewhere (60), if the width of the GE ring is smaller than the CE, the effectiveness of the GE is decreased. The current from the CE may then flow even beyond the GE, especially in the case of passive bars. On the other hand, a GE that is much larger than the CE is impractical and unnecessary. It appears that there is no detectable change in current distribution when the GE width is larger than the concrete cover thickness as shown in Figure 4-8. In the cases of Figures 4-5 through 4-8, the results can be scaled up so that for a proportionately larger geometry the numbers on the abscissa are scaled up by the same factor. For example, if R_{ce} and R_m in Figure 4-8 are 10 and 20 cm, respectively (instead of 1 and 2 cm), the numbers on the axis of the GE width will be multiplied by 10.

Effect of Contact Resistance Between CE/GE and Concrete Surface

When the concrete surface has low resistivity, the contact resistance between CE/GE apparatus and the concrete surface also will be low. Figure 4-9 shows three cases: high resistivity top layer, low resistivity top layer, and uniform concrete resistivity. The results shown in Figure 4-9 indicate that the system exhibits a more uniform signal distribution when the top portion of the concrete structure has a resistance lower or equal to the resistance of the remaining portion of the concrete, whereas an impaired signal distribution is obtained for a high resistivity top layer. Therefore, it can be concluded that variations in the concrete resistance distribution can have a significant influence on the current and potential distributions.

Effect of Macrocells

Typically, some portions of the surface of the reinforcing bar will be exposed to chloride ions or will be exposed to a higher concentration sooner than the other parts of the surface, causing them to become active. Since the chloride concentration is not uniform throughout the structure, some areas become active while others remain in the passive state. It is



Note:

$R_{ce} = 1.0 \text{ cm}$

$R_{in} = 2.0 \text{ cm}$

$\rho_s = 10^3 \Omega\text{cm}$

$R_p = 10^4 \text{ cm}^2$

Figure 4-8. Effect of GE size on signal distribution.

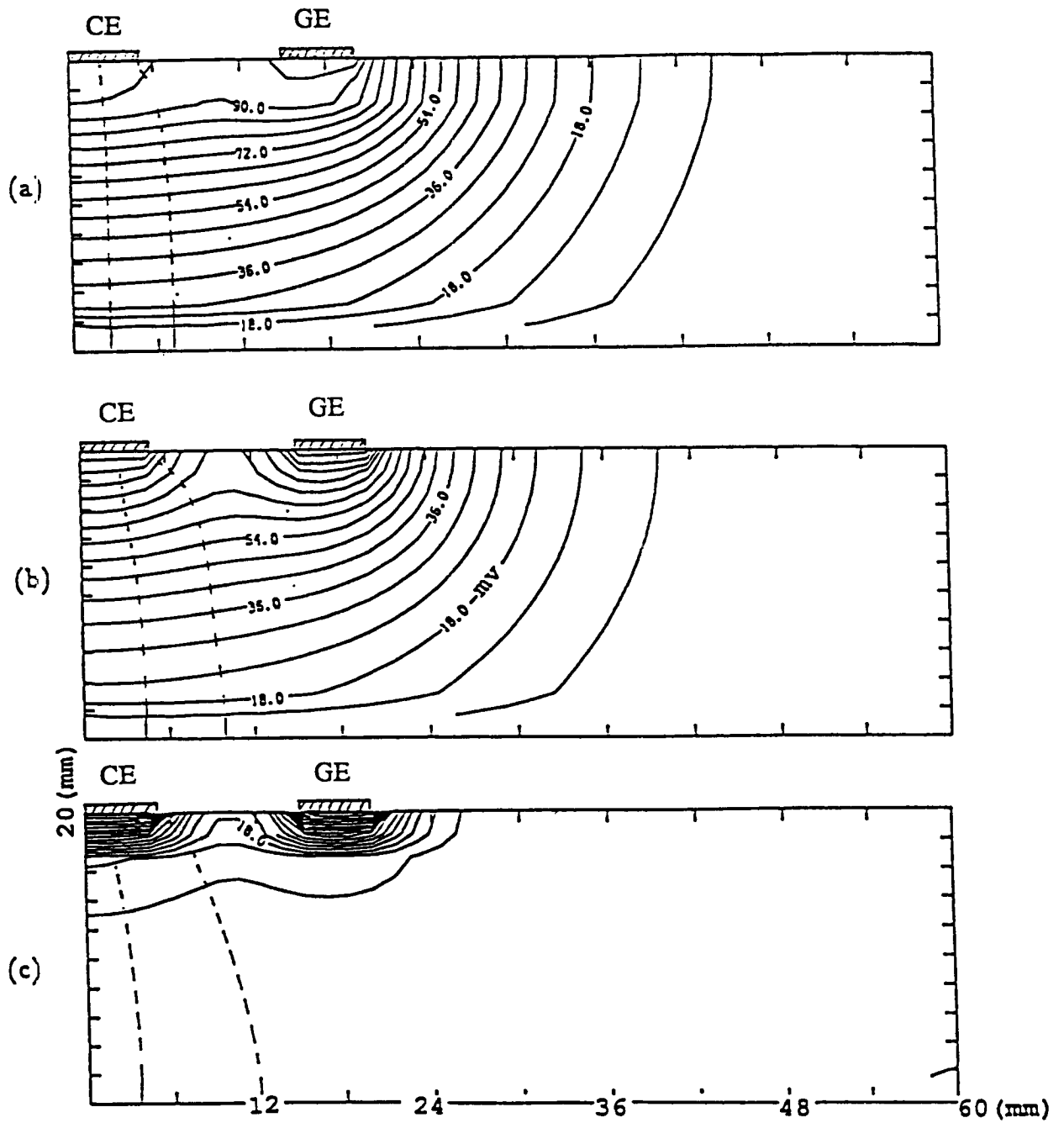


Figure 4-9. Potential/current distribution: (a) low resistivity top layer ($\rho_1 = 1,000\Omega \text{ cm}$, $\rho_2 = 3,000\Omega \text{ cm}$); (b) uniform concrete medium ($\rho = 3,000\Omega \text{ cm}$); (c) high resistivity top layer ($\rho_1 = 3,000\Omega \text{ cm}$, $\rho_2 1,000\Omega \text{ cm}$).

important to notice that the interfacial impedance is position-dependent due to the macrocell effect, i.e., the polarization current is more confined to the corroding area (where R_p is less) than elsewhere on the passive surface.

Typical plots of the potential/current distribution are shown in Figure 4-10 for the cases when the corroding section is located under the CE, between the CE and the GE, and under the GE. Figure 4-11 illustrates the cases in which no GE is used so that the effects of the GE can be easily seen.

The dependence of the polarized area on the macrocell for the three cases identified above show that detection of corrosion on the rebar is possible only when the corrosion spot is under or near the CE; in this case, the polarized area is almost the same as that of the CE. It is worth noting, however, that the possibility of detecting the corrosion spot decreases as the corroding segment moves down the rebar. Thus, if one knows approximately where the corrosion may occur, then, in principle, the position of the corrosion area can be located precisely by using the GE. This, in fact, has been confirmed by experimental results; for example, see Figure 3-9.

An effective method of locating the site of corrosion may involve the potential criterion. The polarization resistance measurement using a GE should preferably be carried out for locations identified as probable corrosion areas. In any event, any of the techniques can apparently be used when the polarization resistance is low.

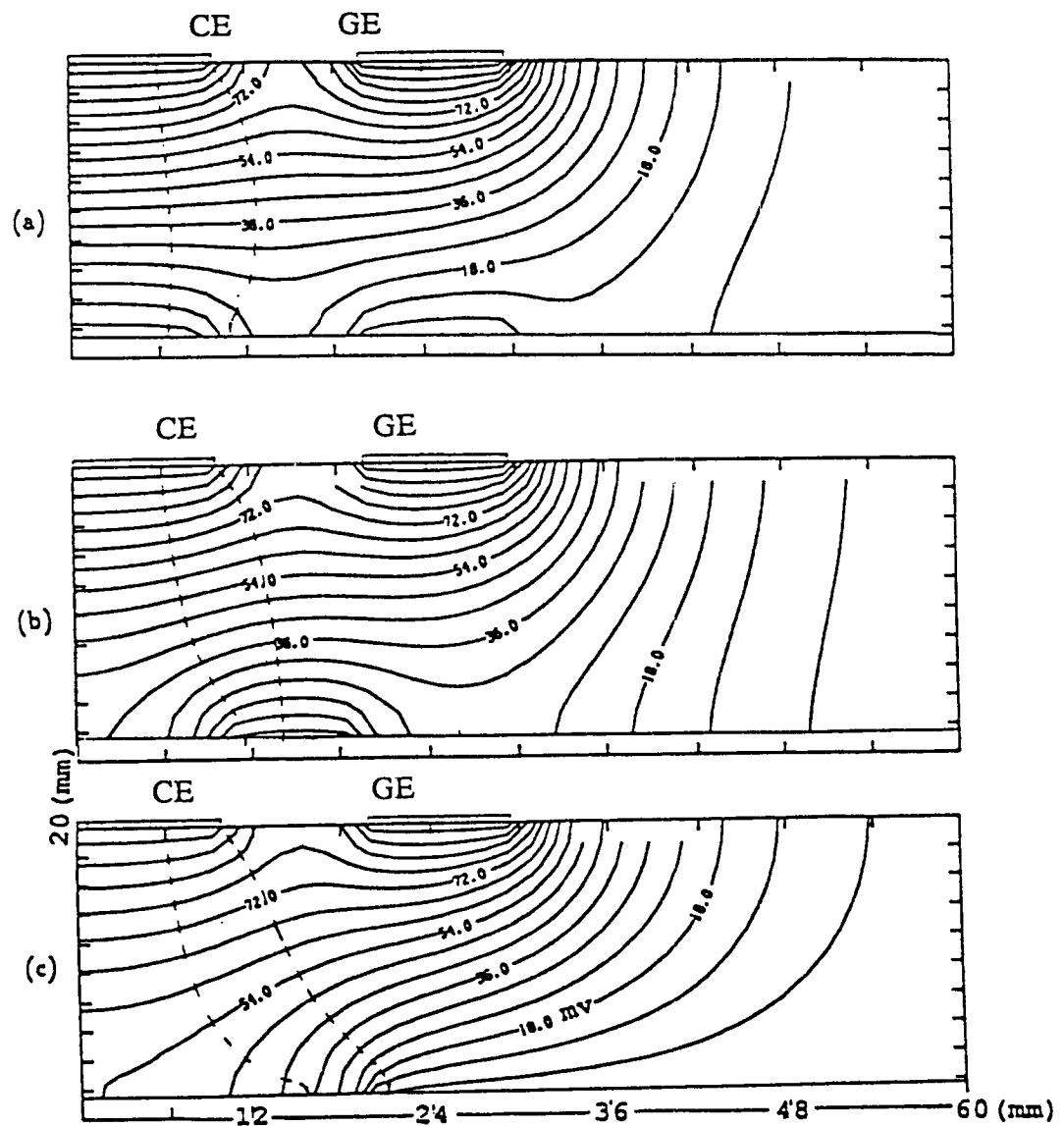


Figure 4-10. Potential/current distribution showing effect of macrocells along rebar: (a) corroding spot under CE; (b) corroding spot between CE and GE; (c) corroding spot under GE.

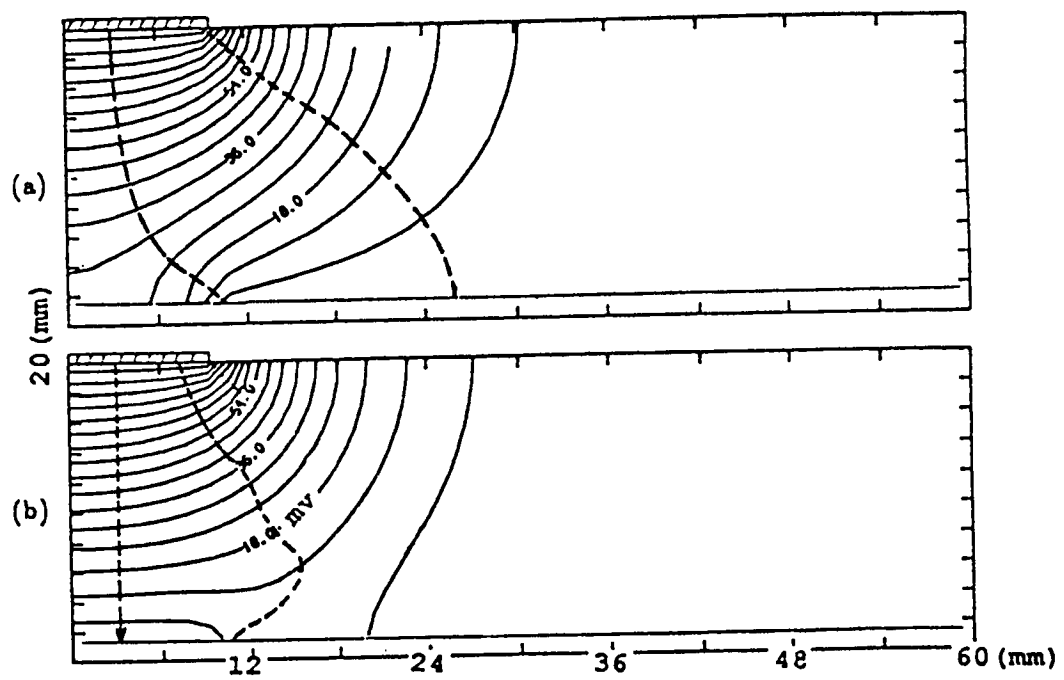


Figure 4-11. Potential/current distribution showing effect of macrocell along rebar without GE: (a) corroding spot displaced to the right of the CE; (b) corroding spot under CE.

5

Field Validation Studies

Introduction

Due to the physicochemical complexity of the steel-in-concrete system, considerable care is required for the interpretation of the results obtained from electrochemical measurements on large concrete structures. The results will depend on the actual conditions of the reinforced concrete, on the concrete/electrode contact, and on the operation of the measuring instrument. For nondestructive determination of the corrosion rate of steel rebars, electrochemical methods are especially suitable. Most often, the linear polarization and AC impedance methods have been examined (12,14,31,61-65) and used for field corrosion monitoring (13,63,64,66). These methods are applied by several instruments that have been developed for corrosion rate measurements on concrete structures (11).

In nondestructive examination of large structures, it is impossible to determine the accuracy of the results obtained, because the actual corrosion rate cannot be measured by any direct method. The best approach for evaluating the applicability of the various instruments involves the use of a set of different instruments in order to compare the data and to assess their consistency.

The objective of this work was to evaluate the corrosion rate data obtained by various devices in the testing of large concrete structures. A procedure for the field testing was developed and used for preparing a draft of a standard test method. The field measurements were performed on several bridge structures with the use of three commercial devices. Corrosion current and corrosion potential (half-cell potential) were measured to assess a

relationship between the information gained from the corrosion potential alone (ASTM C876-87) (42) and from the corrosion rates.

Devices Used for Corrosion Rate Measurements

The instruments used in the field validation studies are the three described in Chapter 3 of this report. They are:

- The Nippon Steel Corporation (NSC) device;
- The instrument developed by K. C. Clear, Inc. (3LP); and
- The instrument developed by GEOCISA in Spain (GECOR).

All are generally of fairly recent development and/or in evolutionary stages. Photographs of the three devices in operation during the field validation studies are shown in Figures 5-1 to 5-3.

Test Sites

For field testing, bridges were chosen in areas representing three types of environments:

- Tropical climate with marine environment (highly aggressive due to a steady exposure to the ocean water at high temperatures). For this environment, the Bahia Honda Bridge in the Florida Keys was chosen (designation: Bahia Honda, Florida).
- Moderate climate with snowfall in winter and a rather frequent use of deicing agents (moderate aggressiveness associated with chloride salts used in winter months only). For this environment, two bridges in Centre County, Pennsylvania, were chosen, one on Route 322 and the other on Route 220 were chosen (designation: 322, PA; 220, PA).



Figure 5-1. NSC device being used to obtain corrosion rate data on a stirrup of a reinforced concrete beam of a bridge on US Route 220 in Pennsylvania.



Figure 5-2. The 3LP instrument gathering corrosion rate data on the underside of a bridge deck on US Route 220 in Pennsylvania.



Figure 5-3. The GECOR device being used to obtain corrosion rate data on a distressed pier column of a bridge on US Route 322 in Pennsylvania.

- Mild climate with only a sporadic use of deicing agents (low aggressiveness owing to low concentration of chlorides). For this environment, two bridges in Virginia, both on Route 81 North, were chosen (designation: 81N-1, VA; 81N-2, VA).

On the Bahia Honda Bridge, the measurements were carried out on the pier and pile cap assembly No. 65, and on pile No. 75. The test sites are shown in Figure 5-4. Sites C on the pile cap and L on pile No. 75 are in the splash zone, where concrete spalling and rust staining appeared most frequently. Sites H are above this area, in the atmospheric zone. Sites T are at mean high tide level (MHTL).

On Bridges 322, 81N-1, and 81N-2, the measurements were made on decks, piers, and abutments, whereas on bridge 220, tests were carried out on the deck, the underside of the deck, and on a beam. The positions of the test sites on the bridge decks are shown in Figure 5-5, and distances for these sites as well as the height of sites on piers and walls are given in Table 5-1. The sites chosen were located at single segments of the rebar grid between rebar intersections so that overlapping of rebars was avoided.

Table 5-1. Distances for test sites on bridge decks and the height of test sites on piers and abutments.

Bridge	Distances on Deck					Height Above Ground Level		Other Sites
	a	b	c	d	f	Pier	Abutment	
322, PA	11'- 7"	6'- 6"	14'- 6"	6'- 8"	9'- 3"	5'- 5"	2'- 9"	---
220, PA	8'- 9" (asphalt)	2'- 0"	8'- 9" (asphalt)	2'- 1"	12'- 10"	---	---	Under- side of Deck; Beam
81N-1, VA	16'- 4"	6'- 9"	---	---	---	5'- 0"	1'- 5"	---
81N-2, VA	14'- 0"	5'- 11"	14'- 0"	4'- 8"	15'- 0"	4'- 7"	1'- 11"	---

* No reading.

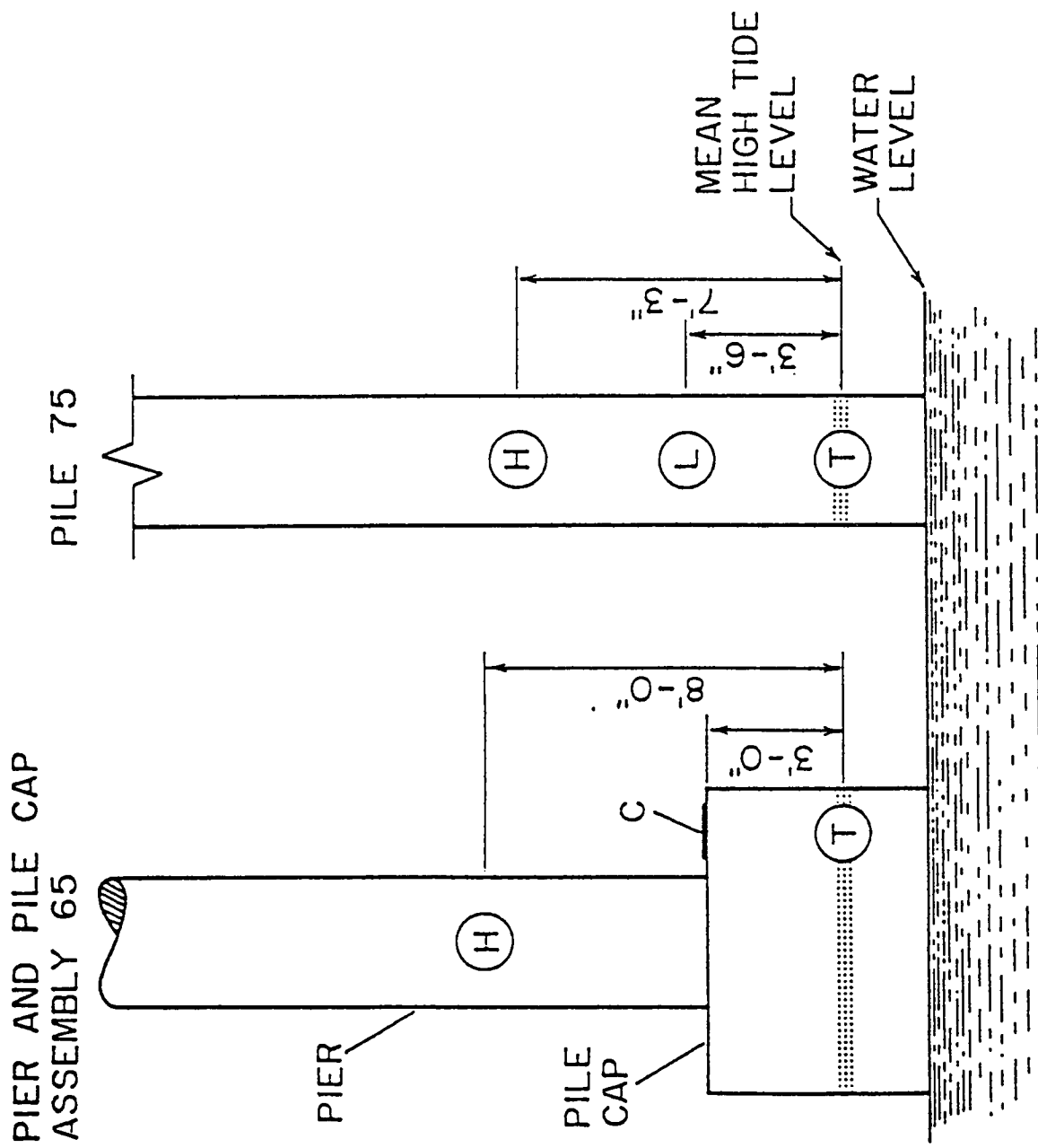


Figure 5-4. Position of test sites H, C, T, and L on Assembly 65 and Pile 75 of Bahia Honda Bridge (northbound), Florida.

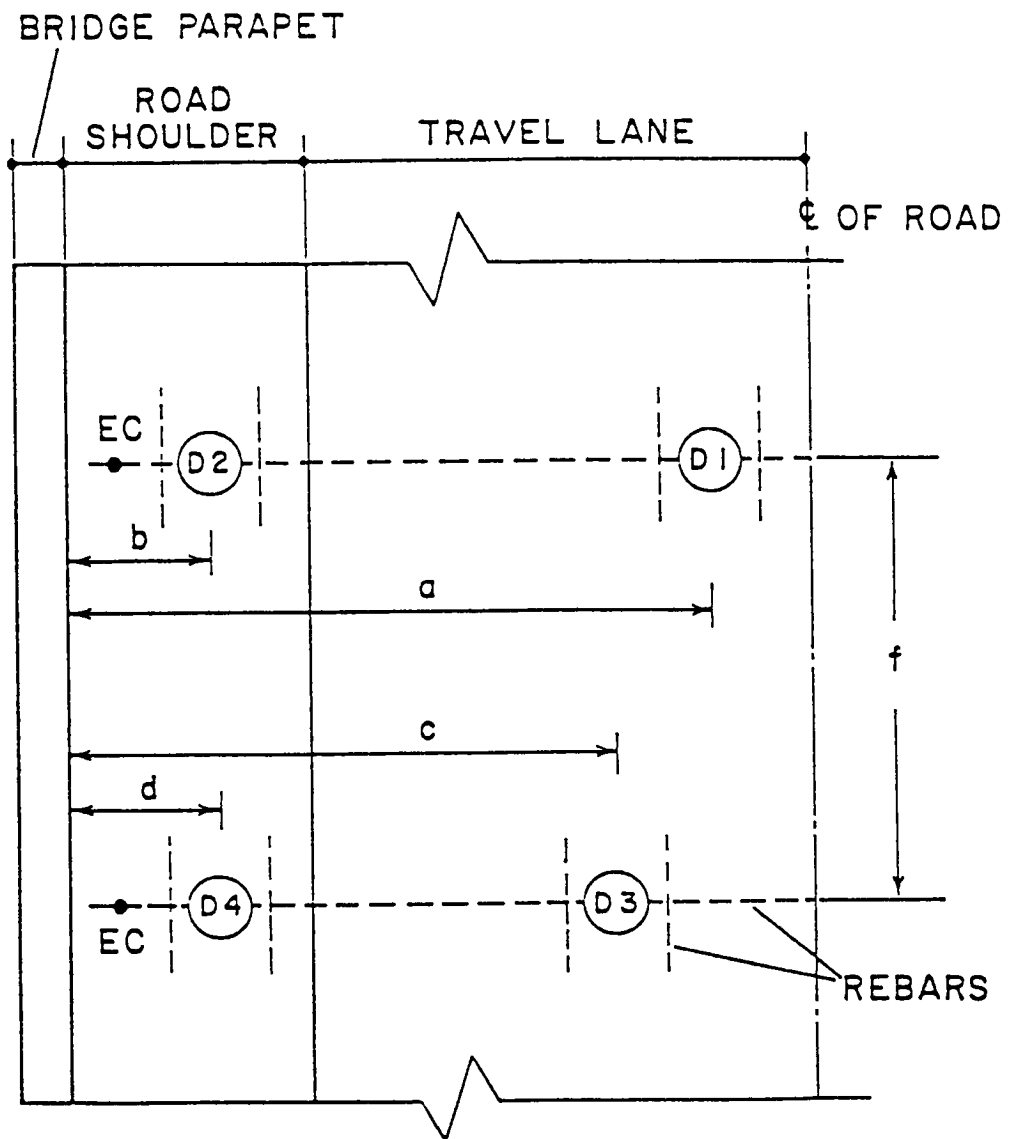


Figure 5-5. Position of test sites D1 to D4 on bridge decks; EC denotes electrical connection with rebars, a to f denote distances (see Table 5-1).

Testing Procedure

After locating rebars with a rebar locator, electrical connection was established for each of the rebars where the test sites were situated (see Figures 5-6 and 5-7). In case of vertical and overhead surfaces, probes of the measuring instruments were affixed to the surfaces using plastic strap tie-downs and drilled wall anchors (see Figure 5-8).

The test sites were adequately wetted with potable water containing 3.2 fl oz (95 mL) of a household detergent per gallon, and an attempt was made to restrict the wetted area to the size of the electrochemical probe used. A few minutes after the wetting, a sponge about 0.2 in. (5 mm) thick and 2.8 in. (70 mm) in diameter was placed on the site and similarly wetted; afterwards, a saturated copper/copper sulfate half cell (Tinker-Rasor, Model 3A) 2.8 in. (70 mm) in diameter was placed on the sponge and the corrosion potential, E_c , of the rebar was measured with the MICRONTA®LCD Digital Multimeter (input impedance 10^7 ohm)--see Figure 5-9. The potential was recorded when the readings did not change more than 2 mV/minute, and this was usually observed after 5 to 10 minutes from the start of the wetting. Next, the polarization resistance, R_p , was measured using each of the devices, first by NSC (the smallest probe), then by 3LP (intermediate size probe), and, finally, by GECOR (the largest probe, including both internal and external CEs).

The probes contacted with the concrete surface through sponges, which matched the size of the probes. The sponges for NSC and GECOR were 0.2 in. (5 mm) thick. The sponge for the NSC probe was wetted with saturated KCL solution (the same solution was used for wetting a polymer in the probe). The sponge for the 3LP probe was wetted with water containing detergent, whereas water without additions was used for wetting the sponge of the GECOR probe.

After installing a probe, three measurements were made with each of the devices. Time requirements varied from 20 to 40 minutes, depending on the device. The time between readings (for the half-cell to return to its initial value and stabilize) is about 10 minutes. Corrosion potential was measured with the Cu/CuSO₄ half-cell each time before installing the probe of another device. The time between the completion of the measurements with one device and the start of the measurements with another device was typically from 20 to 40 minutes.

To estimate the reproducibility of the data, the measurements were carried out on the same sites on two different days.

Corrosion current, i_c , was calculated from the relation:



Figure 5-6. Using a rebar locator to determine the position of the reinforcement.



Figure 5-7. Core drilling in order to expose a rebar for making an electrical connection.



Figure 5-8. Drilling a pier column to install wall anchors for affixing an instrument probe to the concrete surface.



Figure 5-9. Taking corrosion potential readings with the copper/copper sulfate half-cell.

$$i_c \left[\frac{A}{cm^2} \right] = \frac{B}{R_p [ohm \ cm^2]} \quad (5-1)$$

where B was taken as equal to 26 V (23). It was assumed that during the electrochemical measurements the rebar was polarized uniformly around its circumference for a length equal to the diameter or length, L , of the polarizing electrode.¹ Therefore, R_p was calculated from the relation:

$$R_p = R_p(\text{meas}) \cdot \pi \cdot d_{rb} \cdot L \quad (5-2)$$

where R_p (meas) is the polarization resistance measured, d_{rb} is the diameter of the rebar, and L is equal to 1.2 in. (3.0 cm) for NSC, 6.7 in. (17.1 cm) for 3LP, and 5.5 in. (14.0 cm) for GECOR.

Results

Corrosion Current as a Function of Corrosion Potential

Values of the corrosion current, i_c , obtained from the measurements were presented in $\log i_c$ versus E_c plots. This presentation is similar to the conventional presentation of polarization curves, and it provides a good basis for the comparison of the information on the extent of corrosion gained from measurements of i_c with that based solely on E_c (ASTM C876-87).

Figures 5-10 to 5-13 present values of corrosion current, i_c , (arithmetic mean of three measurements) as a function of corrosion potential, E_c , (measured with reference to the

¹Laboratory work showed that it is essentially only the top half of the rebar that is polarized. However, in an effort to keep our results in the same terms as those of other investigators (for purposes of comparison) in determining corrosion rates in field structures, the entire circumference of the rebar was assumed to be polarized.

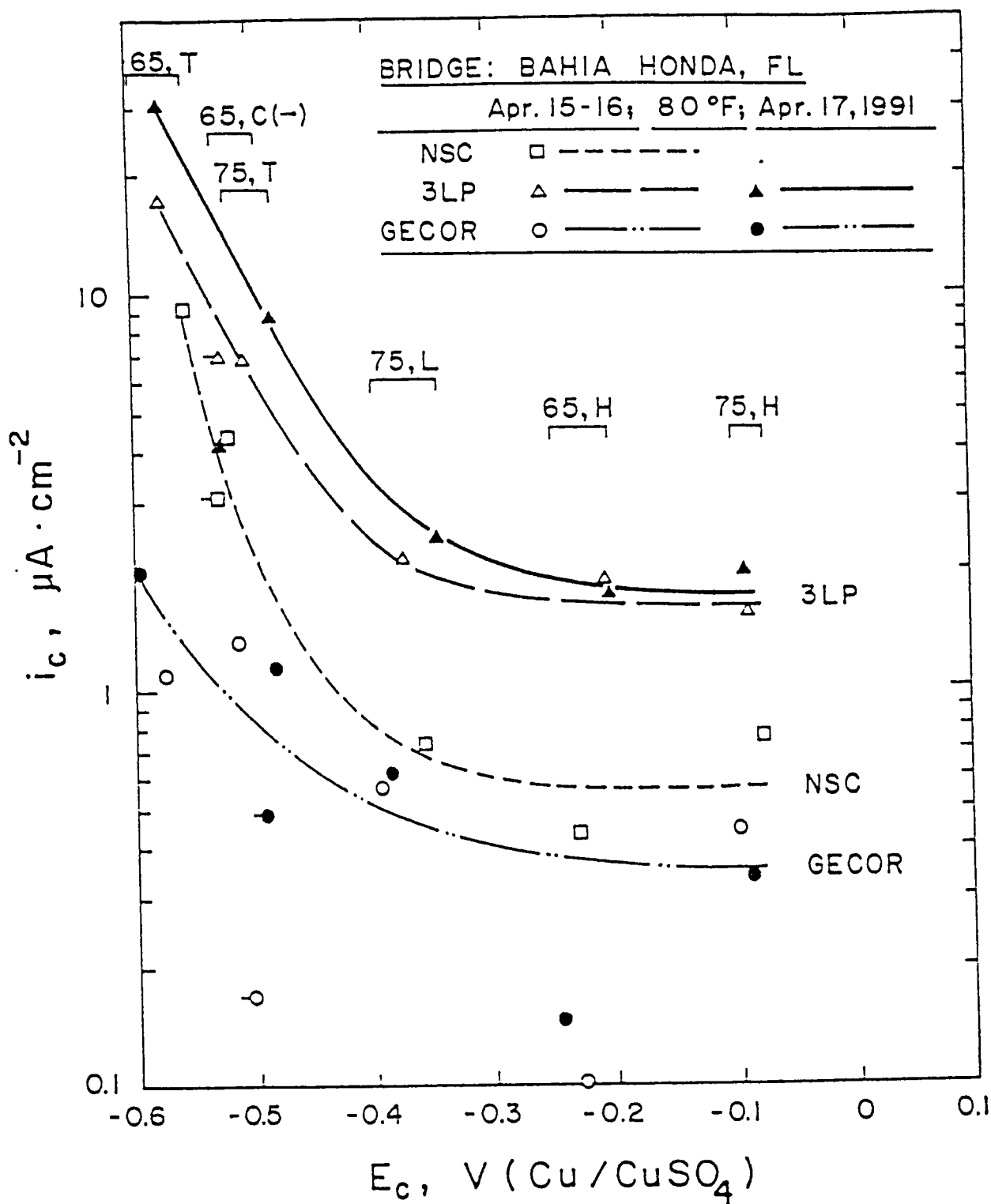


Figure 5-10. Corrosion current i_c versus corrosion potential E_c for Bahia Honda Bridge, Florida, on April 15, 16, and 17, 1991; i_c was determined by devices NSC, 3LP, and GECOR. Designation: 65 and 75 denote the bridge assembly and pile; H, C, L, and T denote the locations of measurements.

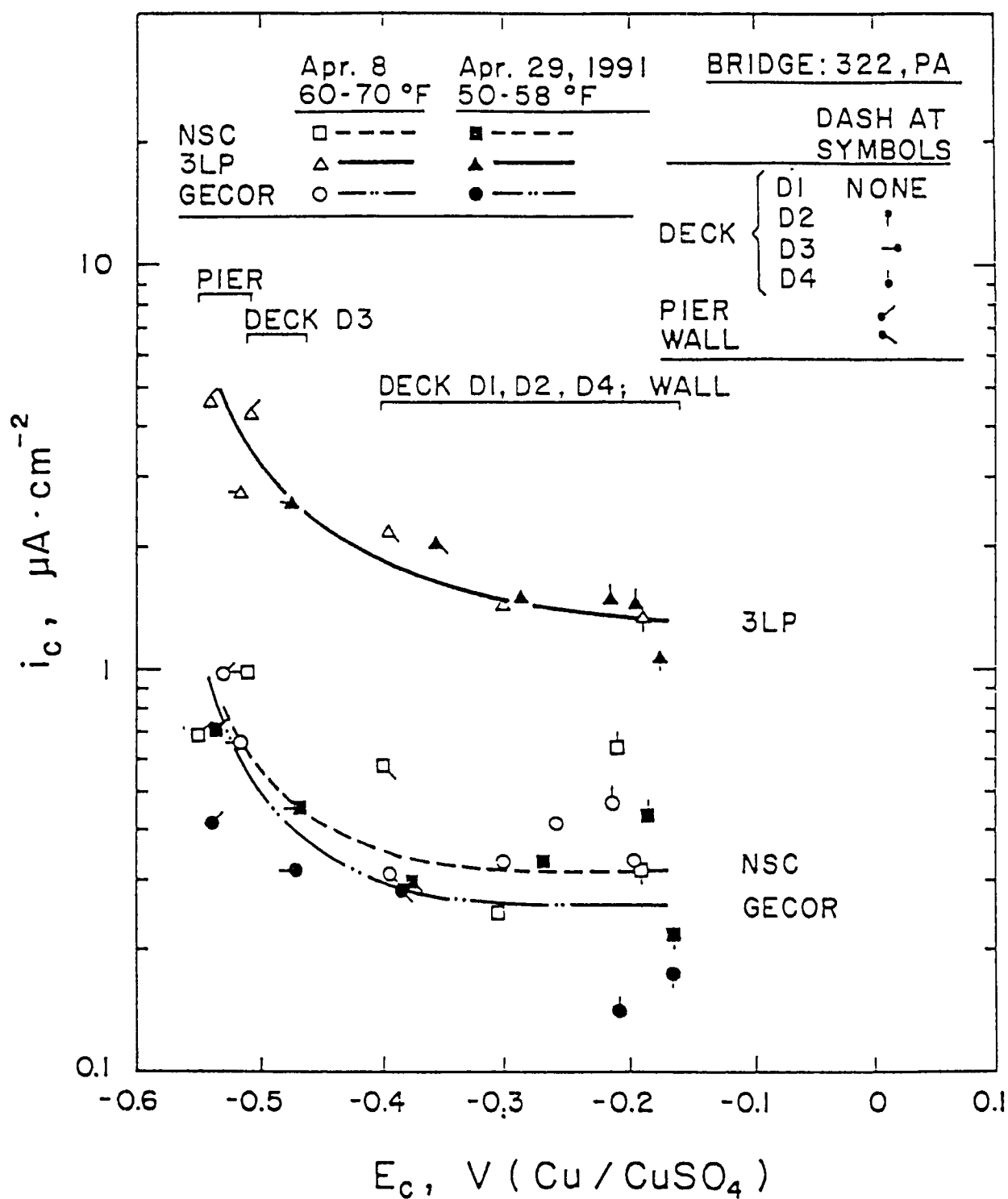


Figure 5-11. Corrosion current i_c versus corrosion potential E_c for Bridge 322, PA, on April 8 and 29, 1991; i_c was determined by devices NSC, 3LP, and GECOR.

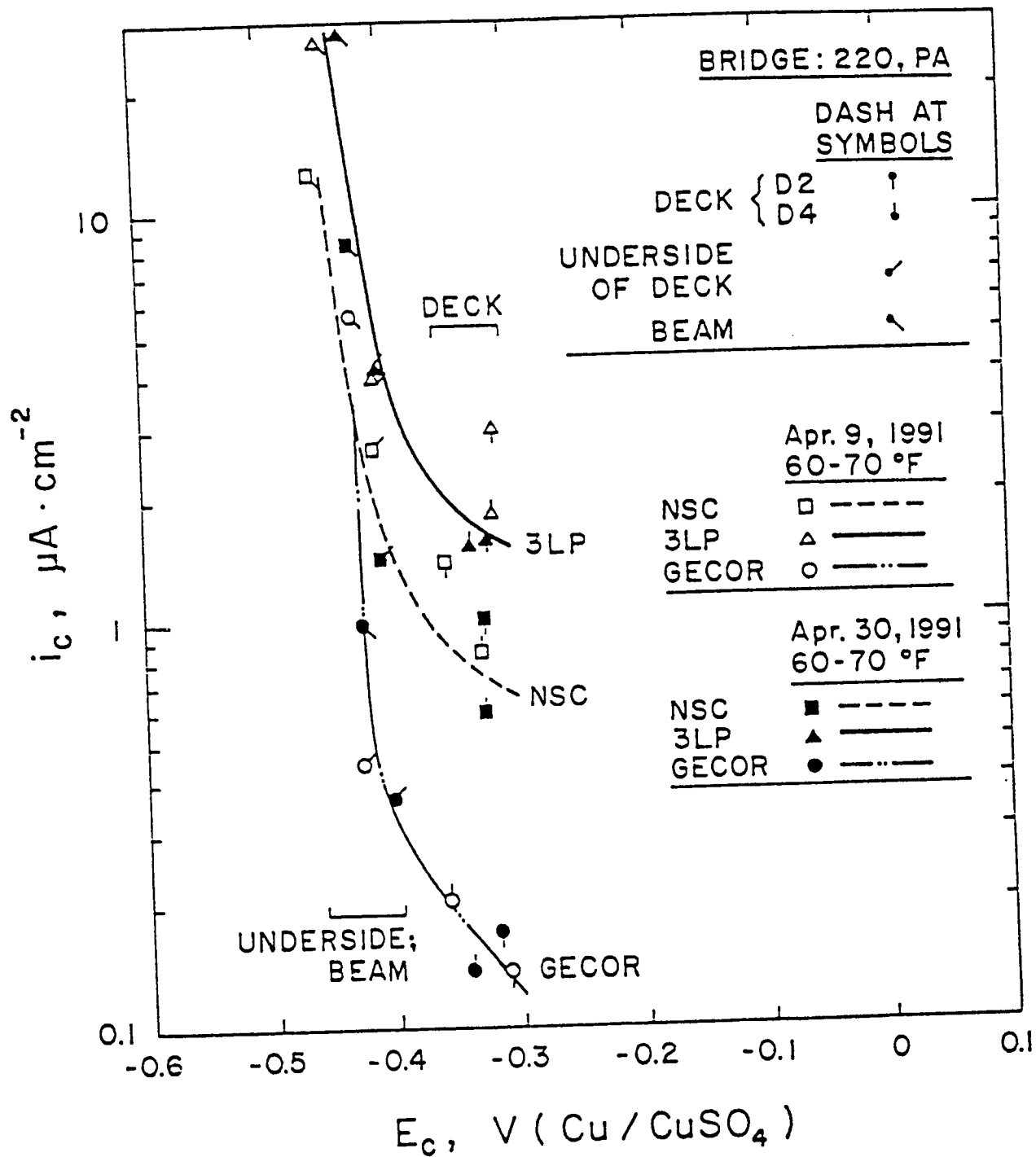


Figure 5-12. Corrosion current i_c versus corrosion potential E_c for Bridge 220, PA, on April 9 and 30, 1991; i_c was determined by devices NSC, 3LP, and GECOR.

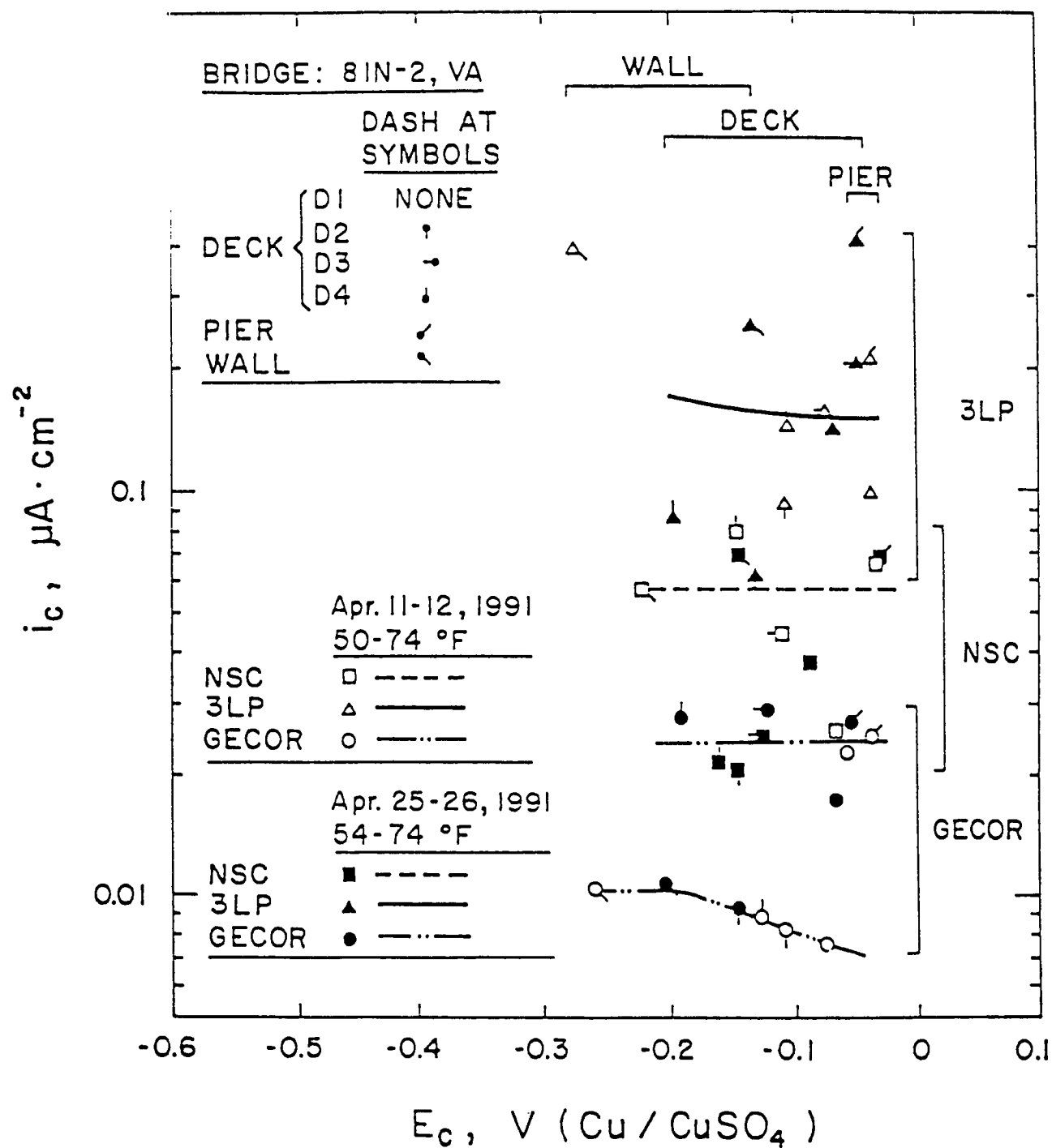


Figure 5-13. Corrosion current i_c versus corrosion potential E_c for Bridge 81N-2, VA, on April 11-12 and 25-26, 1991; i_c was determined by devices NSC, 3LP, and GECOR.

Cu/CuSO₄ half-cell) obtained with the use of the three devices on four bridges. Brackets in the figures show the ranges of E_c for particular sites and bridge elements. In terms of corrosion rate, a current density of $1 \mu\text{A}/\text{cm}^2$ ($0.93 \text{ ma}/\text{ft}^2$) corresponds to $0.0116 \text{ mm}/\text{y} = 0.433 \text{ mpy} = 2.5 \text{ mg} \cdot \text{dc}/\text{m}^2 \cdot \text{d}^{-1}$.

The i_c values for all the devices for the Bahia Honda Bridge (Figure 5-10) showed the same dependence on E_c . The potential dependence was typical for the transition region from the active/passive to the passive state of the metal. The observed dependence correlates well with the prediction of corrosion behavior on the basis of corrosion potential values (39), showing that at potentials around or more positive than -0.2 V , the corrosion current is very low (0.4 to $2 \mu\text{A} \cdot \text{cm}^{-2}$, depending on the device), whereas it rises almost exponentially with the potential shift below about -0.35 V .

As expected, the lowest i_c values were obtained for sites H (high above the water level). The highest i_c values were obtained for sites T (MHTL) and lower i_c values were measured on sites C or L (intermediate height). The latter data are rather unexpected, since they do not match with the appearance of the reinforced concrete; typically, there are no visible signs of corrosion at the MHTL, whereas extensive corrosion with spalling and cracking is frequent at the intermediate heights (sites C and L).

Values of i_c obtained by the devices decreased in the sequence $3\text{LP} > \text{NSC} > \text{GECOR}$. Evidently, this sequence is related to the differences in the current confinement and in the electrode sizes. The highest i_c (3LP) is attributable to the lack of confinement, whereas the lowest i_c (GECOR) apparently results from enhanced confinement and the use of large electrodes.

The measurements on different days (with the same temperature of 80°F) gave similar values. The i_c values on the second day for 3LP were slightly higher than those on the first day. However, as a rule, the reproducibility of the measurements was good.

For Bridge 322, PA (Figure 5-11), the potential dependence of i_c was similar to that for the Bahia Honda Bridge, with i_c values at a given E_c only slightly lower (by about 25 percent at potentials above -0.4 V). The highest i_c and lowest E_c occurred for the pier. Along this pier, water was draining from the deck so that the pier at the measurement site was wet. As in the case of the Bahia Honda Bridge, values of i_c decreased in the sequence $3\text{LP} > \text{NSC} > \text{GECOR}$. No discernible difference was observed in the i_c values measured on the different days.

For Bridge 220, PA (Figure 5-12), E_c for the deck (shoulder area--traffic lanes were overlaid with asphalt) was around -0.33 V, and values of i_c were almost the same as those for the Bahia Honda and 322 bridges at this potential. However, at more negative potentials, the rise of i_c was much steeper, and it took place in the potential range from -0.40 to -0.45 V. This steep i_c rise was observed for the deck underside and beam, both of which were considerably wet. This area of the bridge exhibited much calcium carbonate buildup, corrosion damage, and dripping water. Similar to the bridges described previously, the sequence of i_c values was 3LP > NSC > GECOR, and the data obtained on different days were close to each other.

For Bridges 81N-1 and 81N-2, VA, E_c values were nobler (above -0.3 V), and, accordingly, i_c values were lower than those for the other bridges (data for 81N-2 are presented in Figure 5-13). At these potentials, the i_c values were by about one order of magnitude lower than on the other bridges.

Relation Between Corrosion Current and Concrete Resistance

High i_c values obtained for sites on wet concrete (Figures 5-10 to 5-13) suggest that i_c can be related to concrete resistance, R_s . The i_c versus R_s dependence obtained with NSC for all the test sites is shown in Figure 5-14. Values of i_c increased with decreasing R_s . For the i_c range of about 0.05 to 1.5 $\mu\text{A}\cdot\text{cm}^{-2}$, the relationship can be described by the equation:

$$\log i_c = \log 0.4 - 1.8 \log R_s \quad (5-3)$$

Outside of this i_c region, especially at higher i_c , the i_c versus R_s dependence is characterized by a smaller slope (about -0.7 instead of -1.8), showing that high i_c values are less affected by R_s .

Measurements Under Unfavorable Conditions

Unfavorable conditions included low temperatures (below freezing point), rain, asphalt overlay, poor electrical connection through the rebar grid, and high concrete resistance due to its dryness. Under such conditions, the measurements were difficult to perform, and they gave erratic values.

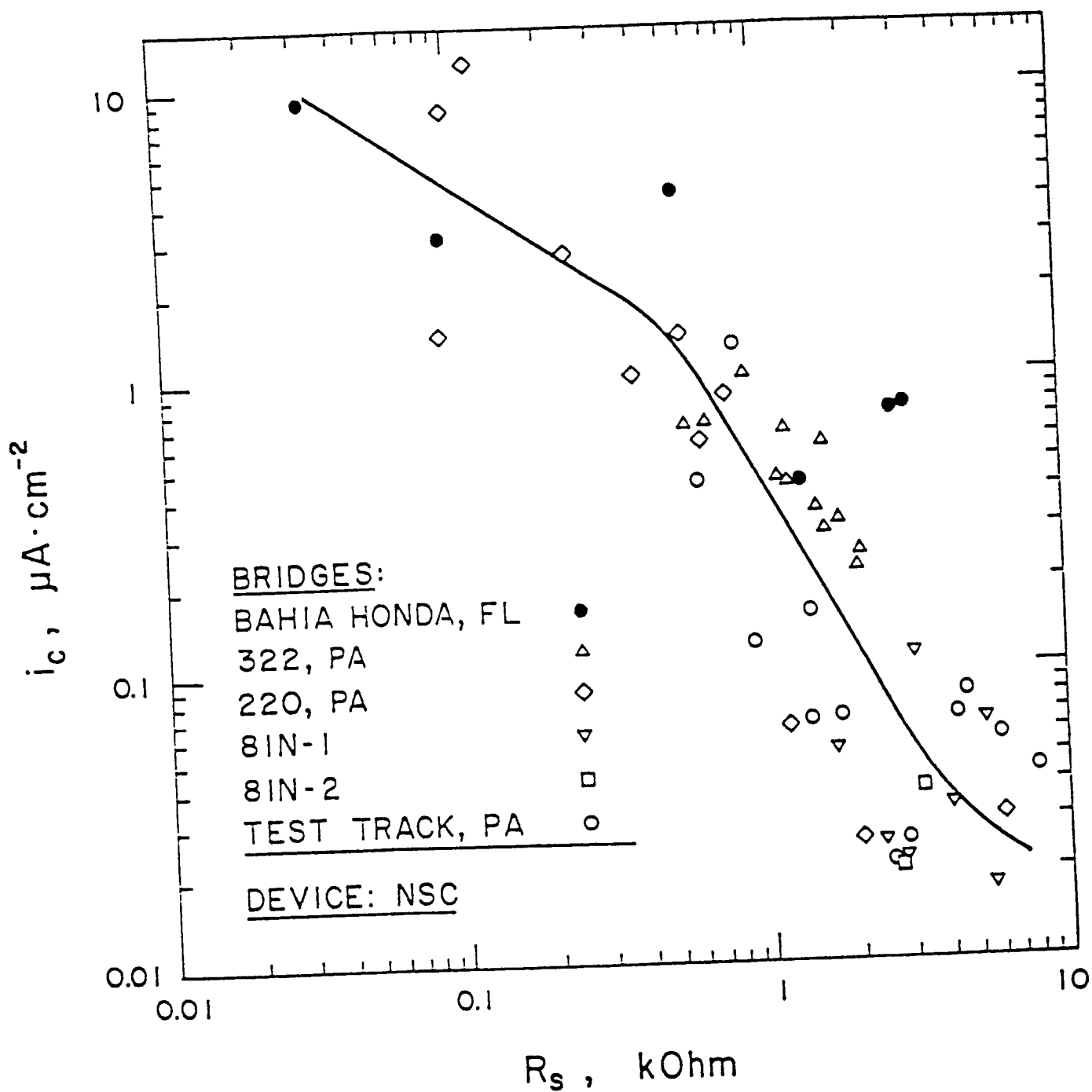


Figure 5-14. Corrosion current i_c versus concrete resistance R_s for the sites tested (i_c and R_s were determined with NSC).

Reproducibility of Data

For large steel-in-concrete systems, such as those investigated in this work, the accuracy of the measurements cannot be determined directly. Hence, the performance of the instruments should be characterized mainly by the reproducibility of the results.

In this work, the reproducibility was expressed by standard error of the mean, EM :

$$EM = S/\sqrt{n} \quad (5-4)$$

where S is the standard deviation, and n is number of measurements on each chosen site with the affixed probe (in these measurements, $n = 3$).

Standard error was plotted versus the mean of corrosion current, i_c , for the sets of data as follows:

- Data from all the devices for each bridge separately;
- Data from all the bridges for each device separately; and
- Data from all the devices for all the bridges together.

For illustration, plots of $\log EM$ versus $\log i_c$ are shown for Bahia Honda Bridge with data from all the devices (Figure 5-15), for the 3LP device with data from all the bridges (Figure 5-16), and for all the devices and bridges (Figure 5-17). These plots show that there exists an approximately linear relationship between $\log EM$ and $\log i_c$. Straight lines can be drawn through the data plotted for each bridge or each device separately.

Parameters of equations for straight lines drawn on the plots are given in Tables 5-2 and 5-3 for the data for each bridge and each device, respectively. The parameters did not differ much for particular bridges or devices. For the bridges, Parameter A was about -1.4, and Parameter B was on average close to unity, though for four bridges it was about 0.8 (but 1.55 for the Bahia Honda Bridge). The scatter of the data can be expressed by the square of the correlation factor (coefficient of determination), R^2 . R^2 for the bridges ranged from 0.54 to 0.82, with the average being 0.67. These data show that the standard error for the mean

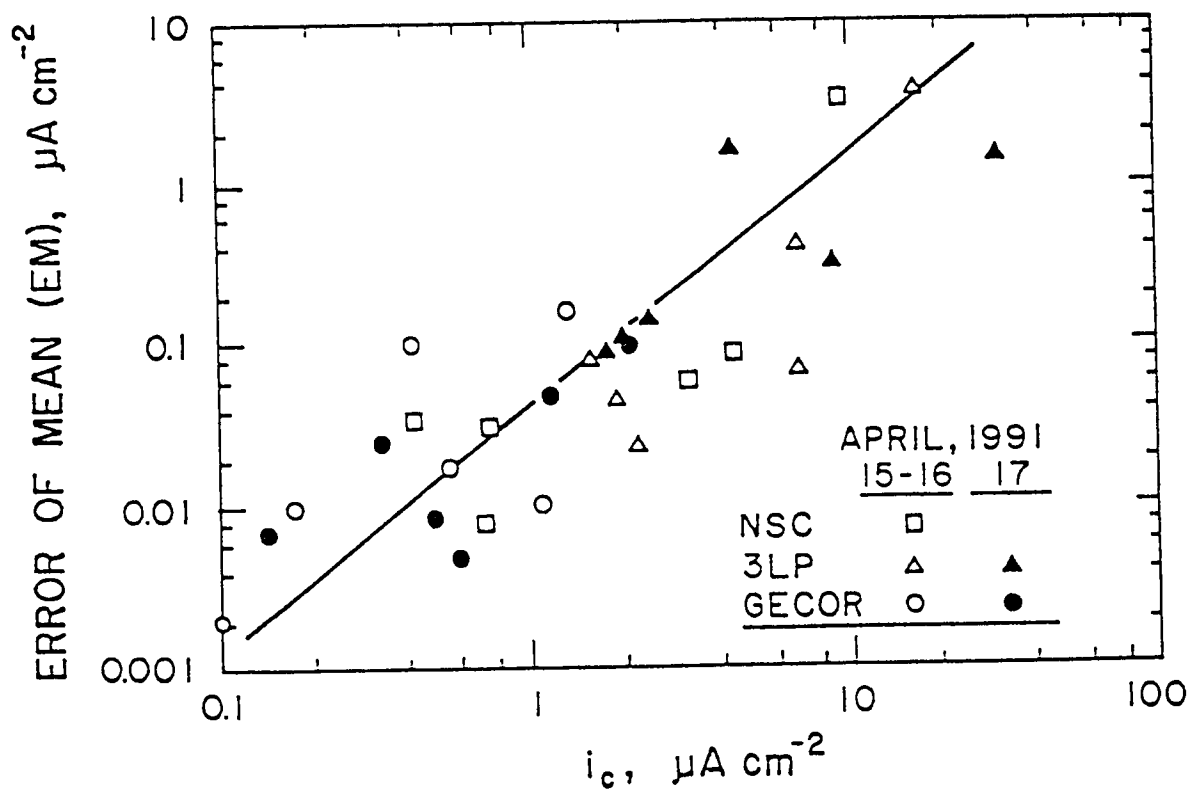


Figure 5-15. Standard error (EM) of i_c as a function of i_c for Bahia Honda Bridge, measured by devices NSC, 3LP, and GECOR on days indicated. The i_c is the mean of corrosion current values from three measurements.

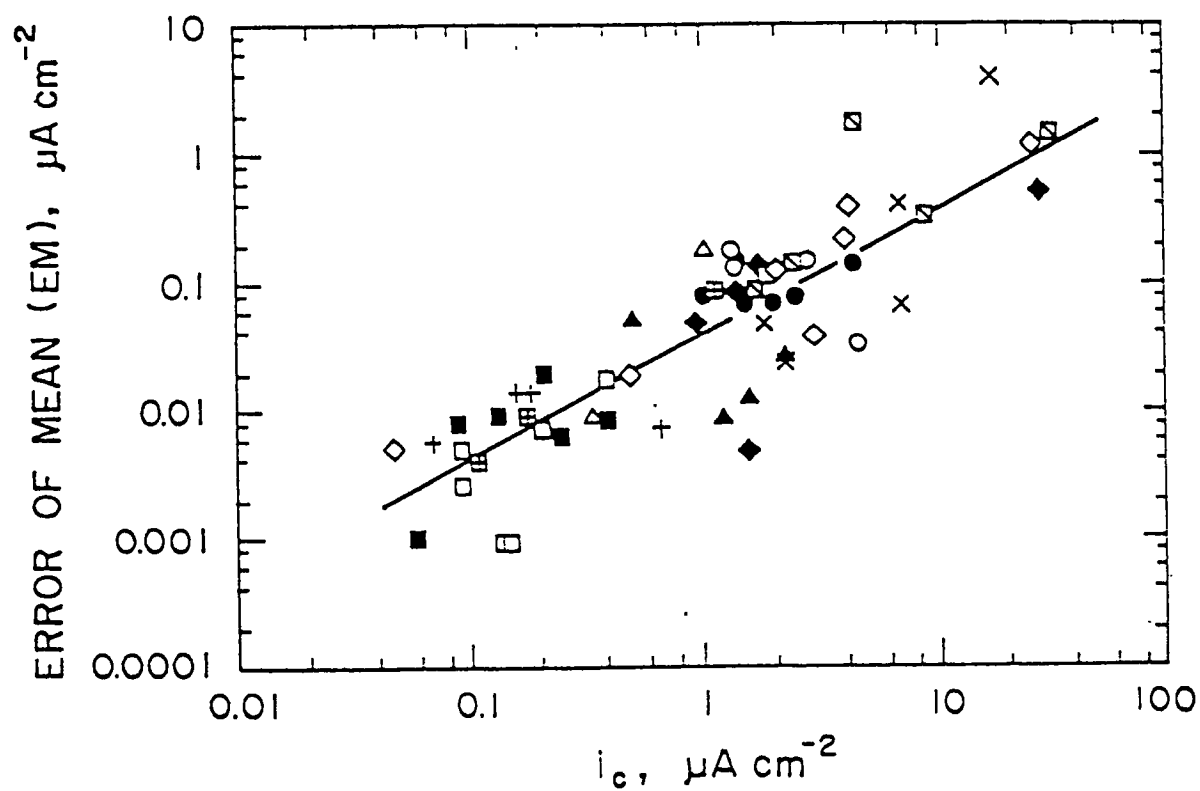


Figure 5-16. Standard error (EM) versus i_c for all the bridges, measured by 3LP device.

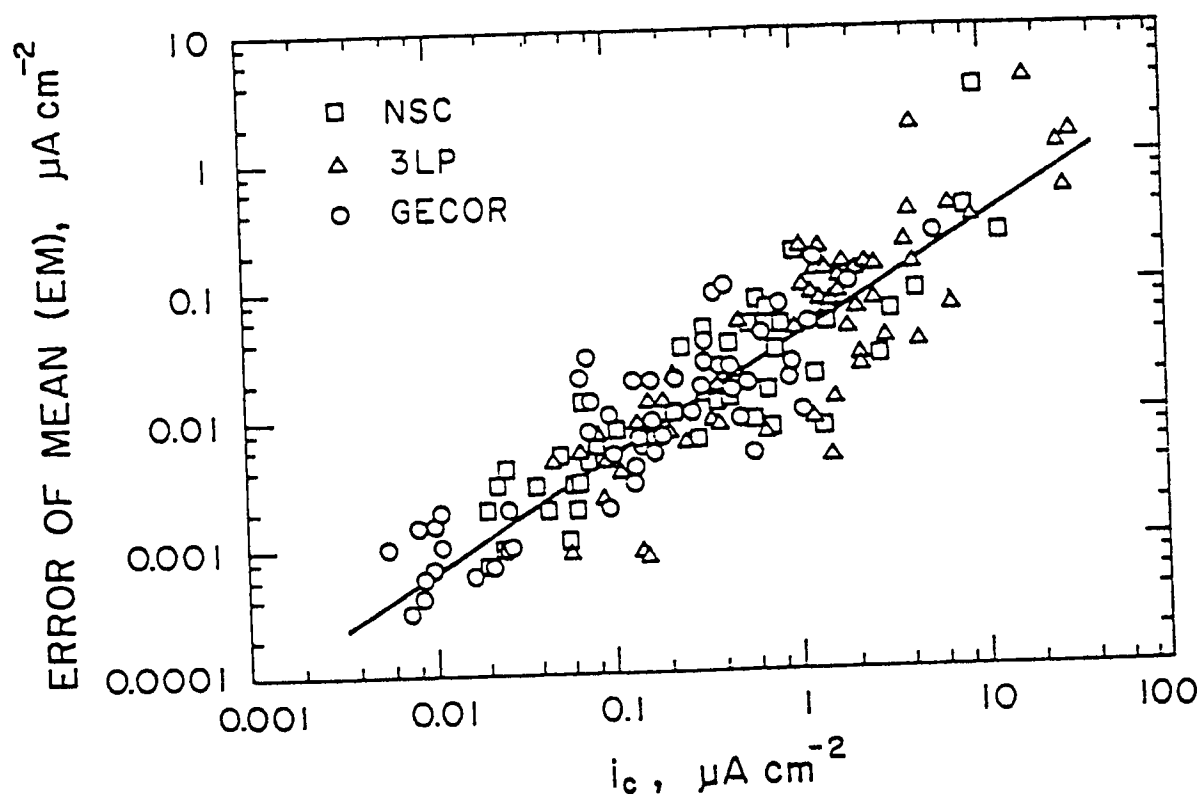


Figure 5-17. Standard error (EM) versus i_c for all the bridges, measured by all the devices.

Table 5-2. Values of A and B in equation $\log EM (\text{Bridge}) = A + B \log i_c$ for data from all the devices for each bridge separately; R^2 is the coefficient of determination.

Bridge	A	B	R^2
Bahía Honda, FL	-1.37	1.55	0.718
322, PA	-1.26	0.87	0.536
220, VA	-1.43	0.82	0.815
81N-1, VA	-1.39	0.75	0.658
81N-2, VA	-1.56	0.83	0.621
Mean	-1.40 ± 0.05	0.96 ± 0.15	0.67 ± 0.05

Table 5-3. Values of C and D in equation $\log EM (\text{Device}) = C + D \log i_c$ for data from all the bridges for each device separately; R^2 is the coefficient of determination.

Device	C	D	R^2
NSC	-1.34	0.88	0.755
3LP	-1.37	1.00	0.737
GECOR	-1.29	0.93	0.779
Mean	-1.33 ± 0.02	0.94 ± 0.03	0.76 ± 0.01
All Devices	-1.33	0.92	0.788

corrosion current is proportional to the mean, but essentially independent of the measurement site. As indicated by R^2 , the scatter of the independence of EM on i_c was rather high; however, it did not vary much among the bridges tested.

Similarly, the dependence of EM on i_c is essentially unaffected by the device used. The difference in parameters C and D and R^2 for the particular devices was insignificant, indicating that the scatter of the i_c values was proportional to the absolute values of i_c , and that it was almost the same for all the devices used.

The relationships between the standard error and the mean i_c values obtained indicate that the scatter of the results of field testing depends only on the magnitude of the i_c , and it is affected neither by the particularities of a bridge nor by the instrument used.

Interrelation Between the Devices

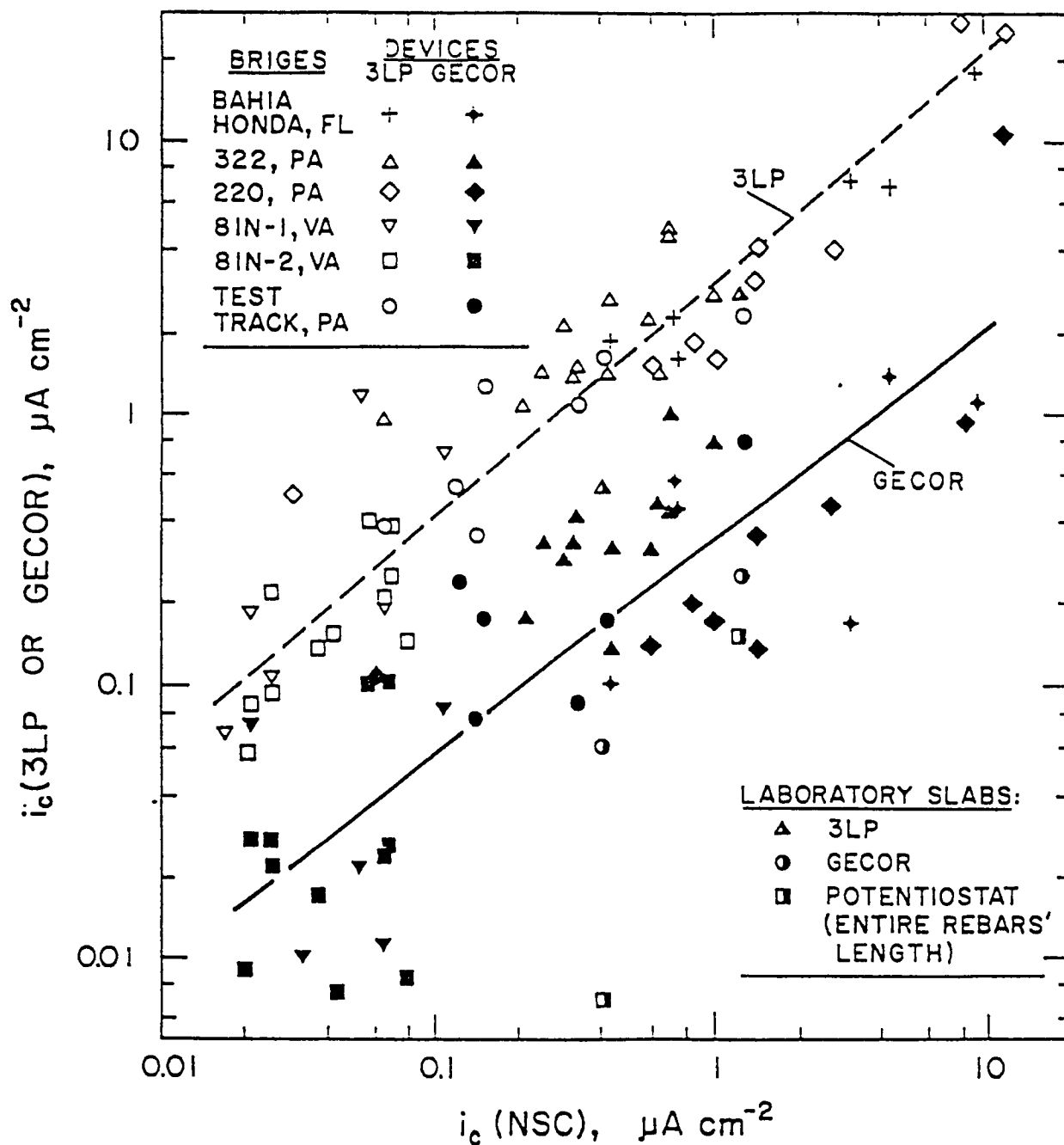
The instruments used for the field testing operate on different principles, so it is reasonable that they give different values of i_c (Figures 5-10 to 5-13). To find out whether these values are interrelated, the data from each of the devices for each of the measurement sites are presented on one plot. Figure 5-18 shows values of i_c from the 3LP and GECOR devices plotted as a function of i_c from the NSC device. Despite a large amount of scatter, there appears to exist a linear relationship between logarithms of i_c values measured by these devices. The respective linear regression equations are:

$$\log i_c (3LP) = 0.47 + 0.84 \log i_c (NSC); R^2 = 0.886 \quad (5-5)$$

$$\log i_c (GECOR) = -0.47 + 0.77 \log i_c (NSC); R^2 = 0.691 \quad (5-6)$$

They indicate the occurrence of a good correlation among the data obtained by different instruments. Thus, it appears that any of these devices gives information related to the real corrosion rate of steel in concrete structures.

In an attempt to estimate the real corrosion rate, measurements were performed on laboratory slabs using the commercial devices and also a potentiostat with IR compensation. In the measurements with a potentiostat, the entire length of an embedded steel bar was polarized through another parallel bar acting as a CE. The data from these measurements are included in Figure 5-18. They show that the values obtained on the laboratory slabs are within the range of the values from the field testing. This demonstrates that the interrelationship



Note: $\log i_c (3LP) = 0.47 + 0.84 \log i_c (NSC); R^2 = 0.886.$
 $\log i_c (GECOR) = -0.47 + 0.77 \log i_c (NSC); R^2 = 0.691.$

Figure 5-18. Relationships between i_c values determined by NSC, 3LP, and GECOR for all the field test sites and for laboratory slabs.

between the instruments encompasses the data both from the large structures and from the laboratory slabs.

Values obtained with a potentiostat can be regarded as "true" corrosion rates. They are lower than those obtained with the commercial instruments. This shows that the commercial instruments overestimate the actual corrosion rate. Among the devices used, the GECOR device gave values of i_c that were closest to the true corrosion rate.

Discussion

The field test data indicate that the corrosion behavior of the reinforcing steel in large concrete structures resembles the anodic behavior of steel in the active-passive transition region. The low i_c values and their lack of dependence on E_c at potentials more positive than about -0.25 V (Cu/CuSO₄) are characteristic of the passive state, whereas the rise of i_c with the shift of E_c in the negative direction is characteristic of the active/passive transition state (Figures 5-10 to 5-13). A similar dependence between potential and corrosion rate was also observed by Escalante (63) on laboratory concrete specimens. This observed relation demonstrates that the potential measurements alone can provide meaningful, though qualitative, information on the corrosion condition of the reinforcing steel. They support the general opinion on the validity of the information obtained from half-cell measurements for estimating the corrosion state of steel reinforcement (42).

The i_c values increased with decreasing concrete resistance (Figure 5-14), indicating a close interrelation between these two parameters. Langford and Broomfield (67) suggested that the resistivity of the concrete should be measured in conjunction with potential mapping, and recently Millard et al. (68) found a clear correlation between negative open-circuit potentials, low concrete resistivities, and instantaneous corrosion rates. The correlation between i_c and concrete resistances is expected, in view of the ionic current involved in corrosion processes. The resistivity of concrete is determined primarily by its moisture content. In the present study, the lowest E_c , highest i_c , and the lowest concrete resistances were obtained for the sites where concrete appeared to be wet for an extended time (MHTL for the Bahia Honda Bridge, a pier with draining water on Bridge 322, PA, and the underside of the deck and a beam of Bridge 220, PA).

Reproducibility of the results was expressed by the standard error of the mean. It varied with the absolute values of corrosion current. However, it was not affected by the measurement site or the device. This provides evidence for a direct connection between measured values and real corrosion rates.

The instruments give different values of corrosion current. However, the values obtained by the different instruments are closely interrelated in the entire range of corrosion currents from the passive to active state. The interrelation among the instruments has a significant practical importance, since it shows that any of these instruments can be used in the inspection, monitoring, and testing of steel rebars in concrete structures.

6

Summary and Conclusions

Basic Laboratory Studies

A variety of laboratory studies was carried out in order to answer numerous questions and to evaluate certain parameters as a necessary prelude to the development of field testing procedures. In summary, the major findings of the laboratory studies are:

- The increase in polarization resistance, R_p , values after wetting can be explained by the refraction of current towards the normal as it goes into a higher resistance medium. This leads to better confinement and, subsequently, an increased R_p .
- The potential of the steel-in-concrete system was found to shift in the cathodic (less noble or more negative) direction after wetting, and it stabilized some time after the wetting of the concrete surface. These trends were observed to become more pronounced as the resistivity of the concrete and the cover thickness of the concrete increased. This is because water fills the concrete pores and impedes the access of atmospheric oxygen to the rebar.
- Reproducibility of the R_p measurements was markedly improved by:
 - making the concrete surface planar (intimate probe contact);
 - decreasing the contact resistance between the probe and concrete surface by using water or conducting paste;

- symmetric positioning of the probe over the rebar; and
- making R_p measurements only after the corrosion potential stabilized.
- A GE confines the polarized area of a steel rebar far more effectively than a single CE. The polarized area decreases by an order of magnitude when a GE is used.
- Improved signal confinement from the CE is achieved by:
 - Decreasing the separation between the CE and the GE.
 - Increasing the width of the GE.
- The top portion of the rebar (facing the electrode) is polarized to a much greater extent (and the polarization can occur exclusively on the top half) during polarization resistance measurements, rather than the entire circumference, as is commonly assumed. This conventional assumption leads to an underestimation of the corrosion rate by up to half of its real value. This unusually strong focusing of the current to the top half is greater than theoretically predicted when a uniform R_p is assumed, but it is more in line with modeling results when considering localized corrosion (macrocells), which has a lower R_p than the adjacent passive surfaces.
- A rebar becomes more corroded when anodic currents are applied from both the CE and the GE, compared to when the polarization is only applied through the CE.
- High polarization resistance values will occur near edges and internal discontinuities (e.g., cracks or voids) due to the limited signal distribution arising from the lack of a medium in which to spread.
- The GE used in the experiments to measure polarization resistance values for locating corroding areas was unable to confine the signal distribution completely below the CE.
- Even with an ineffective GE, polarization resistance measurements can be used to identify and estimate the extent of a corroding area. These measurements can be used in conjunction with corrosion potential measurements to better define corroded areas in reinforced concrete structures.

- When a GE is used in conjunction with an active/passive couple (macrocell), it is the active part of the couple that controls current distribution to the polarized area rather than the whole couple, as is usually assumed.
- The results obtained with a macrocell indicate that confinement is only obtained when measurements are carried out, using a GE, over the active part (which is surrounded by passive areas) of the macrocell. Poor confinement is achieved when measurements are made over the passive part (which is surrounded by active areas of the macrocell).
- The GE was able to confine signal distribution in a highly resistive medium over a separation of 11 in. (28 cm). Therefore, for field testing of concrete structures, which generally have smaller cover thickness (typically 2 or 3 in. [5.1 or 7.6 cm], maximum) much better confinement can be expected.
- A linear correlation observed between polarization resistance values of small mortar specimens shows that the results obtained by EIS and the NSC device will be similar for specimens with comparable WE and CE areas.
- None of the tested devices (NSC, 3LP, and GECOR) were able to confine the signal distribution for a highly resistive, passive, steel-in-concrete system.
- Of the three devices tested (3LP, NSC, and GECOR), the GECOR device gives the best current confinement for active steel-in-concrete systems.

Current Distribution Studies

Numerical methods were used to assess, theoretically, the applicability of GEs for detecting and locating corrosion on rebars embedded in concrete. This work shows that:

- The current distribution pattern around the circumference of the rebar changes somewhat when a GE is used. In general, the top portion of the rebar is subjected to most of the polarization.
- The GE can be an effective tool for defining the polarized area of the rebar surface.
- The degree of success in the application of the GE technique depends on: the magnitude of the polarization resistance, R_p ; concrete cover thickness; and the

design of the CE system used. The most significant parameter is concrete cover thickness. The polarized area increases dramatically as thickness increases. The separation distance between the CE and the GE is another important parameter. If the GE width is larger than the concrete cover thickness, the polarized area does not change very much with increases in GE size.

- Variations in the distribution of the concrete resistivity have a significant influence on the potential/current distribution. If the outer portion of the concrete structure has a lower resistivity compared to the remaining portion of the concrete, the system presents a more uniform signal distribution. It is recommended that the concrete surface be appropriately wetted before R_p measurements in field tests to ensure good electric contact between electrodes and concrete surface for more accurate results.
- In the presence of macrocells, the GE helps to confine current. The position of the CE becomes an important parameter. The best results are obtained when the CE is placed directly over the active portion of the rebar.

Field Validation Studies

Electrochemical measurements were carried out on chosen bridges in three states with the use of three devices (3LP, United States; NSC, Japan; GECOR, Spain) to evaluate their performance in the validation of the corrosion rate of steel reinforcement in concrete. Corrosion currents were estimated from the polarization resistance. The main results and conclusions are as follows:

- Corrosion currents, i_c , were low and almost potential-independent at half-cell potentials nobler than about -0.25 V (Cu/CuSO₄), whereas they increased strongly as the potential shifted to more negative values.
- The observed relationship between corrosion current and half-cell potential correlated well with the predictions of corrosion probability based on the potential measurements alone (ASTM C876-87).
- Corrosion currents were inversely proportional to the concrete resistance. Visual observations indicated that high corrosion currents were found at sites of high moisture content in the concrete. Therefore, it can be supposed that high corrosion currents were closely related to high moisture of the concrete.

- Values of corrosion current obtained using the different devices were compatible, and they indicated the same trend in their dependence on the half-cell potential. The corrosion current values decreased in the sequence $3LP > NSC > GECOR$.
- Reproducibility of the data, as expressed by the standard error of the mean, was nearly the same for all the devices and on all of the bridges. The standard error increased with the increasing mean of corrosion current in almost the same way for all of the bridges and devices.
- Values of i_c from various devices were interrelated. Values obtained by any one of the devices can be, to some approximation, recalculated into values of another device by using empirical formulas. This suggests that any of the three devices can provide meaningful information on the corrosion rate of steel reinforcement in concrete structures.
- Preliminary results on the comparison of the measured and true corrosion currents suggest that among the instruments used, the GECOR device gives the i_c values most closely matching the true values.

Test Procedure

A recommended test procedure, in American Society of Testing and Materials (ASTM) format, has been prepared for the determination of corrosion rate of reinforcing steel in field concrete structures. It is presented in Volume 8, "Procedure Manual," of this report series.

References

1. Slater, J. *Corrosion of Metals in Association with Concrete*. ASTM STP 818. Philadelphia, PA: ASTM, 1983, 83 pp.
2. Cady, P.D. *Chloride Corrosion of Steel in Concrete*. ASTM STP 629. Edited by D.E. Toinini and S.W. Dean, Jr., Philadelphia, PA: ASTM, 1977, pp. 3-11.
3. Litvan, G. and J. Bickley. *Concrete Durability*. Detroit, MI: American Concrete Institute SP 100. Edited by J. Scaloni. 1987, pp. 1503-1515.
4. Borgard, B., C. Warren, S. Somayaji, and R. Heidersbach. *Corrosion Rates of Steel in Concrete*. ASTM STP 1065. Edited by N.S. Berke, V. Chaker, and D. Whiting. Philadelphia, PA: ASTM, 1990, pp. 174-188.
5. AASHTO, FHWA, TRB, NCHRP, Strategic Highway Research Program-Research Plans, Final Report, Technical Research Area 4, TRA 4-1 (May 1986), 60 pp.
6. Isecke, B. *Materials Performance* 21 No. 12 (1982): 36.
7. Heidersbach, R. "Corrosion." Chapter 3 in *Attorney's Guide to Corrosion*, edited by I. Kuperstein and N. Salters. New York: Matthew Bender, 1986.
8. "Salt Flattens Old Garage." *Engineering News Record* 11 (June 4, 1984).
9. U. S. Secretary of Transportation, *Second Annual Report to Congress on the Highway Bridge Replacement and Rehabilitation Program*, May 1981.
10. ENR Washington Observer, *Engineering News Record*. 218 No. 22 (1987): 7.
11. Broomfield, J. P. "The Determination of Rates of Highway Bridge Deterioration. Rehabilitation and Life Cycle Costing Under the Strategic Highway Research Program." Paper presented at NACE Corrodible Structures Conference, Cambridge, U.K. 1991.

12. Matsuoka, K., H. Kihira, S. Ito, and T. Murata. Paper No. 121. Presented at Corrosion '87 NACE, Houston, TX. 1987.
13. Clear, K.C. *Transportation Research Record* 1211 (1989): 28-37.
14. Andrade, C., V. Castelo, C. Alonso, and Y. Gonzalez. ASTM STP 906. Philadelphia, PA: ASTM, 1984, pp. 43-63.
15. Feliu, S., J.A. Gonzalez, S. Feliu, Jr., and M. C. Andrade. "Polarization Resistance in Reinforced Concrete." *ACI Materials Journal* No. 87-M47 (Sept./Oct. 1990): 457-460.
16. Gonzales, J., A. Molina, M. Escudero, and C. Andrade. *Corrosion Science* 25 (1985): 917.
17. Gonzales, J., A. Molina, M. Escudero, and C. Andrade. *Corrosion Science* 25 (1985): 519.
18. Sagues, A.A. *Corrosion of Rebars in Concrete*. Edited by P. Virmani. NACE 87 (1988): 13.
19. Stern, M. and A.L. Geary. *Journal of the Electrochemical Society* 104 (1957): 56.
20. Jackson, P.D. *Geophysical Prospecting* 29 (1981): 601.
21. Wagner, C. *Journal of the Electrochemical Society* 118 No. 158 (1951).
22. Hoar, T.P. and J. N. Agar. *Discussions of the Faraday Society* 1 No. 162 (1947).
23. Shih, H. and H. W. Pickering. *Journal of the Electrochemical Society* 134 No. 551 (1987).
24. Tamura, M., M. Nagayama, and K. Shimozawa. *Corrosion of Reinforcement in Concrete*. Edited by C.L. Page, K.W. Treadway, and K.P.B. Bamforth. New York: Elsevier Applied Science, 1990, p. 372.
25. Andrade, C. and J.A. Gaonzalez. "Quantitative Measurements of Corrosion Rates of Reinforcing Steels Embedded in Concrete Using Polarization Resistance Measurements." *Werkstoffe and Korrosion* 29 (1978): 515.
26. Feliu, S., J.A. Gonzalez, M.L. Escudero, and C. Andrade. *Influence of Counter Electrode size on the on-site Measurement of Polarization Resistance in Concrete Structures*. No. 142. Paper Presented at Corrosion '90, Las Vegas.
27. Macdonald, D.D., H.C.H. McKubre, and M. Urquidi-Macdonald. *Corrosion* 44 No. 1 (1988): 2.
28. Macdonald, D.D., M. Urquidi-Macdonald, R.C. Roche-Filho, and Y. El-Tantawy. *Corrosion* 47 No. 5 (1991): 330.

29. Feliu, S., J.A. Gonzalez, M.L. Escudero, S. Feliu, Jr., and C. Andrade. "Possibilities of the Guard Ring for Electrical Signal Confinement in the Polarization Measurements of Reinforcements." *Corrosion* 46 No. 12 (1990): 1015.
30. Sehgal, A., Y.T. Kho, K. Osseo-Asare, and H.W. Pickering. Paper 39.1. Presented at the 29th Annual Conference of Canadian Institute of Metallurgists, Hamilton, Canada, 1990.
31. Matsuoka, K., H. Kihira, S. Ito, and T. Murata. *Corrosion Rates of Steel in Concrete*. ASTM STP 1065. Edited by N.S. Berke, V. Chaker, and D. Whiting. Philadelphia, PA: ASTM, 1990, pp. 103-117.
32. Jasinski, R.J., and K.D. Efrid. "Electrochemical Corrosion Measurements in Crude Oil." *Corrosion* 43 No. 8 (1987): 476.
33. Jasinski, R.J., and K.D. Efrid. "Electrochemical Corrosion Probe for High Resistivity Hydrocarbon/Water Mixtures." *Corrosion* 44 No. 9 (1988): 658.
34. Guyod, H. "Factors Affecting the Responses of Laterolog-Type Logging Systems (LL3 and LL7)." *Journal of Petroleum Technology* 16 (1964): 211.
35. de Witte, L., K.P. Fournier, and H. Tejada-Flores. "Potential Distribution Due to a Cylindrical Electrode Mounted on an Insulating Probe." *Geophysics* XXII No. 1 (1957): 67.
36. Moran, J.H., and R.E. Chemali. "More on the Laterlog Device." *Geophysical Prospecting* 27 (1979): 902.
37. Babskow, A. "Some Achievements in the Field of Logging and Processing the Focused Resistivity Logs." *Revue Roumaine de Geologie Geophysique et Geographie* 25 (1981): 115.
38. Sagues, A.A. *Critical Issues in Electrochemical Corrosion Measurements Techniques for Steel in Concrete*. Paper No. 141. Presented at Corrosion '91. Cincinnati, 1991.
39. Stratfull, R.F. "Half-Cell Potentials and the Corrosion of Steel in Concrete." *Highway Research Record* 443 (1973): 12-21.
40. Elsener, E., and H. Bohni. "Lokalisierung von Korrosion in Stahlbeton. Potentialfeldmessungen-Möglichkeiten und Grenzen." *Schweizerischer Ingenieur und Architekt* 105 (1987): 528.
41. Berkeley, K.G. and S. Pathmanban. "Practical Potential Monitoring in Concrete." *Proceedings of UK Corrosion '87* (1987): 115-131.
42. "Standard Test Method for Half Cell Potentials of Reinforcing Steel in Concrete." ASTM C876-87. Philadelphia, PA: ASTM.

43. Baker, A.F. Paper No. 3. Presented at the Seminar on Corrosion in Concrete-Monitoring, Surveying and Control by Cathodic Protection. London Press Center, May 13, 1986.
44. Elsener, B., S. Muller, M. Suter, and H. Bohni. Measurement and Testing in Civil Engineering, RILEM, Lyon, France (1988).
45. Guoyd, H. "Examples of Current Distribution About Laterolog Sondes." *The Log Analyst* 7 No. 1 (1966): 27.
46. Wenger, F., and J. Galland. "Analysis of Local Corrosion of Large Metallic Structures or Reinforced Concrete Structures by Electrochemical Impedance Spectroscopy (EIS)." *Electrochimica Acta* 35 No. 10 (1990): 1573.
47. Holm, J. *Corrosion, Concrete and Chlorides*. American Concrete Institute SP 102. Edited by F.W. Gibson. Detroit, MI: ACI, 1987, p. 35.
48. Schießl, P. "Chlorinduzierte Korrosion von Stahl in Beton." *Betonwerk und Fertigteil Technik* 10 (1986): 626.
49. Berke, N.S., D.F. Shen, and K.M. Sundberg. *Corrosion Rates of Steel in Concrete*. ASTM STP 1065. Edited by N.S. Berke, V. Chaker, and D. Whiting. Philadelphia, PA: ASTM, 1990, pp. 38-51.
50. Fontana, M.G. *Corrosion Engineering*. New York: McGraw Hill, 1987, p. 488.
51. Feliu, S., J.A. Gonzalez, C. Andrade, and V. Feliu. *Corrosion* 44 No. 10 (1988): 761.
52. Newman, J. *Journal of the Electrochemical Society* 106 (1951): 833.
53. Ibl, N. *Tech. Ingenieur* 12 (1976): 902.
54. Ibl, N. IUPAC Information Bulletin No. 59, July 1977.
55. John, D.G., P.C. Searson, and J.L. Dawson. *Brit. Corros. J.* 16 (1981): 102.
56. Dawson, J.L., J.A. Richardson, L.M. Callow, and K. Hladky. *Corrosion '87*. NACE, Houston, 1978.
57. King, R.A., J.L. Dawson, and D. Geary. *Proceedings Symposium Corrosion Steel Reinforcement Concrete Construction*. London: Soc. Chem. Ind., 1979, pp. 135-143.
58. Macdonald, D.D. and M.C.H. McKubre. "Electrochemical Impedance Techniques in Corrosion Science." *Electrochemical Corrosion Testing*. ASTM STP 727. Philadelphia, PA: ASTM, 1981.
59. Macdonald, D.D. and M.C.H. McKubre. *Impedance Spectroscopy*. Edited by J.R. Macdonald. Shiley Interscience, 1986.

60. Li, D. Master's thesis, University Park, PA: The Pennsylvania State University, 1991.
61. Escalante, E., S. Ito, and M. Cohen. NBS Report NBSIR 80-2012. Washington, D.C.: NBS, March 1980, 43 pp.
62. Escalante, E., E. Whiteton, and F. Qui. NBS Report NBSIR 86-3456. Washington, D.C.: NBS, October 1986, pp. 1-27.
63. Escalante, E. "Effectiveness of Potential Measurements for Estimating Corrosion of Steel in Concrete." In *Corrosion of Reinforcement in Concrete*, edited by C.L. Page et al. London: Elsevier, 1990, pp. 281-292.
64. Danson, J.L., D.G. John, M.I. Jafar, K. Hladky, and L. Sherwood. "Electrochemical Methods for the Inspection and Monitoring of Corrosion of Reinforcing Steel in Concrete." In *Corrosion of Reinforcement in Concrete*, edited by C.L. Page et al. London: Elsevier, 1990, pp. 358-371.
65. Tamura, H. and M. Yoshida. Detroit, MI: American Concrete Institute. SP-82. 1984, pp. 689-702.
66. Simon, P. Paper No. 380. Presented at Corrosion '89. New Orleans, April 1989.
67. Langford, P. and J. Broomfield. "Monitoring the Corrosion of Reinforcing Steel." *Construction Repair* (May 1987) 32-36.
68. Millard, S.G., M.H. Ghassemi, J.H. Bungey, and M.I. Jafar. "Assessing the Electrical Resistivity of Concrete Structures for Corrosion Durability Studies." In *Corrosion of Reinforcement in Concrete*, edited by C.L. Page et al. London: Elsevier, 1990, pp. 303-313.

Concrete and Structures Advisory Committee

Chairman

James J. Murphy
New York State Department of Transportation

Vice Chairman

Howard H. Newlon, Jr.
Virginia Transportation Research Council (retired)

Members

Charles Arnold
Michigan Department of Transportation

Don Beuerlein
Koss Construction Co.

Bernard Brown
Iowa Department of Transportation

Richard D. Gaynor
National Aggregates Association/National Ready Mixed Concrete Association

Robert J. Girard
Missouri Highway and Transportation Department

David L. Gress
University of New Hampshire

Gary Lee Hoffman
Pennsylvania Department of Transportation

Brian B. Hope
Queens University

Carl E. Locke, Jr.
University of Kansas

Clellon L. Loveall
Tennessee Department of Transportation

David G. Manning
Ontario Ministry of Transportation

Robert G. Packard
Portland Cement Association

James E. Roberts
California Department of Transportation

John M. Scanlon, Jr.
Wiss Janney Elstner Associates

Charles F. Scholer
Purdue University

Lawrence L. Smith
Florida Department of Transportation

John Strada
Washington Department of Transportation (retired)

Liaisons

Ted Ferragut
Federal Highway Administration

Crawford Jencks
Transportation Research Board

Bryant Mather
U.S. Army Corps of Engineers Waterways Experiment Station

Thomas J. Pasko
Federal Highway Administration

John L. Rice
Federal Aviation Administration

Suneel Vanikar
Federal Highway Administration

11/19/92

Expert Task Group

Charles J. Arnold
Michigan Department of Transportation

Jack J. Fontana
Consultant

Ronald I. Frascoia
State of Vermont Agency of Transportation

Andrew D. Halverson
Minnesota Department of Transportation

Gary Hoffman
Pennsylvania Department of Transportation

Crawford Jencks
Transportation Research Board

Paul D. Krauss
Wiss Janney Elstner Associates

Louis Kuhlmann
Larkin Laboratory--Dow Chemicals USA

Alberto Sagues
University of South Florida

Frederick Szczepanek
New York Department of Transportation

Paul Virmani
Federal Highway Administration

10/9/92

Consultant to the Expert Task Group

John Broomfield